8-1-2015

# CFD Simulation of Heat Enhancement in Internally Helical Grooved Tubes

Sogol Pirbastami
*University of Nevada, Las Vegas*, Sogolpb89@gmail.com

# CFD SIMULATION OF HEAT ENHANCEMENT IN INTERNALLY HELICAL GROOVED TUBES

By

Sogol Pirbastami

Bachelor of Science in Biomedical Engineering
University of Science and Research, Tehran, Iran

2011

A thesis submitted in partial
fulfillment of the requirements for the

Master of Science – Mechanical Engineering

Department of Mechanical Engineering
Howard R. Hughes College of Engineering
The Graduate College

University of Nevada, Las Vegas
August 2015

UNLV | GRADUATE COLLEGE

# Thesis Approval

The Graduate College
The University of Nevada, Las Vegas

July 2, 2015

This thesis prepared by

Sogol Pirbastami

entitled

CFD Simulation of Heat Enhancement in Internally Helical Grooved Tubes

is approved in partial fulfillment of the requirements for the degree of

Master of Science in Engineering – Mechanical Engineering
Department of Mechanical Engineering

Samir Moujaes, Ph.D.
*Examination Committee Chair*

Kathryn Hausbeck Korgan, Ph.D.
*Graduate College Interim Dean*

Darrell Pepper, Ph.D.
*Examination Committee Member*

Brendan O'Toole, Ph.D.
*Examination Committee Member*

Samaan Ladkany, Ph.D.
*Graduate College Faculty Representative*

ABSTRACT

CFD SIMULATION OF HEAT ENHANCEMENT IN INTERNALLY HELICAL GROOVED TUBES

By

Sogol Pirbastami

Samir F. Moujaes, Ph.D.,P.E., Examination Committee Chair
Professor, Department of Mechanical Engineering
University of Nevada, Las Vegas

Heat exchanger devices are widely used in industries, air conditioning systems, refrigeration, etc. These devices have a major role in energy conservation; therefore, increasing the performance of heat exchangers helps save energy, costs and materials. The technique to increase the heat transfer performance is called heat augmentation, which can be applied to pipe surfaces and other surfaces which are used in heat exchangers to improve thermal performance. These techniques are categorized into 3 groups: passive, active and compound technique. In this study a helically machined rectangular groove on the inside of a 2.0 m tube with a diameter of 7.1mm was studied for the heat augmentation effect.

A Computational Fluid Dynamics (CFD) investigation has been carried out to study the heat transfer enhancement in a smooth tube and in four grooved tubes with different pitch sizes (7.1, 12.7, 50 and 130 (mm)). The simulations were performed in the Reynolds number range of 4000-20000. The current CFD predicted values were compared with previously collected experimental data [2]. First, the CFD simulation was run for different groove pitches (203, 254 and 305) to compare them with the published experimental work [2]. The results of these simulations for Nu numbers and friction factors showed good agreement with the experimental values. The primary focus of this study

involves evaluating the effect of groove pitch on heat transfer and friction factors. A thermal enhancement factor is defined to evaluate the performance of the internally grooved tubes. By decreasing the pitch size from 130 to 7.1 (mm) at the same Reynolds number, both Nusselt number and friction factor increase. Also, by increasing the Reynolds number, the Nusselt number, as expected, becomes greater. The highest Nusselt number is obtained for smaller pitch size of 7.1 and 12.7 (mm) but at the penalty of a greater pressure drop compared to smooth tubes. It is observed that there is an optimum value of the enhancement factor ($\eta$) at about Re = 15,000 for all investigated grooves and enhancement up to 20% is obtained for grooved tubes with 7.1 mm pitch size.

The heat transfer properties of grooved tubes revealed that the CFD simulations can be used to improve future design considerations, which leads to improvement of performance in heat exchanger devices.

# ACKNOWLEDGMENTS

This journey would not have been possible without the support of my family, professors and friends. Infinite appreciation goes to my family, who have always been proud of me and encouraged me to pursue my interests. Gratitude is extended to my advisor, Dr. Samir Moujaes for invaluable guidance throughout this process and, also, to my thesis committee Dr. Darrell Pepper, Dr. Brendan O'Toole for their tremendous support. And, my sincere appreciation goes to Jann Wright and Joan Conway for helping me through the tough times. Last but not least, a thank you to my friends for their support and encouragement.

TABLE OF CONTENT

ABSTRACT ..... iii
ACKNOWLEDGMENTS ..... v
TABLE OF CONTENT ..... vi
LIST OF TABLES ..... viii
LIST OF FIGURES ..... ix
CHAPTER 1 INTRODUCTION ..... 1
1.1 Heat Exchangers ..... 1
1.2 Heat Enhancement (Augmentation) Techniques ..... 2
1.2.1 Passive Techniques ..... 3
1.2.2 Active Techniques ..... 5
1.2.3 Compound Techniques ..... 6
CHAPTER 2 LITERATURE REVIEW ..... 7
CHAPTER 3 CFD MODELING ..... 15
3.1 Theoretical Methods ..... 15
3.1.1 Governing Equations ..... 15
3.1.1.1 Conservation of Mass ..... 16
3.1.1.2 Conservation of Momentum (Navier-Stokes Equations) ..... 16
3.1.1.3 Conservation of Energy ..... 17
3.2. Experimental Methods ..... 17
3.3. Numerical Methods - Computational Fluid Dynamics (CFD) ..... 18
3.3.1 STAR-CCM+ ..... 19
3.3.2. Finite Volume ..... 19
3.3.3. Turbulence Modeling ..... 20
3.3.3.1 Reynolds-Average Navier-Stokes (RANS) ..... 20
3.3.3.2 STAR-CCM+ Turbulence Modeling: ..... 21
3.4. K-Epsilon Two Equation Model ..... 22
3.5. Wall Function ..... 23
3.6. Work Chart of the CFD Simulation ..... 24
CHAPTER 4 CFD MODEL DESCRIPTION ..... 26
4.1 Description of Geometry Model ..... 26
4.2. Meshing Scheme ..... 27
4.2.1 Mesh Model ..... 29
4.2.1.1 Surface Mesh ..... 29
4.2.1.2 Volume Mesh ..... 30

4.3 Physics of Simulation ..... 31
4.3.1 Boundary Condition ..... 33
CHAPTER 5 RESULTS AND DISCUSSION ..... 35
5.1 Grid Independence Study ..... 35
5.1.1 Wall Y+ for the Grid Model ..... 40
5.2 Parameters of the Present Research ..... 41
5.3 CFD Validation ..... 43
5.3.1 Smooth Tubes Validation ..... 43
5.3.2 Grooved Tubes Validation ..... 46
5.4 Extended CFD Simulation of Internally Grooved Tubes ..... 51
5.4.1 Nusselt Number ..... 51
5.4.2 Friction Factor (*f*) ..... 52
5.4.3 Thermal performance ..... 54
5.5 Center plane plots of temperature for tube pitch 12.7 ..... 58
5.6 Streamlines for Re number of 10000 ..... 62
5.7 Swirl Effect ..... 65
5.8 Turbulent Kinetic Energy ..... 67
5.9 Heat Transfer Coefficient ..... 71
5.9.2 Circumferentially Averaged Value for the Heat Transfer Coefficient ..... 75
5.9 Axial Pressure Drop along the Tube ..... 78
CHAPTER 6 CONCLUSION ..... 82
6.1 Future Work ..... 84
REFERENCES ..... 85
CURRICULUM VITAE ..... 89

LIST OF TABLES

Table 3.1. Constant Variables of the k- $\varepsilon$ Model ..... 23

Table 4.1. Details of the Test Section ..... 27

Table 4.2 Material Properties of the Fluid ..... 33

Table 4.3 Inlet Boundary Condition of Grooved Tubes with different Pitch Size (7.1, 12.7, 50, 130) and with constant inlet temperature of 24 ◦ C ..... 34

Table 5.1 Mesh Properties in Grid Independence Study ..... 38

Table 5.2 Details of Heat Transfer Characteristics for Grooved Tube with 203 mm Pitch Size ..... 47

Table 5.3 Details of Heat Transfer Characteristics for Grooved Tube with 254 mm Pitch Size ..... 47

Table 5.4 Details of Heat Transfer Characteristics for Grooved Tube with 305 mm Pitch Size ..... 47

Table 5.5 Average Outlet Temperatures in all cases ..... 59

Table 5.6 Calculated Local Heat Transfer for Reynolds of 10000 in Grooved Tube with Different Pitch Size (7.1, 12.7, 50 and 130 (mm)) ..... 76

Table 5.7 Calculated Local Heat Transfer for Grooved Tube with 12.7 (mm) Pitch ..... 77

Table 5.8 Axial Pressure drop ..... 78

LIST OF FIGURES

Figure 1.1 Passive Technique Devices [13] ..... 5
Figure 2.1 Sketch of the Grooved Tube [2] ..... 7
Figure 2.2 Geometric Shapes of the Grooved Tube [4] ..... 8
Figure 2.3 Twisted Tape Insert in Internally Grooved Tube [3] ..... 9
Figure 2.4 Grid for the Plain Tube with Alternate Axis Twisted Tape Insert [20] ..... 10
Figure 2.5 Rectangular Channel with Ribs and Grooves [27] ..... 11
Figure 2.6 The Configurations of Square Duct with Cylindrical Groove [15] ..... 12
Figure 2.7 Geometry of a) Spiral Groove and b) Herring Bone Groove [14] ..... 13
Figure 4.1 2D Sketch of a Grooved Tube ..... 27
Figure 4.2 Schematic Diagram of the Grooved Tube ..... 28
Figure 4.3 Surface Mesh a) Initial Surface b) Remeshed Surface ..... 30
Figure 4.4. Volume Mesh of the Grooved Tube ..... 31
Figure 5.1 Schematic Diagram of a Radial Probe Line of A-A on the Cross Section Plane Used for Axial Velocity and Temperature ..... 36
Figure 5.2 Different Volume Mesh Used in Grid Independence Study ..... 37
Figure 5.3 Comparison of Axial Velocity for Four Different Mesh ..... 38
Figure 5.4 Comparison of Axial Temperature for Four Different Mesh ..... 39
Figure 5.5 Wall Y+ Distribution for chosen Mesh with 2398319 cells ..... 41
Figure 5.6 Comparison of CFD Nusselt Number of a Smooth Tube with Experimental Data ..... 45
Figure 5.7 Comparison of CFD Friction Factor of a Smooth Tube with Experimental Data ..... 45
Figure 5.8 Comparison of CFD and Experimental Nusselt Number for Tube with 203 (mm) Pitch Size ..... 48
Figure 5.9 Comparison of CFD and Experimental Friction Factor for Tube with 203 (mm) Pitch Size ..... 48
Figure 5.10 Comparison of CFD and Experimental Nusselt Number for Tube with 254 (mm) Pitch Size ..... 49
Figure 5.11 Comparison of CFD and Experimental Friction Factor for Tube with 254 (mm) Pitch Size ..... 49
Figure 5.12 Comparison of CFD and Experimental Nusselt Number for Tube with 305 (mm) Pitch Size ..... 50

Figure 5.13 Comparison of CFD and Experimental Friction Factor for Tube with 305 (mm) Pitch Size ..... 50

Figure 5.14 Nusselt Numbers as a Function of Reynolds Number for Four Different Grooved Tubes ( Pitch Size 7.1, 12.7, 50 and 130 (mm)) and a Smooth Tube ..... 52

Figure 5.15 Friction Factor as a Function of Reynolds Number for Four Different Grooved Tubes ( Pitch Size 7.1, 12.7, 50 and 130 (mm)) and a Smooth Tube ..... 53

Figure 5.16 Thermal Enhancement Factor for Grooved Tube with 203 (mm) Pitch Size ..... 56

Figure 5.17 Thermal Enhancement Factor for Grooved Tube with 254 (mm) Pitch Size ..... 57

Figure 5.18 Thermal Enhancement Factor for Grooved Tube with 254 (mm) Pitch Size ..... 57

Figure 5.19 Thermal Enhancement Factor as a Function of Reynolds Number for Four Grooved Tubes ..... 58

Figure 5.20 Center-plane Temperature Profile of Tube with12.7 (mm) Pitch at 4000 Re Number ..... 59

Figure 5.21 Temperature Profile near the Groove ..... 60

Figure 5.22 Center-plane Temperature Profile of Tube with12.7 (mm) Pitch at 6000 Re Number ..... 60

Figure 5.23 Center-plane Temperature Profile of Tube with12.7 (mm) Pitch at 8000 Re Number ..... 61

Figure 5.24 Center-plane Temperature Profile of Tube with12.7 (mm) Pitch at 10000 Re Number ..... 61

Figure 5.25 Streamlines within the Fluid Region in Tube without Groove. ..... 63

Figure 5.26 Streamlines within the Fluid Region in Tube with 7.1 mm Pitch Size ..... 63

Figure 5.27 Streamlines within the Fluid Region in Tube with 12.7 mm Pitch Size ..... 64

Figure 5.28 Streamlines within the Fluid Region in Tube with 50 mm Pitch Size ..... 64

Figure 5.29 Streamlines within the Fluid Region in Tube with 130 mm Pitch Size ..... 65

Figure 5.30 Vector Velocity of [i]+[j] at Re of 10000 for Tube with 7.1 mm Pitch Size 66

Figure 5.31 Vector Velocity of [i]+[j] at Re of 10000 for Tube with 12.7 mm Pitch Size ..... 66

Figure 5.32 Contour Plot of TKE for Tube with 12.7 Groove at Re number of 4000 .... 68

Figure 5.33 Contour Plot of TKE for Tube with 12.7 Groove at Re Number of 6000 .... 68

Figure 5.34 Contour Plot of TKE for Tube with 12.7 Groove at Re Number of 8000 ... 69

Figure 5.35 Contour Plot of TKE for Tube with 12.7 Groove at Re Number of 10000 . 69

Figure 5.36 Contour Plot of TKE for Tube with 12.7 Groove at Re Number of 15000 . 70

Figure 5.37 Contour Plot of TKE for Tube with 12.7 Groove at Re Number of 20000 70

Figure 5.38 Local Heat Transfer Coefficient on Surface of the Tube with 12.7 mm Pitch Size at Re Number of 4,000 ..... 72

Figure 5.39 Local Heat Transfer Coefficient on Surface of the Tube with 12.7 mm Pitch Size at Re Number of 6,000 ..... 72

Figure 5.40 Local Heat Transfer Coefficient on Surface of the Tube with 12.7 mm Pitch Size at Re Number of 8,000 ..... 73

Figure 5.41 Local Heat Transfer Coefficient on Surface of the Tube with 12.7 mm Pitch Size at Re Number of 10,000 ..... 73

Figure 5.42 Local Heat Transfer Coefficient on Surface of the Tube with 12.7 mm Pitch Size at Re Number of 15,000 ..... 74

Figure 5.43 Local Heat Transfer Coefficient on Surface of the Tube with 12.7 mm Pitch Size at Re Number of 20,000 ..... 74

Figure 5.44 Schematic Diagram of cross sections at Different Axial Position Along Different Grooved Tubes. ..... 76

Figure 5.45 Circumferentially Averaged Heat Transfer for Reynolds of 10000 in Grooved Tube with Different Pitch Size (7.1, 12.7, 50 and 130 (mm) ..... 77

Figure 5.46 Pressure Drop along the Smooth Tube for Reynolds Number ranged between 4000-20000 ..... 79

Figure 5.47 Pressure Drop along the Grooved Tube with Pitch Size of 12.7 (mm) for Reynolds Number ranged between 4000-20000 ..... 79

Figure 5.48 Pressure Drop along the Grooved Tube with Pitch Size of 12.7 (mm) for Reynolds Number ranged between 4000-20000 ..... 80

Figure 5.49 Pressure Drop along the Grooved Tube with Pitch Size of 50 (mm) for Reynolds Number ranged between 4000-20000 ..... 80

Figure 5.50 Pressure Drop along the Grooved Tube with Pitch Size of 130 (mm) for Reynolds Number ranged between 4000-20000 ..... 81

Figure 5.51 Comparison of Pressure Drop along the Grooved Tube at Re of 4000 for All Cases ..... 81

# CHAPTER 1

# INTRODUCTION

Improving the heat transfer performance in heat exchanger devices, which is called heat augmentation or intensification, can play a major role in saving energy and material consumption. This also leads to reducing the manufacturing cost of heat exchanging equipment which has been used in various industrial, commercial and domestic applications. Since the energy resources of the earth are decreasing and their costs are increasing, design of energy efficient heat exchangers has significant impact on energy conservation. The demand for improving heat performance leads to developing heat enhancement techniques which help in equipment size reduction, saving operating costs, and reducing pumping power in heat exchangers. Therefore, based on the purpose of the equipment, designers can focus on one of these heat enhancement criteria and provide these benefits [2] [17].

In recent years, the study of different techniques of heat transfer enhancement in heat exchanger devices has gained valuable attention and much research has been done in both heat transfer and thermodynamic consideration [2] [17]. Learning about heat exchanger devices and different heat transfer techniques is the purpose of this chapter.

## 1.1 Heat Exchangers

Heat exchangers are extensively used in HVAC systems (heating, ventilating and air conditioning), chemical and power plants, refrigeration systems, petroleum plants, etc. These devices provide efficient heat transfer between two or more fluids or solid surfaces and between fluids or solid particles with fluids at different temperatures. Heat exchangers

are thermal devices, which have a major role in energy conservation and impact on climate change. They are categorized based on their transfer process, heat transfer mechanism, number of fluids, surface compactness, construction characteristics and flow arrangement. The categories of heat exchangers where the fluids are in direct contact for exchanging heat are called direct transfer types, or simply recuperators. In contrast, in other heat exchangers, there is a separating wall between hot and cold fluids which are referred to as indirect transfer types, or simply regenerators [17]. Most of the heat exchangers have the potential to be considered for heat enhancement, however, each potential application should be tested to see if the enhancement is practical. Nearly all heat enhancement techniques are used for heat exchangers in the refrigeration and automotive industries [26].

## 1.2 Heat Enhancement (Augmentation) Techniques

Augmentation techniques help increase heat convection in heat exchanger devices and decrease the thermal resistance. In many applications such as for chemical reactors, air conditioning and refrigeration systems, there are many techniques being investigated for increasing the heat transfer rate and reducing the size and cost of the devices. Studies have proved that applying enhancement techniques, improve the thermal performance significantly [16]. However, increasing the rate of enhancement is at the penalty of pressure drop. Therefore, in any heat augmentation design, the heat transfer coefficient and pressure drop needs to be analyzed. These techniques are categorized into 3 groups: passive, active and compound technique [26] [16].

### 1.2.1 Passive Techniques

In these techniques external power is not required; rather geometry or surface of the flow channel will be modified to increase heat transfer coefficients. The inserts and rough surfaces will be employed to promote the swirl in the flow, which leads to increase in heat transfer enhancement. In case of extended surfaces, effective heat transfer area on the side of the extended surface will be increased. Passive techniques are a good method due to the lower cost of set up and compact size of the heat exchangers [16]. Heat transfer enhancement by passive technique can be achieved by using:

**Coated or Treated Surfaces** involve using different surface finishes and coating methods with metallic and nonmetallic material. These modifications are used for boiling and condensing applications. For example, in boiling systems, a coating layer of hydrophobic material such as PTFE (polytetraflouroethylene) is used to promote dropwise condensation and a porous coating is used in enhancing nucleate boiling and a higher heat transfer coefficient. Sintered, multilayered and coated surfaces are among some examples of treated surfaces [26].

**Rough surfaces** are provided in two different methods: Integral method, where the roughness is integrated on the surfaces and made by machining or restructuring. The other is a non-integral method, which is done by placing roughness close to the surface to increase heat transfer. Both methods are generally surface modifications that increase turbulence flow, but do not increase heat transfer surface area in the field and are primarily used in a single phase flow. Also, any structure with a regular pattern that repeats and disturbs the boundary layer like a coil insert is an example of non-integral roughness [26].

**Extended surfaces** expand the heat transfer area which increases the heat transfer coefficient. The plain fin may just increase the area, but special structured extended surfaces can increase the heat transfer coefficient, too. In applications for gases, mostly extended surfaces are used to provide both higher heat transfer coefficient (h) and area (A). Since the heat transfer coefficient of liquids is higher than gases, shorter fin height is used for fluid application. Segmented fins on the surface cause a separation in the boundary layer. Therefore, after each separation a new boundary will be formed and will improve the heat transfer rate. These techniques are used in automotive, refrigeration systems and air conditioning applications [13].

**Displaced enhancement devices** are placed into a flow channel and move the fluid through the tube and displace it from the core to the surfaces with lower or higher temperatures. The objective of this technique is to increase the fluid mixing, which leads to improve energy transport. Inserts like conical ring devices, metallic mesh, disks and wire inserts are among displaced enhancement devices [26].

**Swirl flow devices** include different geometrical configurations which provide secondary flow and recirculation in fluids such as: helical twisted tape, inlet vortex generator, static mixer. These are creating swirls in both clockwise and counterclockwise directions. Swirl generator devices can be used in both single and multiple phase flows [26] [13].

**Additives for liquids and gasses** involve the addition of solid particles, soluble trace additives, gas bubbles and liquid droplets. These particles are added to the liquids or gasses to reduce the fluid resistance in the case of single phase flows. In the case of boiling systems, trace additives are added to reduce the surface tension of the liquids [26].

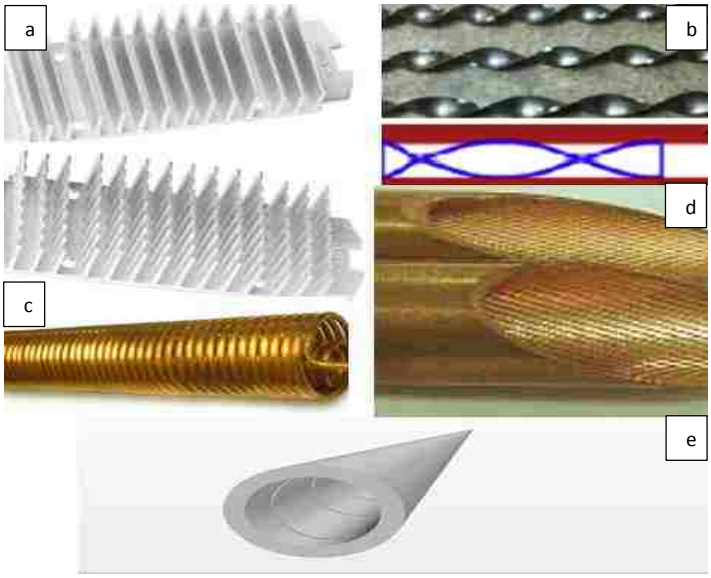


Figure 1.1 Passive Technique Devices. a) Segmented Fin Sink, b) Helical Tape Inserts, c) Coiled Tubes, d) Internally Finned Tube, e) Grooved Tube [13]

### 1.2.2 Active Techniques

These techniques need external power to promote the heat transfer rate. Active techniques are complicated due to design and higher cost of the devices in comparison with passive methods. Therefore, their application is limited. Some active methods are as follows [13]:

**Mechanical Aids** involve devices that are rotating or stirring by mechanical methods. For example, rotator heat exchanger ducts are commercially used and surface scrapers are used for stirring the fluids in chemical processes for viscous fluid.

**Surface Vibration** is applied to improve heat transfer with low or high frequency, such as piezoelectric devices.

**Fluid Vibration** is where pulsation is created in the fluid itself instead of on surfaces. It is useful for single phase flows.

**Electrostatic Fields** are electric and magnetic fields or a combination of the two forms of DC or AC current. Electrostatic fields are applied to heat exchanger systems, which induces greater bulk mixing, force convection or electromagnetic pumping to enhance heat transfer. This technique is applicable in heat transfer processes involving dielectric fluids.

**Injection** is supplying gas or liquid through a porous heat transfer surface into the fluid flow. This technique is used for single phase heat transfer processes.

**Suction** is used to remove vapor or fluid from porous surfaces.

**Jet Impingement** is used for both two phase and single phase heat transfer processes. In this method, single phase fluid is forced normally or in a perpendicular or diagonal direction towards the heat transfer surface [26] [16] [13].

### 1.2.3 Compound Techniques

A compound augmentation technique is a combination of more than one enhancement method (either from active or passive) to improve the thermal performance of heat exchanger devices [13].

Besides heat enhancement techniques, mode of transfer and geometry classification are important. In this study the single phase flow with forced convection mode for the flow inside internally grooved tubes is used. In this current study the effect of groove geometry on heat transfer and pressure drop is investigated. Groove geometry acts as roughness and promotes the flow mixing and interrupts boundary layers.

# CHAPTER 2

# LITERATURE REVIEW

Aroonrat et al. (2013) experimentally investigated the effect of pitch size in internally helical grooved tubes (Figure 2.1) on heat transfer and flow characteristics in stainless steel tubes. The effect of the grooves has shown that the Nusselt number and friction factor obtained from the helical grooved tubes were higher than those of the smooth tubes. Moreover, the Nusselt number and friction factor increased with the decrease of the pitch size. Overall, Thermal performance has improved for the internally grooved tubes [2].

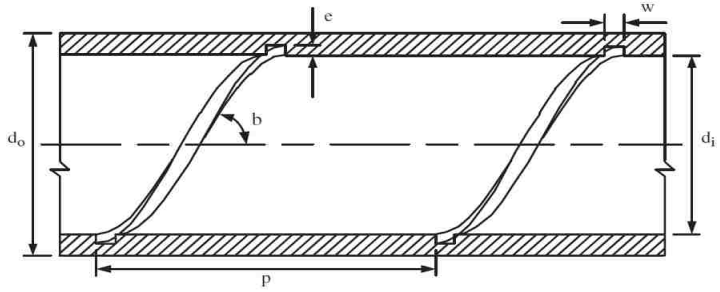


Figure 2.1 Sketch of the Grooved Tube [2]

Bilen et al. (2009) [4] experimentally investigated the effect of groove geometry on heat transfer and friction characteristics of fully developed turbulent flow in grooved tubes (circular, trapezoidal and rectangular). Maximum heat transfer enhancement is obtained up to 63% for circular groove, 58% for trapezoidal groove and 47% for rectangular groove, compared to smooth tubes. Also, the correlation equation is developed experimentally for Nusselt number and friction factor for each tube. In the range of

Reynolds between 10000 to 38000 thermal performance (η) for all grooved pipes is in the range of 1.24-1.28 for circular groove, 1.22–1.25 for trapezoidal groove and 1.13–1.26 for rectangular groove at constant pumping power.

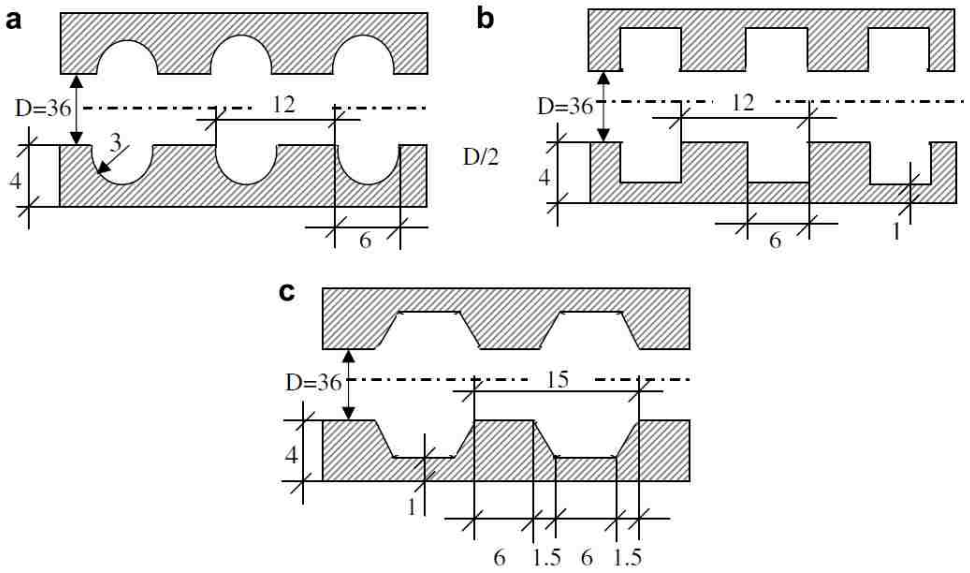


Figure 2.2 Geometric Shapes of the Grooved Tube, Dimension in mm (a) Circular, (b) Rectangular and (c) Trapezoidal Grooves [6]

Bharadwaj, Khondge and Date (2009) [3] experimentally investigated the compound method of heat enhancement with a constant wall heat flux for water flow in the internal spiral grooved tube with twisted tape. Different twist ratio ((Y = 10.15, 7.95 and 3.4) is considered for this study (Figure 2.3), then pressure drop and heat transfer characteristics are defined. Heat transfer enhancement yields 400% in laminar flow and 140% in turbulent flow for spirally grooved tubes without twisted tape compared with smooth tubes. Adding a twisted tape to a spirally grooved tube, increases the enhancement to 600% for laminar and 140% for turbulent flow. However, in both cases, the reduction in heat enhancement observed is 2000<Re< 13000. Among all twisted ratios, the twisted

ratio of Y = 7.95 has the highest heat transfer performance in both laminar and turbulent flows [3].

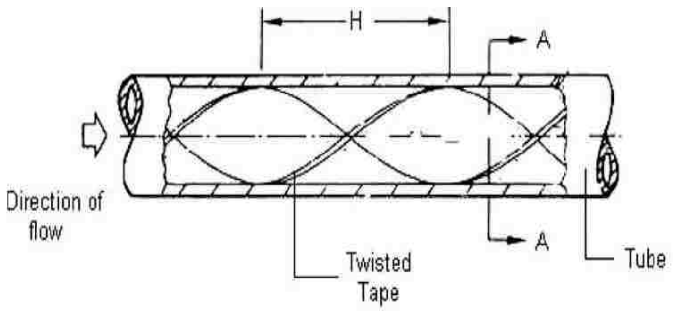


Figure 2.3 Twisted Tape Insert in Internally Grooved Tube [3]

In the study by Graham, Chato and Newell (1999) [8] the performance of an axial micro fin grooved tube with helical angle of 0 for refrigerant R023a was conducted and the results compared with a similar tube with a helical angle of (18°) in different ranges of mass fluxes. The 18° helix angle tube performs better than the axially and grooved tube. Heat enhancement factors have shown 62% and 20% improvement in enhancement for helical and axially grooved tubes compared to smooth tubes at lower mass fluxes [11].

Salman et al. (2014) used Computational Fluid Dynamics (CFD) to investigate heat transfer characteristics and friction factors in a circular tube fitted with twisted tape inserts in a laminar flow region at constant heat flux. Fluent software is used to simulate plain tube and a tube with twisted tape inserts with different twist ratios ($y$ = 2.93, 3.91, 4.89) and alternative angles (β = 30°, 60°, 90°) (Fig 2.4). The results are validated with theoretical and experimental work in literature. Therefore, CFD Simulation is a reliable method for investigating the heat augmentation. Tubes with different twist ratios and angles of helix have shown higher value for The Nusselt number and friction factor

compared to plain tubes and tubes equipped with plain twisted tapes. In this study, the highest heat transfer enhancement belongs to the alternate axis β= 90°and twisted tape ratio of ($y$ = 2.93) [20].

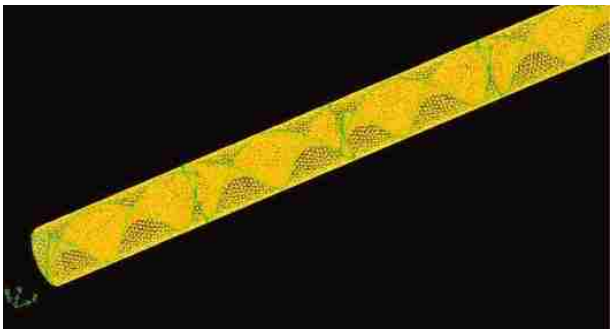

Figure 2.4 Grid for the Plain Tube with Alternate Axis Twisted Tape Insert [9]

Xinyi and Zhou (2012) [27] investigated an overall heat transfer performance and friction factor of water flow in an enhanced surface rectangular channel both experimentally and numerically. Discontinuous crossed ribs and rib-grooves provided in tubes and the flows were examined in a turbulent region. CFD Nusselt number and friction factor are 10% -13.6% higher for ribbed-grooved channel in comparison to experimental data. Furthermore, the effect of rib angels on the heat transfer characteristics was studied by Fluent software. The simulation results showed a rib angle of 45° has the best overall thermal performance, about 18%-36% higher than a rib angle of 0 (figure 2.5).

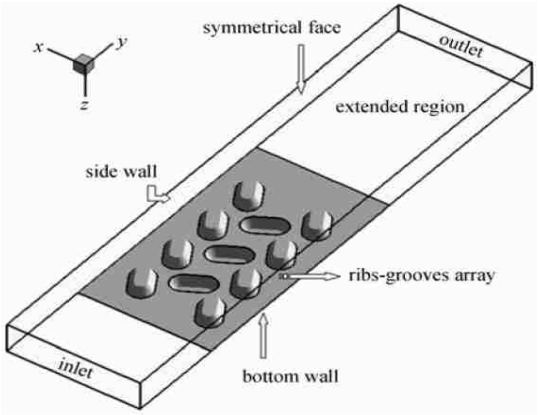


Figure 2.5 Rectangular Channel with Ribs and Grooves [27]

Rahman, Zhen and Kadir (2013) [19] carried out a CFD analysis of flow of refrigerant (R22) through internal grooved copper tubes with Fluent software and investigated heat transfer enhancement in the tubes. Experimental study is too costly and takes a longer time in gathering necessary information. Therefore, numerical simulation is conducted instead of experimental research. The geometry model of an inner grooved tube was designed with SolidWorks software and the grid was generated with GAMBIT software. Then the model was imported to Fluent software to set up the boundary condition and solve the simulation model. The results were obtained and compared with published experimental results. Refrigerant (R22) was used as fluid through a copper tube for two different purposes: condensation and evaporation. The heat transfer coefficient improved for enhanced tube in comparison with smooth tube. The CFD results and experimental data showed strong agreement in this study [19]. In Salman et al. (2013) a study of quadrant-cut twisted tape (QCT) inserts were used as a swirl generator inside the tube, then heat transfer and friction factor characteristics were investigated [21]. They used Sieder and

Tate correlation to validate their data for smooth tube. The results for uncertainty for the Nusselt and Friction factor were determined to be around 8% and 10%, respectively. Results were in the range of Reynolds of 0-2000. The Nusselt number increased with an increasing Reynolds number. The (QCT) inserts by generating vortices and disrupting the boundary layer, improved the fluid mixing and respectively the heat enhancement [21]. Liu, Xie and Simon (2015) [15] studied the heat transfer performance of turbulent flow (Re: 10,000-25,000) in square duct with cylindrical groove. The purpose of this study is to find out the desirable design for better enhancement rate and minimum pressure drop penalties. In this study, 4 different cylindrical shaped grooves in a square rib groove tube were considered (Figure 2.6) and the results were computed with CFD modeling. The pressure drop is less for cylindrical shaped groove tubes in comparison to the square rib tube. The rounder the edges of the cylindrical groove, the better total heat enhancement.

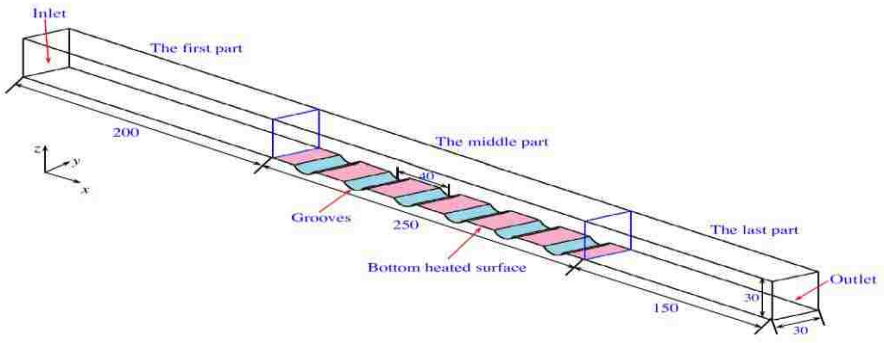


Figure 2.6 The Configurations of Square Duct with Cylindrical Groove [15]

Kaji, Yoshioka and Fujino (2012) [14] experimentally investigated the heat transfer performance of smooth and internally grooved tubes in an air-cooled heat exchanger using CO2 as a refrigerant and Poly alkyl glycol (PAG) oil flow as a lubricant in both cooling and evaporating heat exchanger systems. Two internal grooved configurations

(Herringbone and spiral) (Figure 2.7) are examined for this study. The heat transfer coefficients which are obtained experimentally are 1.8 and 2.1 higher than smooth tube for the spiral and herringbone tubes respectively.

a)  b)

Figure 2.7 Geometry of a) Spiral Groove and b) Herring Bone Groove [14]

Heat transfer performance can be improved by using inner grooved tubes with suitable patterns. Also, the oil's effect was investigated by using an instrument to visualize flow inside the tube. It was observed that herring bone groove has better performance in comparison to spiral and smooth tube in the presence of oil. Therefore, inside geometry can affect oil's behavior [14].

Heat augmentation of internally enhanced surfaces particularly roughness became quite important since the method is economically beneficial for commercial applications. In refrigeration industries mostly rough surfaces are used on the water side of evaporators and condensers in large equipment. Also studies showed that roughness is used in gas turbine blade and gas-cooled nuclear reactors [26]. There are many different geometries that are used for heat enhancement which was explained in this chapter. Some important key factors which should be considered in design and investigation of different roughness including grooves are as follows: roughness height (e), spacing or pitch size (p), roughness width (w) and geometry shape of the roughness. Also two other factors in groove are

applied such as helix angle and number of starts. The integral helical groove may be made as single or multi-start elements. Studies showed that the greatest material saving is for helical internal groove which is about 12% greater than axial grooves. Furthermore, most studies have been conducted on multiple start groove tube, and even Turbo chill tube has commercially made theses tubes for different applications [26]. Based on experimental study that was chosen to compare with the CFD results [2], the heat transfer enhancement in internally grooved tubes was conducted for Reynold in the transient region while fully turbulent. Recently, CFD simulations are used to validate experimental studies. The CFD modeling technique has been recognized as a powerful and effective tool to gain better understanding of the complex heat transfer and fluid problems. Furthermore, due to good agreement between CFD simulation results and experimental studies, scientist could save a great amount of time and money by using simulation techniques to predict the heat transfer characteristics of a flow in heat augmentation methods. Based on this review, many experimental works can be simulated and analyzed by CFD software. In the current study the CFD software STARCCM+ is used to study the heat transfer performance of internally grooved tubes with different pitch sizes in turbulent flow.

# CHAPTER 3

# CFD MODELING

Most flows on earth and around us are in a turbulent region, similarly, so are the turbulent flows inside a cylindrical tube of a combustion engine. These flows have different mechanisms which are categorized by a dimensionless factor called Reynolds number [28]. To describe and predict the characteristics of flow is difficult particularly for turbulent flows. There are three approaches to obtain the solution of fluid flow and heat transfer problems:

- Theoretical approach
- Experimental approach
- Numerical approach, Computational Fluid Dynamics (CFD) [28]

## 3.1 Theoretical Methods

This method has the advantage of providing an exact result by solving the governing equations of flow. However, this method is limited to a few classes of problems since the analytical solution for 3D and 2D flows are highly complex to solve [28].

### 3.1.1 Governing Equations

There are three fundamental laws describing fluid flow, heat transfer and mass transfer. The governing equations of flow are simply a version of conservation laws of physics and may described by both integral and partial differential equations [28] [12].

The governing equations can be presented in Cartesian, cylindrical and spherical coordinates. In this study, the conservation laws are expressed in Cartesian coordinates as follows:

3.1.1.1 Conservation of Mass

Mass flow that is entering the control volume (dxdydz) should be equal to the mass flow that is leaving the control volume.

$$\frac{D\rho}{Dt} + \rho\nabla.\bar{V} = 0 \qquad \text{Conservation of Mass} \qquad (1)$$

3.1.1.2 Conservation of Momentum (Navier-Stokes Equations)

Conservation of momentum or Navier-Stokes equations consists of 3 equations in each direction. These equations are generated based on Newton's second law of motion which stated the momentum of an object is proportional to the net force that is acting on it in the same direction. The net force includes: body forces such as gravity and surface forces that acts on the surface of the element [28] [12]. The three equations in cylindrical coordinates by assuming Newtonian fluid with constant density, viscosity are as follows:

$$\rho\left(\frac{\partial u}{\partial t} + u\ \frac{\partial u}{\partial x} + v\ \frac{\partial u}{\partial y} + w\ \frac{\partial u}{\partial z}\right) = \rho g_x - \frac{\partial p}{\partial x} + \mu\left[\frac{\partial^2 u}{\partial x^2} + \frac{\partial^2 u}{\partial y^2} + \frac{\partial^2 u}{\partial z^2}\right] \text{(x direction)} \qquad (2)$$

$$\rho\left(\frac{\partial v}{\partial t} + u\ \frac{\partial v}{\partial x} + v\ \frac{\partial v}{\partial y} + w\ \frac{\partial v}{\partial z}\right) = \rho g_y - \frac{\partial p}{\partial y} + \mu\left[\frac{\partial^2 v}{\partial x^2} + \frac{\partial^2 v}{\partial y^2} + \frac{\partial^2 v}{\partial z^2}\right] \text{(y direction)} \qquad (3)$$

$$\rho\left(\frac{\partial w}{\partial t} + u\ \frac{\partial w}{\partial x} + v\ \frac{\partial w}{\partial y} + w\ \frac{\partial w}{\partial z}\right) = \rho g_z - \frac{\partial p}{\partial z} + \mu\left[\frac{\partial^2 w}{\partial x^2} + \frac{\partial^2 w}{\partial y^2} + \frac{\partial^2 w}{\partial z^2}\right] \text{(z direction)} \qquad (4)$$

where:

$\rho$: Fluid density

$g_x$ , $g_y$ , $g_z$: Body forces

$\mu$: Fluid viscosity

$p$: Static Pressure

$t$: time

### 3.1.1.3 Conservation of Energy

The first law of thermodynamics states that energy cannot be created or destroyed, but energy can be transformed from one form to another. In fluid it is better to define it as a rate of internal energy and kinetic energy that is equal to energy transported by convection and conduction, and the net rate of work has been done by elements. [12]

$$\rho c_p \frac{DT}{Dt} = \nabla . k \nabla T + \mu \varphi \tag{5}$$

$$\varphi = 2\left[\left(\frac{\partial u}{\partial x}\right)^2 + \left(\frac{\partial v}{\partial y}\right)^2 + \left(\frac{\partial w}{\partial z}\right)^2\right] + \left(\frac{\partial u}{\partial y} + \frac{\partial v}{\partial x}\right)^2 + \left(\frac{\partial v}{\partial z} + \frac{\partial w}{\partial y}\right)^2 + \left(\frac{\partial w}{\partial x} + \frac{\partial u}{\partial z}\right)^2 \tag{6}$$

Where:

$c_p$ : Specific heat

$k$: Thermal conductivity

$\varphi$: Dissipation function

## 3.2. Experimental Methods

Experimental methods provide acceptable solutions for flow problems, but setting up an experiment in the lab is costly and time consuming. For instance, Wind Tunnel experiments help in designing of airplanes, ships and other objects, but it might take several years to resolve all technical problems of the experimental set up and it is expensive. [28]

## 3.3. Numerical Methods - Computational Fluid Dynamics (CFD)

Numerical methods for solving partial differential equations to describe fluid flow and heat transfer process were started in early twentieth century. Computational Fluid Dynamic (CFD) started with the development of the computer which sped up the numerical simulation in the early 1970's [17] [5]. Computational methods are not free of difficulties, but have advantages over other methods such as: universality, flexibility, accuracy, and cost [28]. CFD is a subdivision of fluid mechanics integrated with physics, mathematical solution and computer technology for simulating and solving fluid flow and heat transfer problems [5]. The ability of CFD methods to solve complex flow problems is highly dependent on the development of computer technology. The simulation of inviscid flows (Euler equations) and computation of the viscous flow (Navier-Stokes equation) was started in 1980s. Various turbulent modelling with different complexities gradually developed and lead to significant models such as Direct Numerical Simulation (DNS) and Large Eddy Simulation (LES) [5]. Today, many different numerical techniques are used in CFD software which is employed into a variety of fields for flow and heat transfer simulation of aircraft, car, ship design, heat exchangers, etc [5]. Therefore, CFD became an acceptable design and research tool in engineering and science which complements both experimental and numerical solutions by speeding the process and lowering the cost of solving fluid dynamics problems [5] [28]. In the current study, STAR-CCM+ is chosen, which is a software among the limited CFD softwares. STAR-CCM+ has the capability to approximate partial differential equations of different types of flow problems by using the numerical discretization method. There are different discretization methods used in

commercial CFD such as, finite volume method, finite element method and finite difference method; STAR-CCM+ is based on the finite volume method.

### 3.3.1 STAR-CCM+

STAR-CCM+ is an integrated and powerful physics simulation package with ability of processing flow, heat transfer and stress problems in both fluids and solids. This software was created by CD-Adapco in 2004 and is updated constantly. The STAR-CCM+ unique client-server architecture, lets users solve most parts of their simulation on a remote machine. Therefore, it can handle meshing and solving of large models for a variety of engineering and design problems. STAR-CCM+ consists of pre-processing, solving and post processing features such as; CAD modelling, surface preparation tools, automatic mesh generation, physics modelling, turbulence modelling, and visualization and analysis.(STAR view) [25].

### 3.3.2. Finite Volume

The Finite Volume Method is based on the integral form of the governing equations (Navier-Stokes/Euler equation) and discretize the physical space to large numbers of the arbitrary polyhedral control volumes. Mostly cell-centered and cell vortex schemes are used for defining the shape and position of the control volume. This method is very flexible and widely used in CFD because of its attractive properties. It can be used in both structured and unstructured grids [5].

### 3.3.3. Turbulence Modeling

Reynolds discovered two modes of flows, Laminar and Turbulent, based on a dimensionless number which is called Reynolds number in 1883. [5]. The transition phase between laminar and turbulent starts when the Reynolds number passes the 'critical' value. (Re =2300) [12] The simulation of turbulent flow despite laminar and inviscid flow has significant problems. Turbulence models cannot provide the exact solution for every flow simulation. Therefore, there are different major approaches in CFD software used to try to predict the mean (average) flow fields.

- Reynolds-Average Navier-Stokes (RANS equation)
- Large Eddy Simulation (LES)
- Detached Eddy Simulation (DES)

Most simulations rely on the first approach in STARCCM+ and then the second two approaches should be chosen very carefully. [25] In this study, the first approach is explained.

#### 3.3.3.1 Reynolds-Average Navier-Stokes (RANS)

RANS model was presented by Reynolds in 1895 by dividing the Navier-Stokes equation into mean and fluctuating parts. The average processing can be time or ensemble averaging for steady-state situations and transient situations [5] [25]. This approach is popular in engineering applications due to its simplicity, low computational cost and also, broad selection of models to choose from. The RANS equation is the same as Navier-Stokes equation for mean variables, but with Additional terms of Reynolds Stress Tensor.

$\rho \frac{\partial \bar{v}_i}{\partial t} + \rho \bar{v}_j \frac{\partial \bar{v}_j}{\partial x_i} = -\frac{\partial \bar{p}}{\partial x_i} + \frac{\partial}{\partial x_i}(\bar{\tau}_{ij} - \rho \overline{v_i{}' v_j{}'})$ Reynold Averaged Navier-Stokes equations

(7)

$\bar{\tau}_{ij} = -\rho \overline{v_i{}' v_j{}'}$ Reynolds- Stress tensor (8)

[25]

In STAR-CCM+ two approaches are used to model Reynold Stress tensor in the form of mean flow quantities to provide an approximation of the governing equations. [25]

•Eddy viscosity model: in this model, the concept of turbulent viscosity term $\mu_t$ is used to model the Reynolds stress tensor as a function of mean flow quantities. Boussinesq approximation is the most common model.

•Reynolds stress transport model: in this model, the transport equation is solved for each component of Reynolds Stress Tensors.

3.3.3.2 STAR-CCM+ Turbulence Modeling:

Four major Reynolds average turbulence models are used in STARCCM+ software. First, Spalart-Allmaras model, which mostly is used in aerospace and good for flow since the boundary layer is attached and separation is rare. Second, K-Epsilon model which provides a good agreement between accuracy, computational cost and robustness and also is widely used in industrial applications. Third, Standard K-Omega model which is similar to K-epsilon and is applied in aerospace and tubomachinary industries. The last one, is the Reynolds Transport model which has the most computational cost and is used for complex flow such as swirling flow in a cyclone.

### 3.4. K-Epsilon Two Equation Model

In this project, $k$-$\varepsilon$ model is chosen for simulation [25]. In the $k$-$\varepsilon$ two equation model, the velocity and length scale of turbulence are defined with two additional partial differential equations: turbulent kinetic energy $k$ and dissipation rate $\varepsilon$ [16] [18]. Various $k$-$\varepsilon$ models are widely used in industrial applications during the recent decades. There have been countless attempts to improve it. The most significant of these improvements have been incorporated into STAR-CCM+ [25]. The final form of $k$ equation is as below:

$$\rho\frac{\partial k}{\partial t}+\rho\langle u_j\rangle\frac{\partial k}{\partial x_j}=2\mu_t\langle s_{ij}\rangle\frac{\partial\langle u_i\rangle}{\partial x_j}-\rho\varepsilon+\frac{\partial}{\partial x_j}\left[\left(\mu+\frac{\mu_t}{\sigma_k}\right)\frac{\partial k}{\partial x_j}\right] \quad (9)$$

- Left hand side 1st term: Rate of change of k in a fluid particle transported by the mean flow.
- Right hand side; 1st term: Rate of energy production; 2nd term: effect of viscous dissipation, 3rd term: Molecular diffusion of k and 4th term: Diffusion by turbulent motion [16]

The equation for dissipation $\varepsilon$ is derived from the Navier-Stokes equations and simplified to

$$\rho\frac{\partial \varepsilon}{\partial t}+\rho\langle u_j\rangle\frac{\partial \varepsilon}{\partial x_j}=C_{\varepsilon 1}P_k\frac{\varepsilon}{k}-C_{\varepsilon 2}\rho\frac{\varepsilon^2}{k}+\frac{\partial}{\partial x_j}\left[\left(\mu+\frac{\mu_t}{\sigma_\varepsilon}\right)\frac{\partial \varepsilon}{\partial x_j}\right] \quad (10)$$

$k$-$\varepsilon$ consists of two partial differential equations and algebraic demonstrations for eddy viscosity. [16]

$$\mu_t=C_\mu\rho\frac{k^2}{\varepsilon} \quad (11)$$

The k and $\varepsilon$ equations should be solved along with the Navier-Stokes equations for the average flow as part of Partial Differential Equation (PDE) systems.

Table 3.1 Constant Variables of the k- $\varepsilon$ model.

| | |
|---|---|
| $C_\mu$ | 0.09 |
| $C_{\varepsilon 1}$ | 1.44 |
| $C_{\varepsilon 2}$ | 1.92 |
| $\sigma_k$ | 1.3 |
| $\sigma_\varepsilon$ | 1 |

STAR-CCM+ has a choice of eight different k- $\varepsilon$ turbulence models. The most successful recent development is the realizable K-Epsilon model that has been chosen for current CFD work. This model contains a new transport equation for the turbulent dissipation rate $\varepsilon$.

Also a critical coefficient $C_\mu$ , of the turbulent model , is expressed as a function of mean flow and turbulence properties, rather than assumed to be constant as in the standard model [25].

## 3.5. Wall Function

One of the challenges in CFD solvers is how to deal with the near wall layer. RANS model is not able to model the turbulent stresses near the wall; therefore, the wall function approach is used. Wall function is a group of mathematical relations used to solve boundary conditions near the wall region. Therefore, turbulence model is only applied to the rest of the fluid region. The advantage of using wall function is to increase the accuracy of the

solution and also reduce the computational cost by using lower density in core meshes. [20][25] The turbulent flow region is divided into three layers near the wall as follows:

- Viscous Sublayer $0<y^+<5$
- Buffer Layer $5<y^+<30$
- Inertial Sublayer (logarithmic) layer $30<y^+<150$

In STAR-CCM+ there are three near wall modeling assumptions for each turbulent model. Also, applying wall function in some turbulent cases needs fine mesh close to the walls to capture the flow characteristics near the wall.

- The High $y^+$, in this assumption the cells in the vicinity of the wall are placed in the logarithmic region of the boundary layer. This leads to significant reduction in the number of cells in boundary layer and reduces the computational cost.
- The Low $y^+$, this treatment is proper for a low Reynolds number turbulence model and needs excessive grid generation near the wall.
- The All $y^+$, is a hybrid or adaptive treatment for both coarse and fine meshes. It provides a reasonable solution for cells lying in buffer regions as well. [25]

### 3.6. Work Chart of the CFD Simulation

The first step of any CFD simulation is preprocessing which starts with generating a geometry model of the problem to be solved and analyzed. There are many 3D CAD softwares which can be used to design and create solid models such as SolidWorks, CATIA V5, Pro/ENGINEER. Also, the solid model can be created with the 3D CAD package

inside the STAR-CCM+. Then the model can be imported into STAR-CCM+. After importing the geometry model, it is time to prepare the surface for mesh generation. STARCCM+ has a powerful tool for surface preparation, which provides diagnostic on any surface errors and tools to fix them manually or automatically. In Starccm+, there are several mesh strategies that can be used to discretize different geometries, such as surface mesher which includes surface wrapper, surface remesher tools and volume mesher which includes polyhedral mesher, trimmed mesher, etc. After preprocessing, the physics model and solver should be set up for the problems to be analyzed. The physics model and the solution are dependent on the defined problem and can be different for different cases. The physics set up for internal flow is different from flow on the surface. Some post processing features can be set up before running the model such as monitor plots and reports. Then, the model is ready to run, and visualization tools allow the user to view the results along the iteration or after convergence.

.

# CHAPTER 4

# CFD MODEL DESCRIPTION

## 4.1 Description of Geometry Model

Geometry model of the CFD simulation can be designed either by the Computational aid design (CAD) tools which are built in the STAR-CCM+ CFD package or imported from another CAD design software into the CFD software for further analysis. In this project, all models were generated in SolidWorks which is a CAD software for designing solid models. Geometry starts with a 2D sketch which is defined by numeric and geometric parameters. Then, the tube is extruded from the 2D model and becomes a 3D part. The groove is cut swiped from the inside of the tube in a helical pattern. With this software, parts and assemblies can be created for both simple and complex geometry purposes. Figure 4.1 and 4.2 depict the 2D and 3D sketches of the grooved tube. Test tubes include four horizontal cylindrical tubes with internal helical grooves and, also, another three helical grooved tubes for comparison with the experimental study. The detail of the each test section is provided in table 4.1. Tubes are made of stainless steel with inner diameter 7.1 mm, outer diameter 9.5 mm and length of 2000mm.

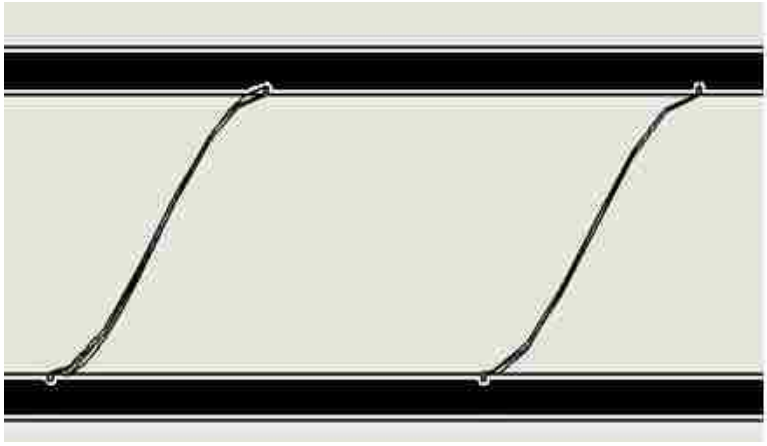

Figure 4.1 2D Sketch of a Groove Tube

Table 4.1. The Details of the Test Sections

| **Tube** | **Groove Width (w)** | **Groove Depth (e)** | $d_i$ **(mm)** | **Pitch Length (mm)** | **Length (mm)** |
|---|---|---|---|---|---|
| GT 7.1 | 0.2 | 0.2 | 7.1 | 7.1 | 2000 |
| GT 12.7 | 0.2 | 0.2 | 7.1 | 12.7 | 2000 |
| GT 50 | 0.2 | 0.2 | 7.1 | 50 | 2000 |
| GT 130 | 0.2 | 0.2 | 7.1 | 130 | 2000 |
| GT 203 | 0.2 | 0.2 | 7.1 | 203 | 2000 |
| GT 254 | 0.2 | 0.2 | 7.1 | 254 | 2000 |
| GT 305 | 0.2 | 0.2 | 7.1 | 305 | 2000 |

## 4.2. Meshing Scheme

Grid generation is an important aspect of any CFD modeling; therefore, in order to have an accurate simulation of flow and heat transfer, the geometry models should have good quality meshes. In the finite volume method, the geometry model is discretized to a number of small elements which are called cells by partial differential equation and

algebraic methods. Then, the integral form of the conservation equations is applied to the cells to get the discrete equations for them [5]. Precise meshes are needed to capture the complexity of the flow characteristics and geometry from near the wall to the bulk of the fluid. STAR-CCM+ provides several meshing strategies that are suitable for different applications [25]. Before starting the simulation, the best mesh should be picked for the model. For this purpose, the mesh generation for a geometry model is started with coarse meshes and then the mesh sizes will be refined. The results will be analyzed until slight changes are observed in them. This is called mesh- independent study in CFD modeling. The CFD results are highly dependent on the mesh such as cell size, shape and grid density and including stretching ratios between cells and skewness angles, etc.

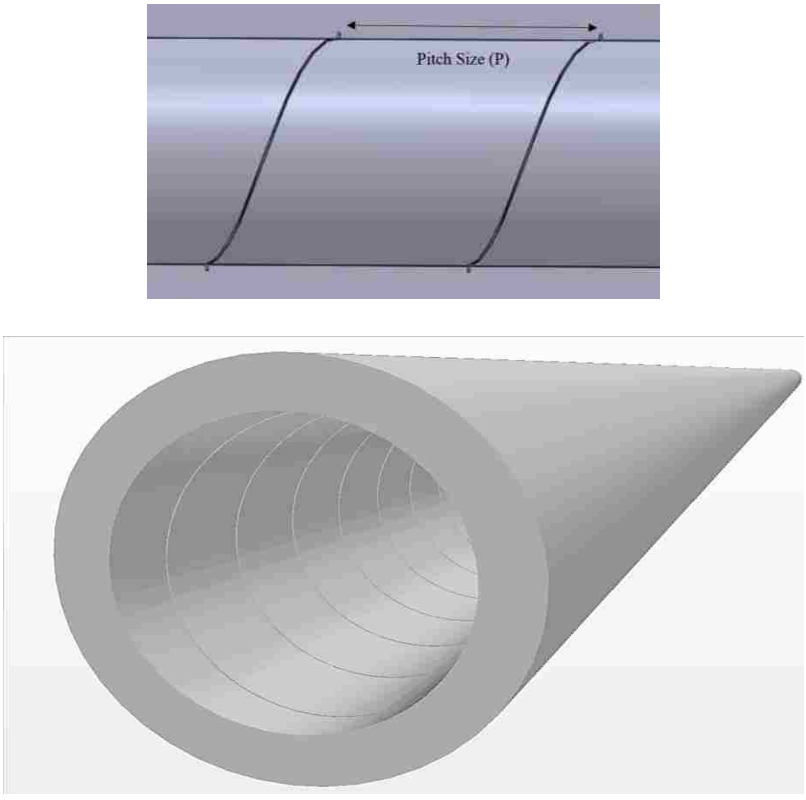


Figure 4.2 Schematic Diagram of the Grooved Tube

### 4.2.1 Mesh Model

The imported geometry surfaces were checked for any errors. In most cases, the surface errors were minor and solved automatically by STAR-CCM+. There are two different strategies for meshing: part based meshing and region based meshing. Region based meshing is chosen to mesh all different tubes in this study, since the geometric parts are assigned as a fluid region.

#### 4.2.1.1 Surface Mesh

The imported surface mesh in all cases was tessellated and needed refinement. The surface repair tool was used to close the manifolds, fix the errors and assign fluid flows through the tubes. This tool is only used for simple geometry and minor surface errors, however, fixing the surface in cases with many errors, surface wrapper should be used instead [25]. For the grooved tube models, "Surface Remsher" was chosen to create triangulated faces on surface geometry to improve surface quality for volume meshing. Most bad volume mesh is caused by poor surface mesh; therefore, surface remesher plays an important role in the final results [25]. Figure 4.3 shows the initial surface and remeshed surface. The finer meshes require more computational time and memory, but they are important for capturing the properties of the model in the process of solving the simulation, especially inside the grooved channels.

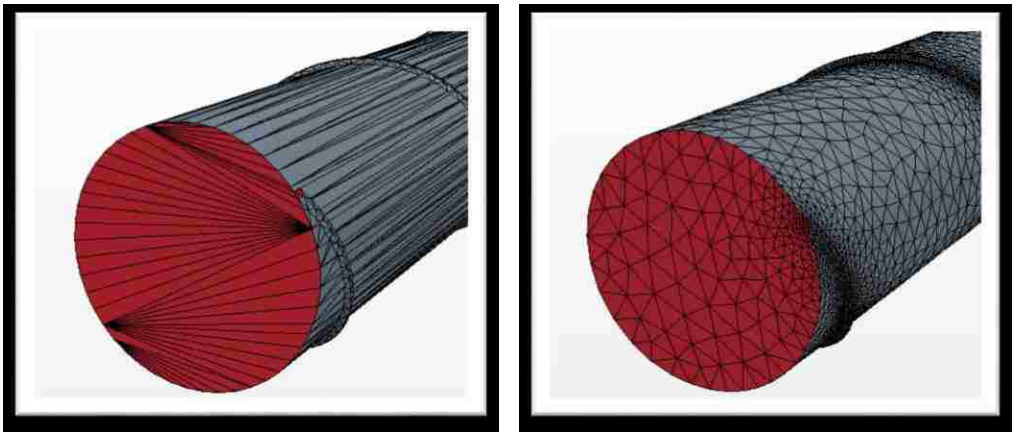

Figure 4.3 Surface Mesh a) Initial Surface b) Remeshed Surface

4.2.1.2 Volume Mesh

STAR-CCM+ has different types of volume meshing models, such as tetrahedral, polyhedral, trimmed and thin mesher. Different mesh types can be used for different regions based on the desired model. The polyhedral mesh model is selected for generating the core mesh of the grooved tubes. This model provides stable solution for complex mesh generation problems with less number of cells. Therefore, this type of mesh required lowest computational cost, which makes it easier and more efficient to be used as core mesh in comparing with other models. In addition to polyhedral mesher, prism layer model is used to mesh near the wall and boundaries as shown in Figure 4.4. This type of mesh generates orthogonal cells next to the boundaries to allow the solvers to improve the accuracy of the flow solution near the wall. [25] Prism layers help to determine the forces and heat transfer on walls and some effective features on drag and pressure drop such as separation, which greatly enhances the results. Prism layer thickness, number of layers and distribution of the mesh are defined based on the turbulence modeling approach and wall function. In

order to generate prismatic layers in the gaps and corners of small grooves, the expert properties of prism layer are changed from the default mode in STAR-CCM+ [25].

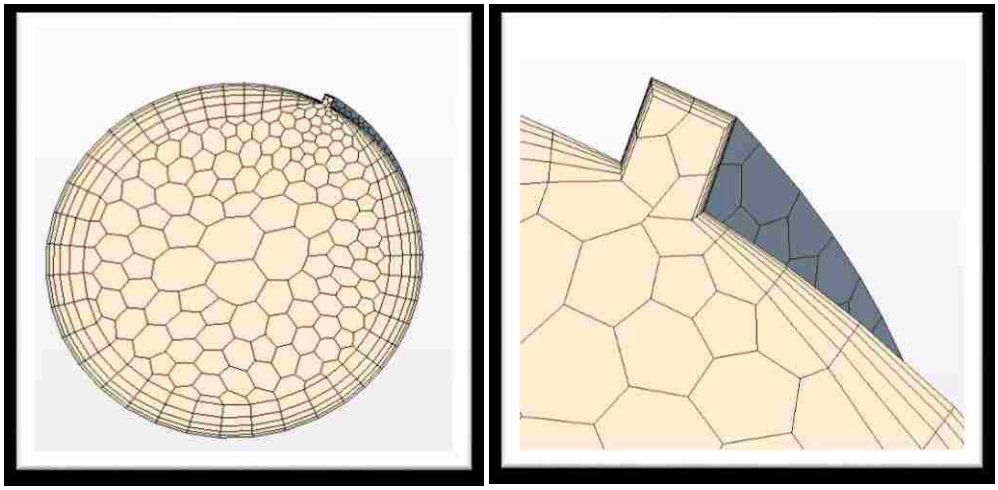

Figure 4.4. Volume Mesh of the Grooved Tube

## 4.3 Physics of Simulation

In this CFD study, since the focus of the study is on flow characteristics of water, the solid part of the tube is neglected in all cases. This assumption has been made by deleting the stainless steel tube part, but by considering the percentage of heat loss. The heat loss is obtained from the experimental study with which the CFD results are validated.The purpose of neglecting the solid part of the tube, is to reduce the computational cost and make the simulation simpler by having one region as a fluid. Water entered the grooved tubes at a constant temperature of 24 ◦C with different mass flow rates. The Reynolds number varies from 4000 to 20000. Heat transfer loss occurring between the applied power on the surface and the actual heat picked up by the water flow was

estimated to be in the neighborhood of 10% heat loss [2]. Therefore, the heat gained by the water inside the tube is calculated by the following energy conservation equation:

$$Q = m_f \, C_p \, (T_o - T_i) \tag{12}$$

Where:

$m_f$: Mass flow rate of water at inlet
$C_p$: Specific Heat of water
$T_o$: Outlet temperature
$T_i$ : Inlet temperature

Both temperatures are acquired by mass flow average temperature in STAR-CCM+ which typically is calculated over the cross section of the inlet and outlet by consideration of mass flow rate and radial temperature profile at the relevant section. This method provides more accurate average temperature for flow which is called mean bulk temperature [12]. The physics model of liquid water is assumed to be incompressible, turbulent, three dimensional, steady in state and constant in density. Based on the turbulent model, some other related models should be activated too. When these physical models are assigned, they provide relevance to the transport energy and dissipation equations and semi empirical coefficients for the solvers. In this study, a segregated fluid energy model is chosen. In this method, flow equations are solved for velocity and pressure component, respectively, and need less memory space for solving the problem compared to coupled solvers which solve the transport equation simultaneously. This method is appropriate and provides accurate results for incompressible flow or mildly compressible flow [12]. Realizable K-epsilon is one of the eight different k-epsilon models that is provided in STAR-CCM+. Realizable k-epsilon which was developed by Shih et al.[23] contains a new

formulation of a transport equation for the dissipation rate and works with a two layer approach in STAR-CCM+. This model works considerably better than standard k-epsilon for many applications. Also, one of the advantages of this method is the ability of using an all y+ wall treatment, which is able to correctly resemble near-wall turbulence for a variety of mesh densities. After choosing a physical model, boundary condition and initial value should be set up. Initial value consists of pressure, static temperature and velocity plus turbulent characteristics of the flow.

Table 4.2 Material Properties of the Fluid

| Material Properties ( water at 24 C) | |
|---|---|
| Density ($kg/m^3$) | 997.13 |
| Thermal conductivity (W/m-K) | 0.58 |
| Specific heat (j-kg/k) | 4181 |

### 4.3.1 Boundary Condition

In the STAR-CCM+ boundaries are initially assigned to the surfaces of a region. In this research work there are 3 surface boundaries considered: inlet, outlet and interface. The boundaries and initial condition are set up to capture the physical characteristics of flow accurately. These boundary conditions are:

**Inlet**: The entrance of the grooved tube is considered as a mass flow inlet type. The uniform velocity is entering a channel and this boundary should be chosen when the mass flow rate is known in the problem. The table 4.1 shows the mass flow rate of different Re number. The inlet temperature is considered as constant 24 C.

**Interface:** The wall boundary condition is chosen for the tube's internal surface. The slip condition and constant heat flux 3150 $w/m^2$are assumed for interface in all cases.

**Outlet**: The boundary is considered as a flow split outlet, but the split ratio is set as 1 and all flow exit through this boundary and pressure is assumed to be at atmospheric pressure.

Table 4.3 Inlet Boundary Condition of Grooved Tubes with different Pitch Size (7.1, 12.7, 50, 130) with Constant Inlet Temperature of 24 ◦ C

| Groove tube inlet Mass Flow rate (kg/s) | Groove tube inlet Velocity (m/s) | Reynolds number |
|---|---|---|
| 0.0198 | 0.504 | 4000 |
| 0.0294 | 0.754 | 6000 |
| 0.0393 | 1.005 | 8000 |
| 0.0491 | 1.257 | 10000 |
| 0.0734 | 1.877 | 15000 |
| 0.983 | 2.514 | 20000 |

# CHAPTER 5

# RESULTS AND DISCUSSION

## 5.1 Grid Independence Study

Before starting to generate the CFD production runs, a mesh independence study was carried out for the tube with 12.7 (mm) pitch size and 2.0 m length. In a grid independence study, the goal was to find the best mesh properties for accurate solution [24]. The process is to vary the mesh density to eventually provide a desired numerical accuracy for engineering purposes at the same time achieving an optimum computational time. Four different mesh densities were generated for a 12.7 mm (pitch) grooved tube in STAR-CCM+ and models were solved by the software. The final results of some heat transfer variables such as axial velocity and axial temperature were compared with each other in all cases and the results showed small differences by changing the mesh density. Therefore, based on the results, the solution was concluded to be independent of the number of cells. The grid generation started with coarse mesh; then the mesh was refined by dividing the base size by two. The mesh density on inlet cross section for different mesh densities is shown in figure 5.2. By increasing the mesh densities, i.e. number of cells near the groove area, the flow area of the groove is suspected to have potentially a large effect on velocity and temperature profile distributions in the flow. The simulation is solved for a fluid region with the mass flow rate of 0.0198 kg/s (Re=4000) and with constant heat flux of 3150 $w/m^2$which was applied on the outer surface of the tube. The coarse mesh has 1168923 cells, then the number of cells were refined to three other meshes, 1503014, 2398319, 5530812 respectively (Table 5.1). Axial velocity and temperature were observed for four cases at radial line probe, which is shown in figure 5.1. The line probe was placed

on a cross section plane at the distance of 1 meter from the inlet. Axial velocity and temperature values were taken as criterion for grid independence for all cases plotted in figure 5.3 and 5.4.

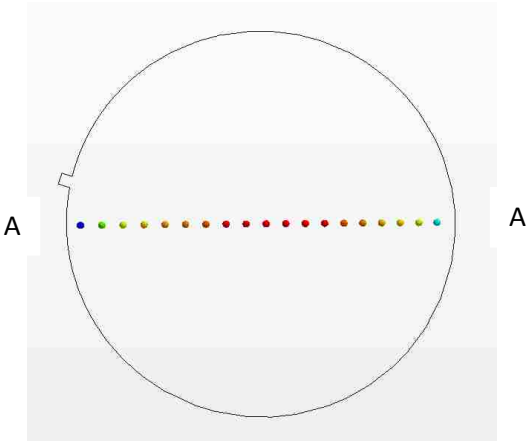


Figure 5.1 Schematic Diagram of a Radial Probe Line of A-A on the Cross Section Plane Used for Axial Velocity and Temperature

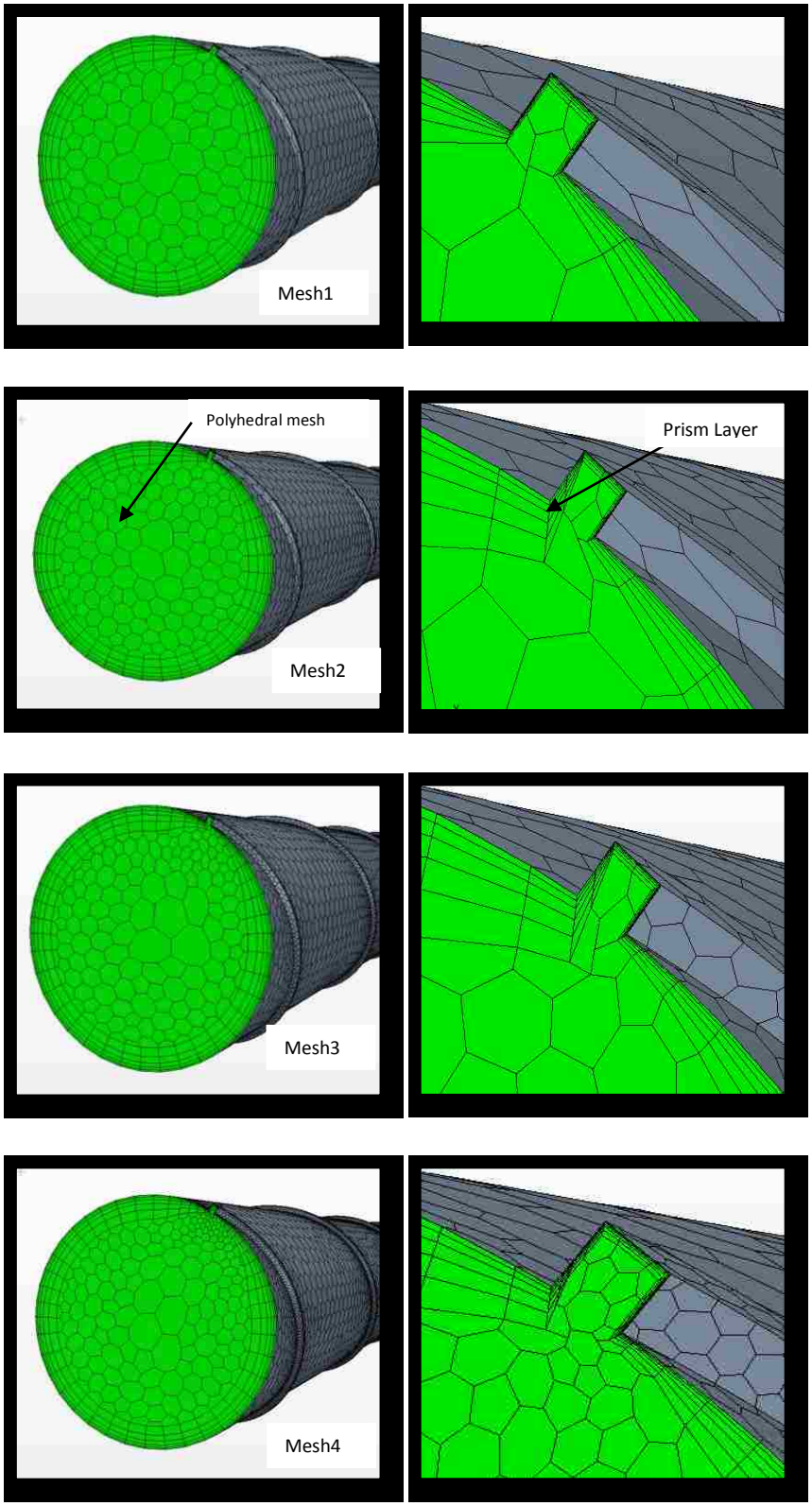


Figure 5.2 Different Volume Mesh Used in Grid Independence Study

Table 5.1 Mesh Properties in Grid Independence Study

| Mesh | Base Size (mm) | Number of Prism Layer | Number of Cells | CPU Time per Iteration (S) |
|---|---|---|---|---|
| Mesh1 | 6 | 5 | 1168923 | 54.04 |
| Mesh2 | 4 | 5 | 1503014 | 60.009 |
| Mesh3 | 2 | 5 | 2398319 | 96.34 |
| Mesh4 | 1 | 5 | 5530812 | 209.35 |

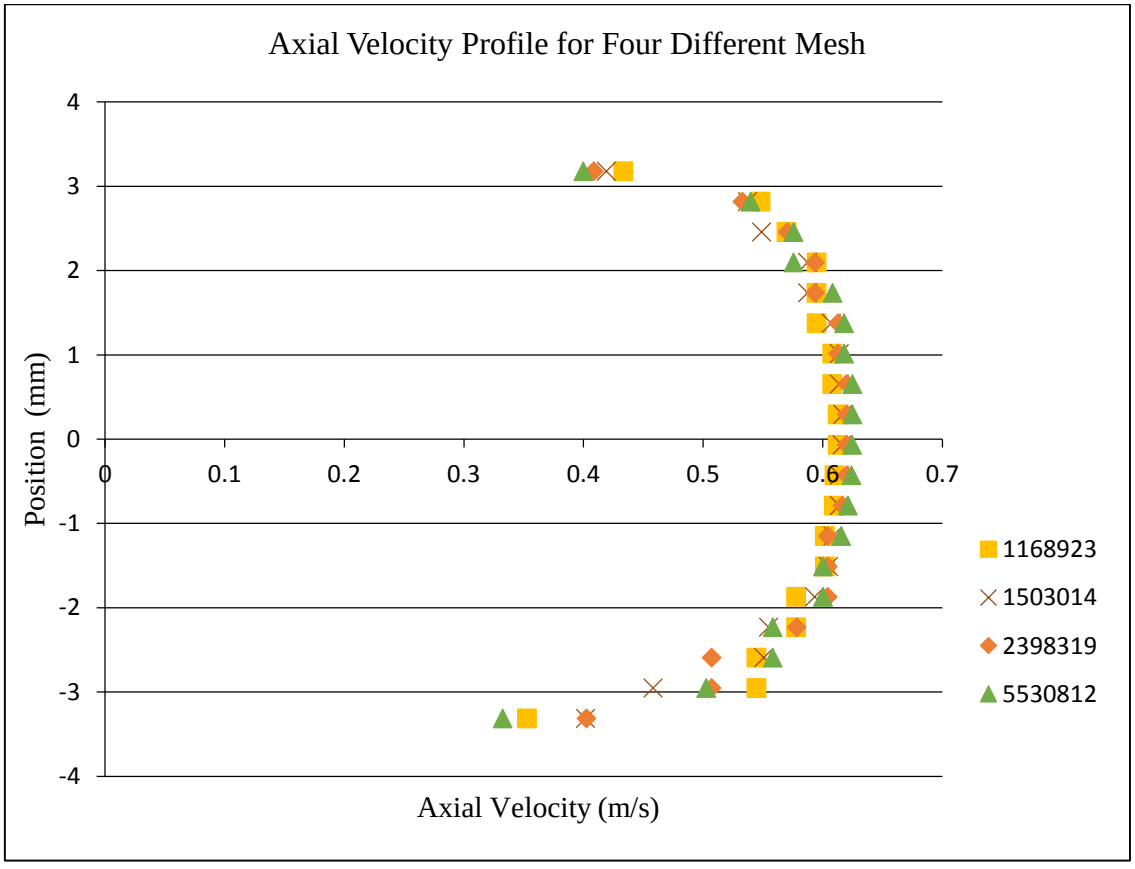


Figure 5.3 Comparison of Axial Velocity for Four Different Mesh.

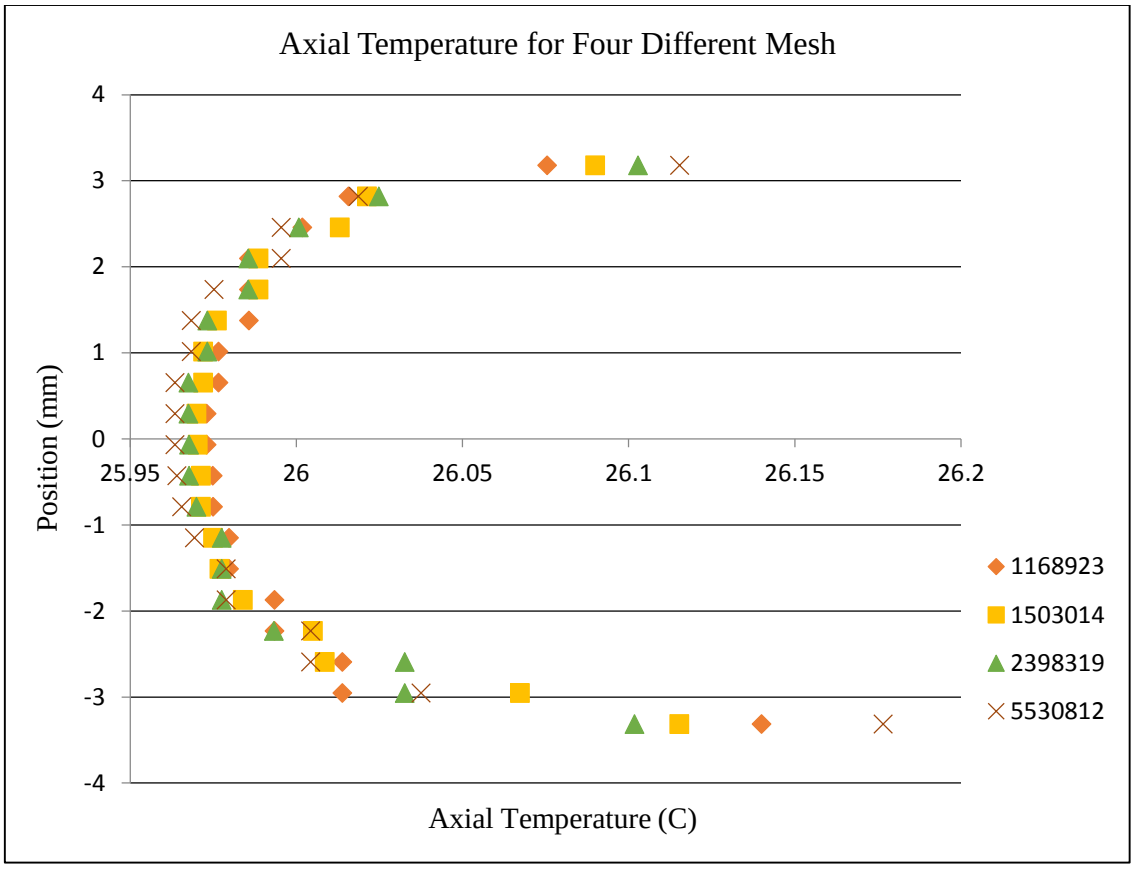


Figure 5.4 Comparison of Axial Temperature for Four Different Mesh

The axial velocity and temperature at A-A line probe were plotted (Figures 5.3 and 5.4) and the change was observed to be less than 1% by increasing the mesh density between the Mesh 4 and Mesh 3 model. Therefore, any one of these meshes can be chosen, but to save the computational time, the mesh with 2398319 cells was selected. A special effort has been made, including personal contacts with a CD-Adapco support group for their advice, to include enough mesh detail around the helical groove to ensure flow field and temperature accuracy.

### 5.1.1 Wall Y+ for the Grid Model

The fluid region in all grooved tubes is modeled as turbulent flow based on Reynolds number ranges between 4000 to 20000. Although the Re number range between 4,000-8,000 would theoretically be more in the transitional regime [18] the STAR-CCM+ manual suggests choosing turbulent model for Reynolds greater than 4000 [25]. Recognizing that with this grooved channel geometry the traditional turbulent flow developing length would probably be severely curtailed; and because of the expected "tripping" of the boundary layer thickness, the flow is expected to be close to the turbulent regime. In STAR-CCM+ manual, it was recommended to use "The All $y^+$ Wall Treatment" for all turbulence models whenever it was available, because it offers the most meshing flexibility. "The All $y^+$ wall treatment'' was the default wall treatment method for the chosen model, and "realizable k-epsilon turbulent model", and was explained in chapter 3 in detail. The validity of each model can be estimated by analyzing the values of the "Wall $y^+$" function at every wall boundary [25]. The chosen wall treatment is a hybrid approach that can be used for very fine or very coarse meshes [10]. The wall y+ value for this case study is around 1 as shown in Figure 5.5.

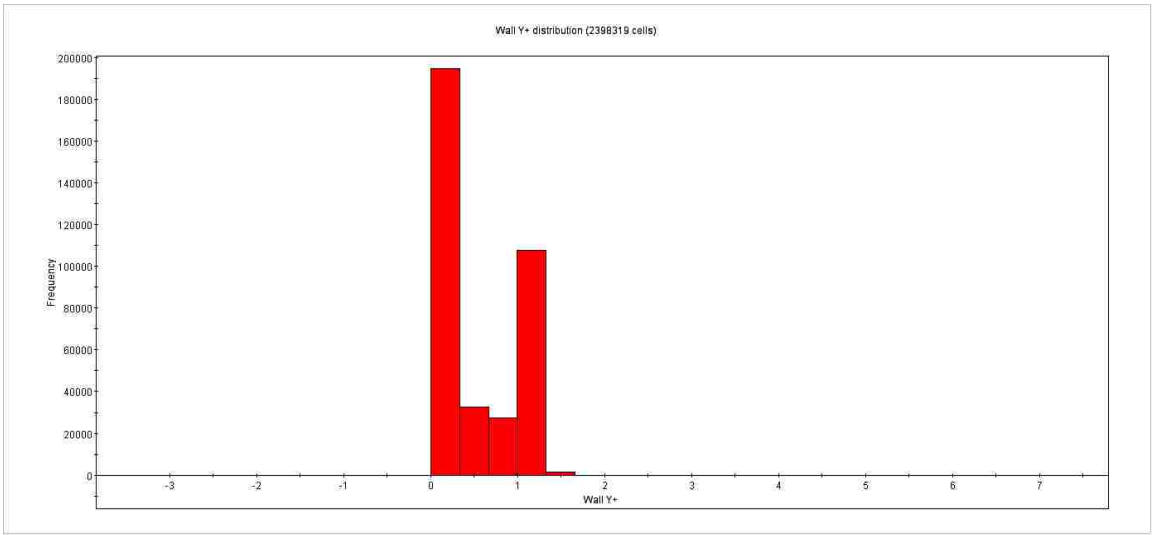


Figure 5.5 Wall Y+ Distribution for chosen Mesh with 2398319 Cells

## 5.2 Parameters of the Present Research

In the past decades, several studies had been focused on heat transfer augmentation in tubes [16], [11], [22], [26]. The purpose of this research is to provide a predictive method for this type of heat augmentation geometry where a rectangular helical groove is machined on the inside surface of a typical tube. The range of Re numbers considered are from 4000 to 20000 and the pitch size is from 7.1 mm to 130 mm. Pitch is defined as the straight distance between each helical turn of the groove inside the tube as shown in Figure 4.2 in chapter 4. The reasons for using a turbulent model have already been discussed in the previous section.

A previously experimental study [2] has been found in the literature for comparison and validation purposes. In that study heating is provided by an electric resistor and heat flux can be calculated by measuring current (I) and voltage drop (V) to calculate the electric power provided. Also in that study an estimate of a 10% loss of heat applied to the outside of the test section was made. This knowledge was applied in our study to reduce the actual

heat flux by 10% as our model did not consider actively modeling the heat flow from the outside of the tube. Thermocouples were used to measure surface temperature at several uniformly distributed locations along the length of the pipe with a typical distance of 250 mm as being the distance between adjacent thermocouples. The mean bulk temperature of the fluid was not strictly calculated as defined in the literature; rather a single temperature measurement at the center of the tube cross-section was used to calculate that temperature. No attempts were made in the experimental study to measure the velocity or temperature transverse distribution. In that study also by knowing the surface temperature and total actual heat flow the average heat transfer coefficient (h) (over the entire surface of the pipe) was calculated by Equation (13) for the experimental study and the current study [2]. With the CFD approach a better estimate is made for the mean bulk temperature and the temperature distribution.

$$h_{ave} = \frac{Q}{A(T_{ave,w} - T_{ave,f})} \tag{13}$$

Following the calculation of $h$ in equation (15) one can calculate the Nusselt number as shown in equation (14). Following the calculation of the Nu number a calculation of the pressure drop follows in the form of a non-dimensional friction factor obtained as shown in equation (15) and comparisons with smooth pipe results can be made. The pressure drop plays an important role in the efficiency of a heat augmentation technique and its relative performance, since it can affect the pumping power and total operating costs [6]. Both equations 14 and 15 were used in the experimental study to calculate Nusselt number and friction factor [2].

$$Nu = \frac{h_{ave} d_i}{k} \quad (14)$$

$$f = \frac{\Delta p}{\left(\frac{d_i}{L}\right)\rho u^2} \quad (15)$$

Where:

ρ: Water density

u : flow velocity of water at the inlet

di is the inner diameter of the test tube,

μ: is the dynamic viscosity of water.

Q: Energy supplied on the surface

$A$ = Surface area of the tube

*L: Tube length*

$T_{ave,w}$ : Average temperature of the tube surface (inside)

$T_{ave,f}$ : Average temperature of inlet and outlet.

## 5.3 CFD Validation

A validation of the numerical code results with experimental data is desirable to ensure that the code is predicting the desired values i.e. Nu and $f$ are predicted with quantitative accuracy. The published experimental results [2] were used for comparison with our CFD data.

### 5.3.1 Smooth Tubes Validation

The geometric model of a tube with 2 meter length was created in SolidWorks and imported to STAR-CCM+. The grid was generated with 5 prism layers near the wall and

polyhedral meshes as a core mesh of the plain tube which was explained in chapter 4.2. Boundary conditions and physics of the problem were applied in agreement with the experimental work [2] on stainless steel tubes. A uniform velocity is assumed to enter the tube for different Reynolds numbers ranging from 4000 to 10000.

In the current work, the CFD Nu number and *f* were calculated by equation 16 and 17, then, compared to the experimental results [2]. In the paper [2], the average surface temperature over the length of the tube was found by averaging the temperature of eight thermocouples on the tube surface; also the inlet and outlet temperatures were measured at the pipe axial center of these surfaces. Figures 5.6 and 5.7 show the comparison of the CFD results for Nu number and *f* for the current study and the experimental data [2] for a Re number range from 4000 to 10000. The obtained results for Re of 4000 is not well predicted by K-epsilon model since it is transitioning from laminar flow to turbulent flow. For other ranges of Reynolds, the plotted results show good agreement within the error estimates of the experimental data. The error bounds given for the Nu is ±18% and for the *f* value is ±1%.

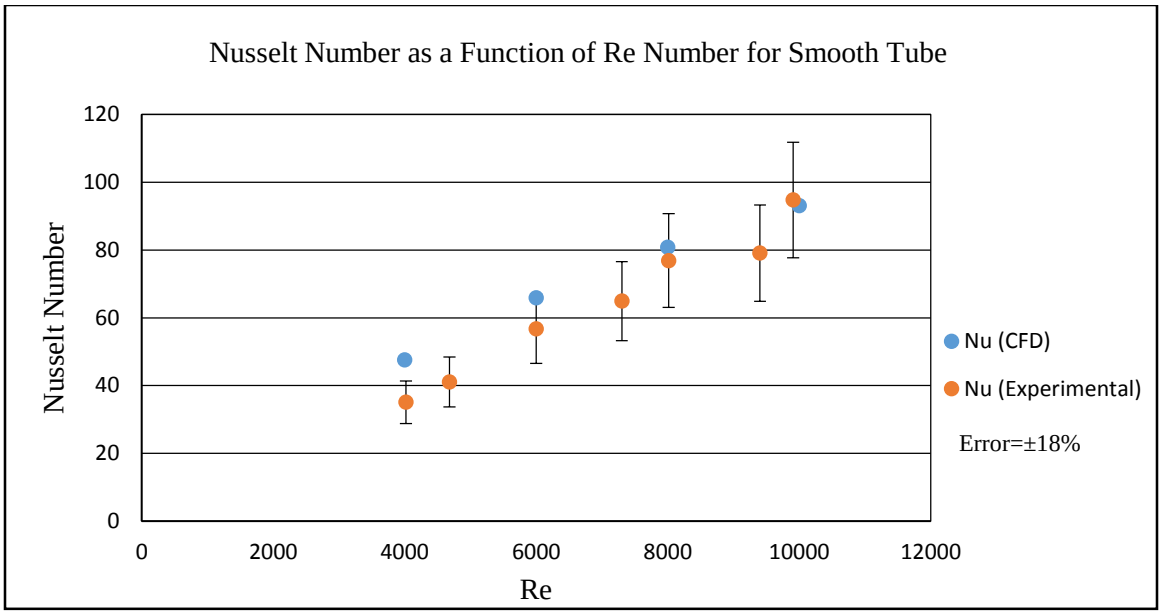


5.6 Comparison of CFD Nusselt Number of a Smooth Tube with Experimental Data.

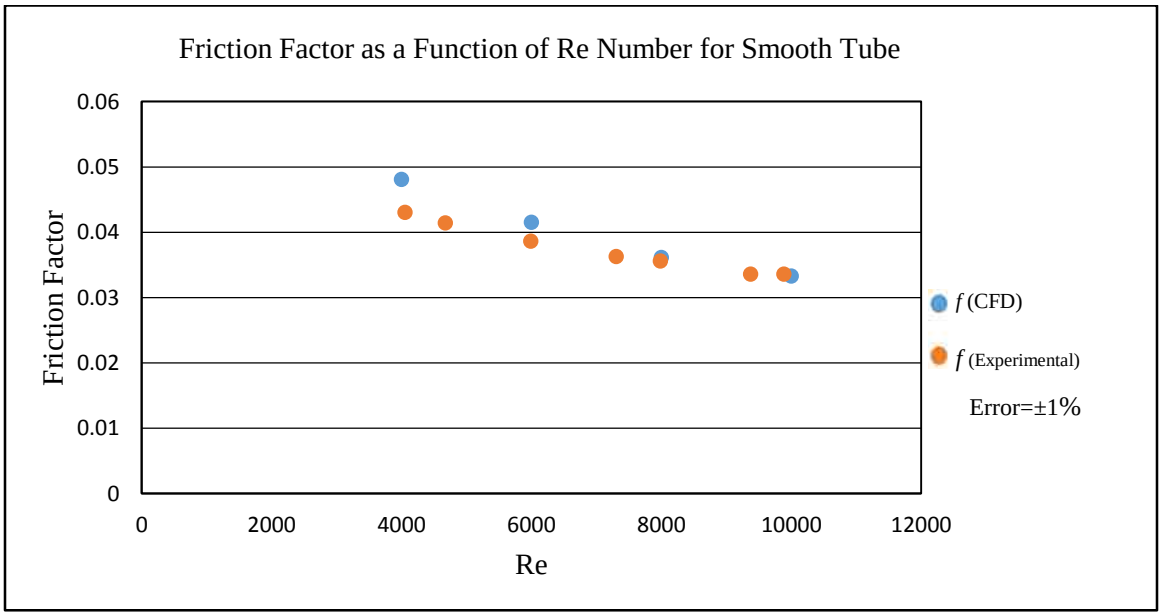


Figure 5.7 Comparison of CFD Friction Factor of a Smooth Tube with Experimental Data

### 5.3.2 Grooved Tubes Validation

The tubes with an internal helical groove and pitch distance of 203, 254 and 305mm of the experimental work [2] were considered for validation with the current simulation work. A comparison between the two methods was made by using similar boundary conditions for the CFD work as was provided in the experimental work. In most cases of the current CFD study, results are within the uncertainty of the experimental study which has been shown in Figure 5.8 through Figure 5.12 (±18% for Nu and ±1%). The agreement between experimental results and CFD is considered quantitative and the CFD model can be used for expanding the study for different pitch sizes and Re number ranges. For further investigation of effect of pitch sizes on heat enhancement, four different pitches to diameter ratios were considered. These new ratios are smaller in comparison with the experimental ones to fill in the gaps between the parameters of interest. In general, a better heat enhancement (i.e. higher Nu) is expected with decreasing pitch to diameter as this increases the occurrence of "tripping' of the boundary layer to try to maintain a smaller thickness of that layer. In the experimental study, the effect of larger pitch size (pitch to diameter ratio P/d =28, 35, 42) was investigated and showed the Nusselt number is increasing with increasing Re number in all cases. The details of heat transfer characteristics are shown for the grooved tube with the pitch size of 203, 254 and 305 (mm) in 5.2, 5.3 and 5.4 tables. Heat transfer coefficient and Nu number show a decreasing trend with increase in the pitch size (i.e. higher P/d values) for the same Re number. The friction factor shows the slight changes.

Table 5.2 Details of Heat Transfer Characteristics for Grooved Tube with 203 mm Pitch Size

| Reynolds Number for Tube 203 | Heat Transfer Coefficient | Nusselt Number | Friction Factor |
|---|---|---|---|
| 4000 | 3571 | 44 | 0.049 |
| 6000 | 5738 | 70 | 0.042 |
| 8000 | 7292 | 89 | 0.037 |
| 10000 | 8333 | 102 | 0.030 |

Table 5.3 Details of Heat Transfer Characteristics for Grooved Tube with 254 mm Pitch Size

| Reynolds Number for Tube 254 | h | Nu | $f$ |
|---|---|---|---|
| 4000 | 3792 | 46 | 0.049 |
| 6000 | 5303 | 65 | 0.042 |
| 8000 | 6604 | 81 | 0.037 |
| 10000 | 8140 | 100 | 0.034 |

Table 5.4 Details of Heat Transfer Characteristics for Grooved Tube with 305 mm Pitch Size

| Reynolds Number for Tube 305 | h | Nu | $f$ |
|---|---|---|---|
| 4000 | 3571 | 44 | 0.049 |
| 6000 | 4730 | 58 | 0.042 |
| 8000 | 5863 | 72 | 0.037 |
| 10000 | 7143 | 87 | 0.034 |

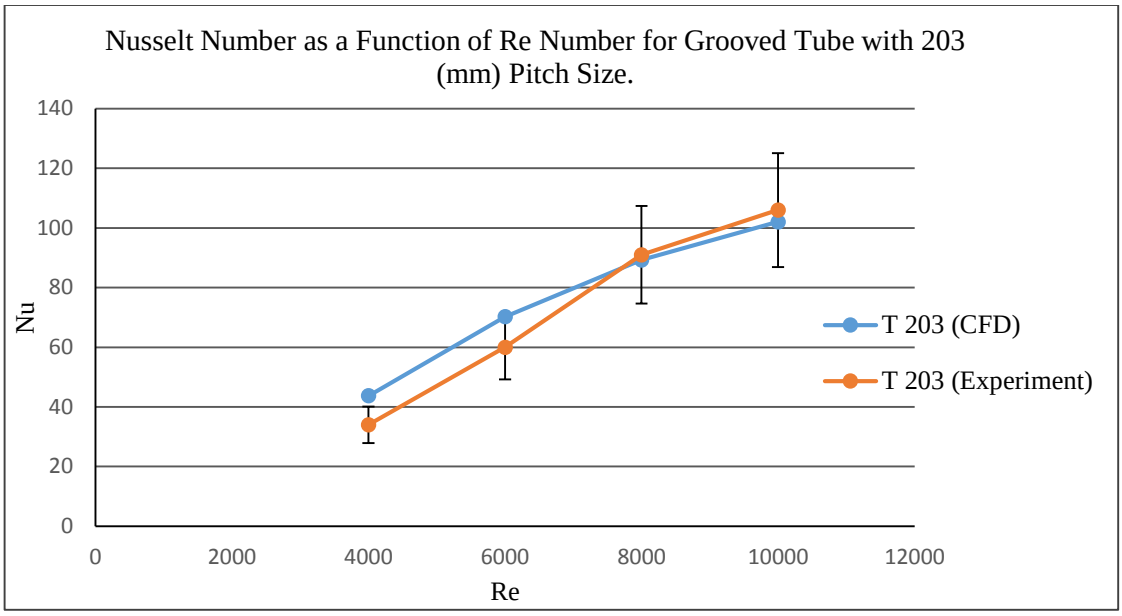


Figure 5.8 Comparison of CFD and Experimental Nusselt Number for Tube with 203 (mm) Pitch Size

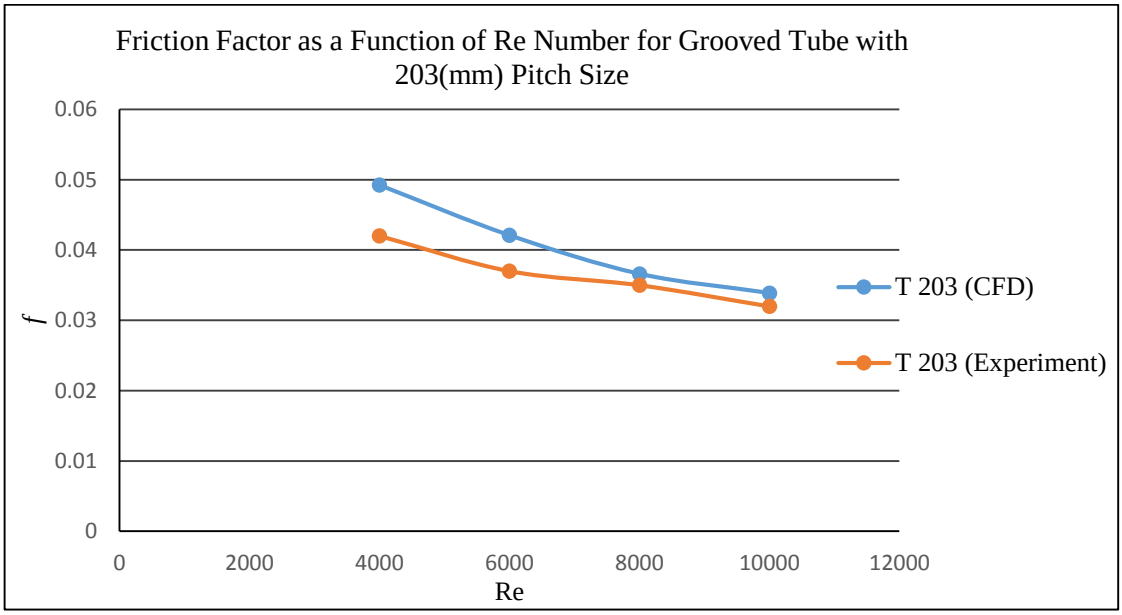


Figure 5.9 Comparison of CFD and Experimental Friction Factor for Tube with 203 (mm) Pitch Size

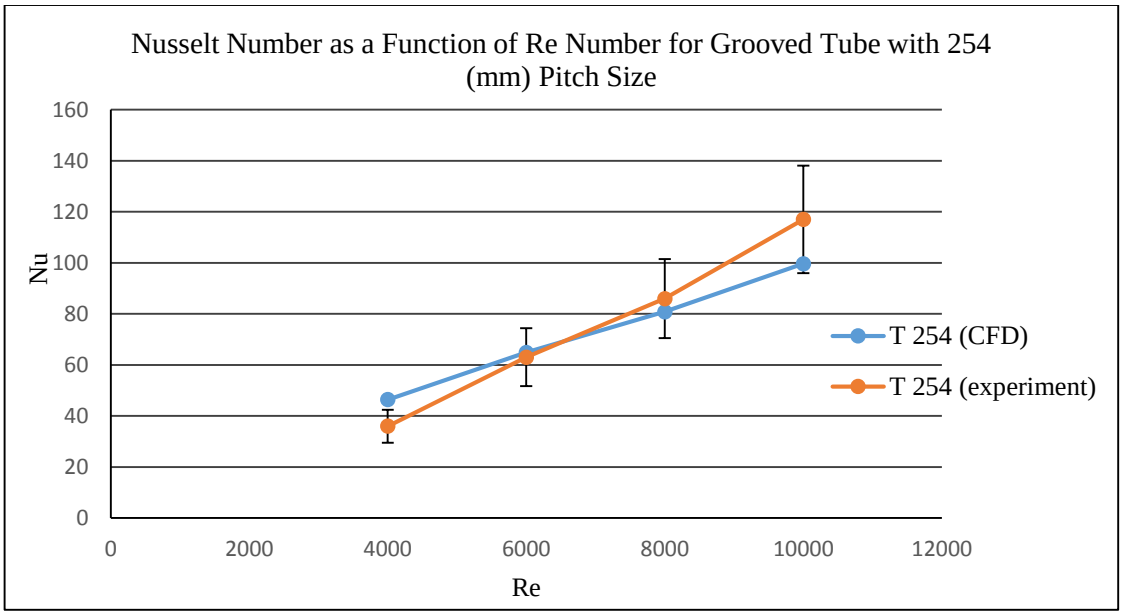


Figure 5.10 Comparison of CFD and Experimental Nusselt Number for Tube with 254 (mm) Pitch Size

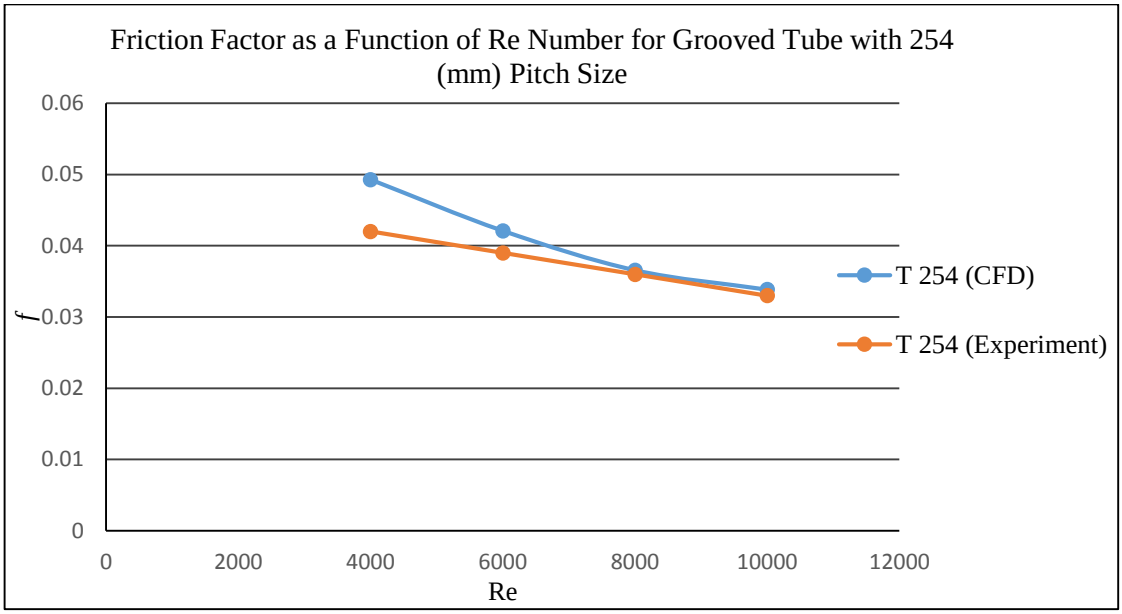


Figure 5.11 Comparison of CFD and Experimental Friction Factor for Tube with 254 (mm) Pitch Size

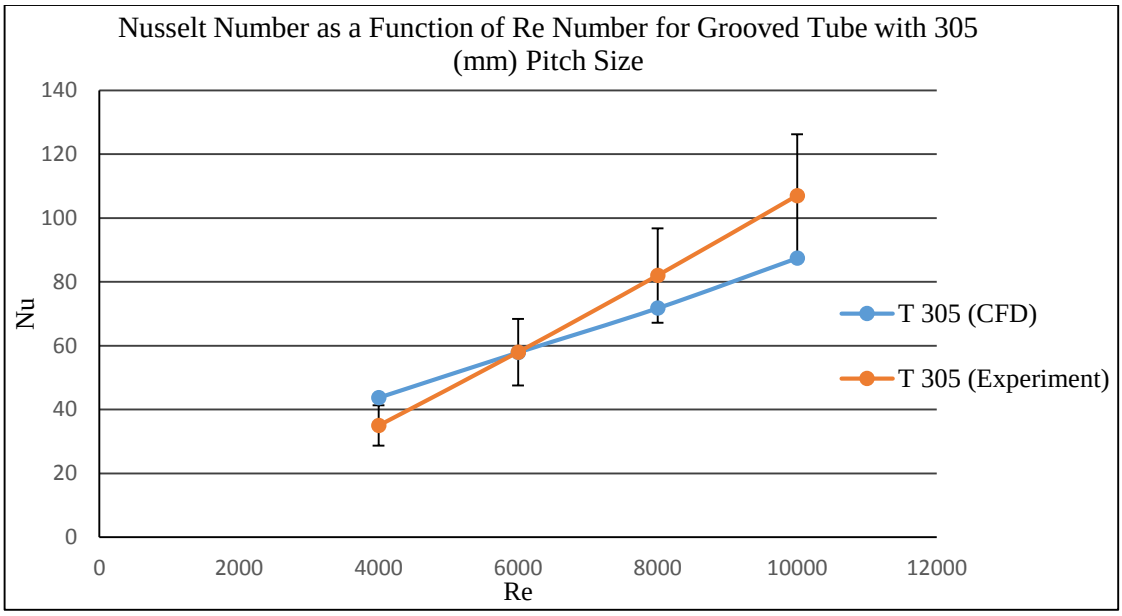


Figure 5.12 Comparison of CFD and Experimental Nusselt Number for Tube with 305 (mm) Pitch Size

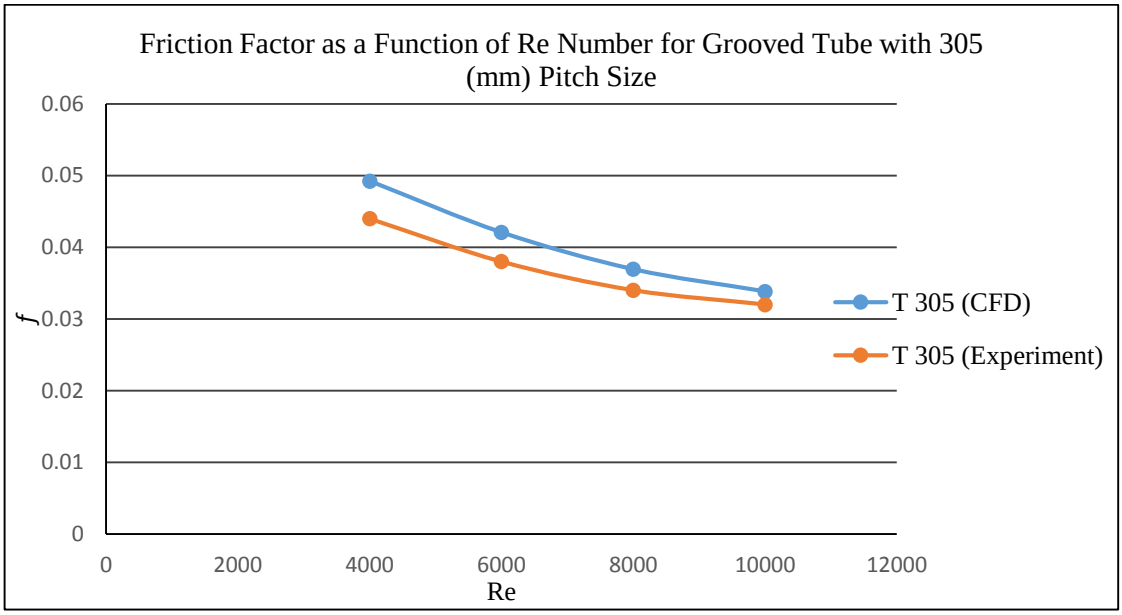


Figure 5.13 Comparison of CFD and Experimental Friction Factor for Tube with 305 (mm) Pitch Size

## 5.4 Extended CFD Simulation of Internally Grooved Tubes

After the validation of the numerical model was done in the previous sections, the CFD simulation was expanded for tubes with 7.1, 12.7, 50 and 130 (mm) pitch size which amounts to a P/d range between 1 to18 being considered. In the current study, the groove width (e) and height (h) were kept constant, to clarify the effect of pitch size on heat transfer augmentation. As before Nu number and *f* were presented for those additional runs.

### 5.4.1 Nusselt Number (Nu)

In the CFD study, the effect of pitch size on Nu number as a function of Re number results for four helical grooved tubes are shown in Figure 5.14 The same constant heat flux of 3150 kW/m2 applied on the tube surface and Re number for each grooved tube is varied from 4000 to 20,000. The heat transfer coefficient h and Nu number were calculated using Equation 16. Figure 5.14 shows that the Nu number increases with Re numbers from 4000 to 20000, and as the pitch distance decreases, indicating as expected, an increase in the frequency of "tripping" and hence the "thinning" of the hydrodynamic and thermal boundary layers is also shown.

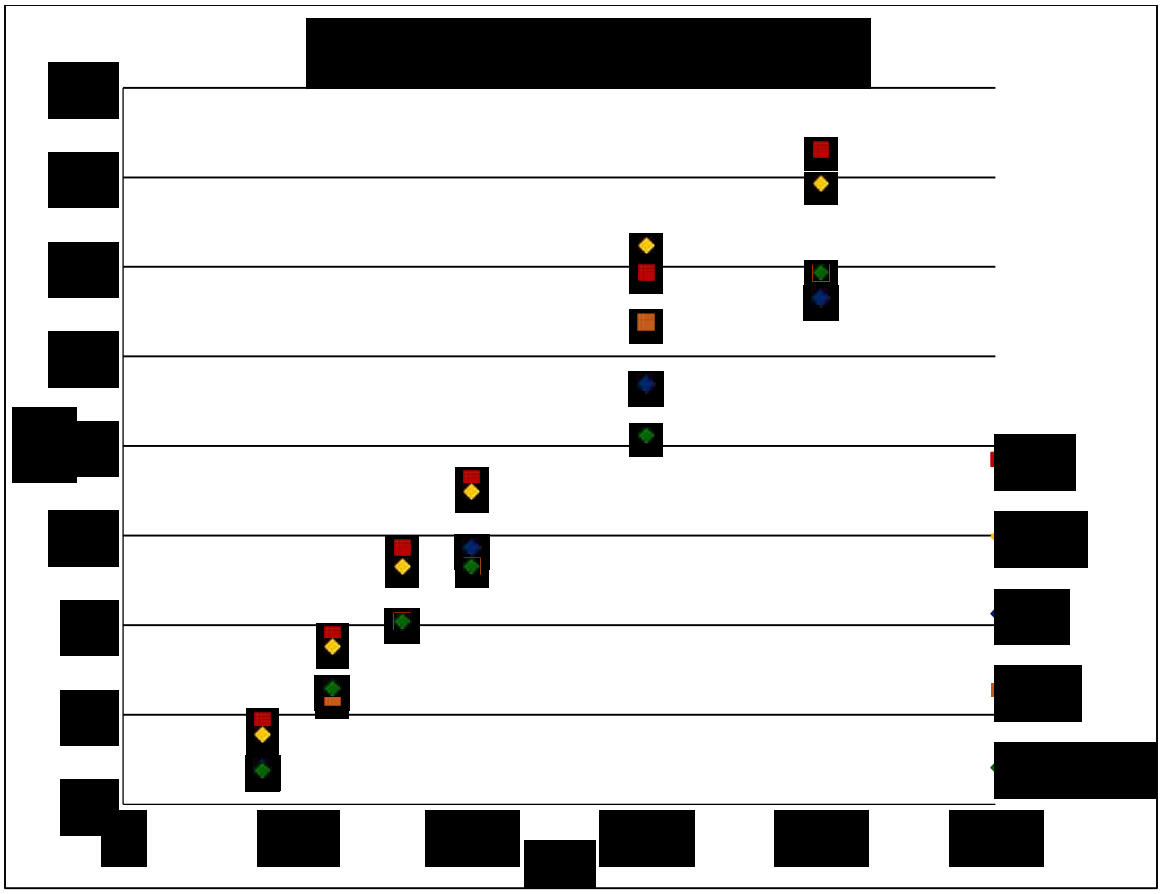

Figure 5.14 Nusselt Numbers as a Function of Reynolds Number for Four Different Grooved Tubes (Pitch Size: 7.1, 12.7, 50 and 130 (mm)) and a Smooth Tube.

5.4.2 Friction Factor (*f)*

*f* is a non-dimensional parameter calculated to show the variation of the pressure drop as a function of Re ranging between 4000 to 20000 using equation 17. Figure 5.15 shows the *f* values for helical grooved tubes decrease monotonically with increasing Re. The grooves inside these tubes in general will increase flow swirl and potentially recirculation around these grooves leading to a higher *f*. Also an increase of the *f* is shown to exist for smaller pitch size values for the same Re due to similar reasons as before [9]. Figure 5.15 is in good agreement with the trends of the Moody diagram which shows that

*f* decreases with increasing Re number. Also as the relative roughness ε/d increases, in the Moody diagram, the value of $f$ increases for the same Re value.

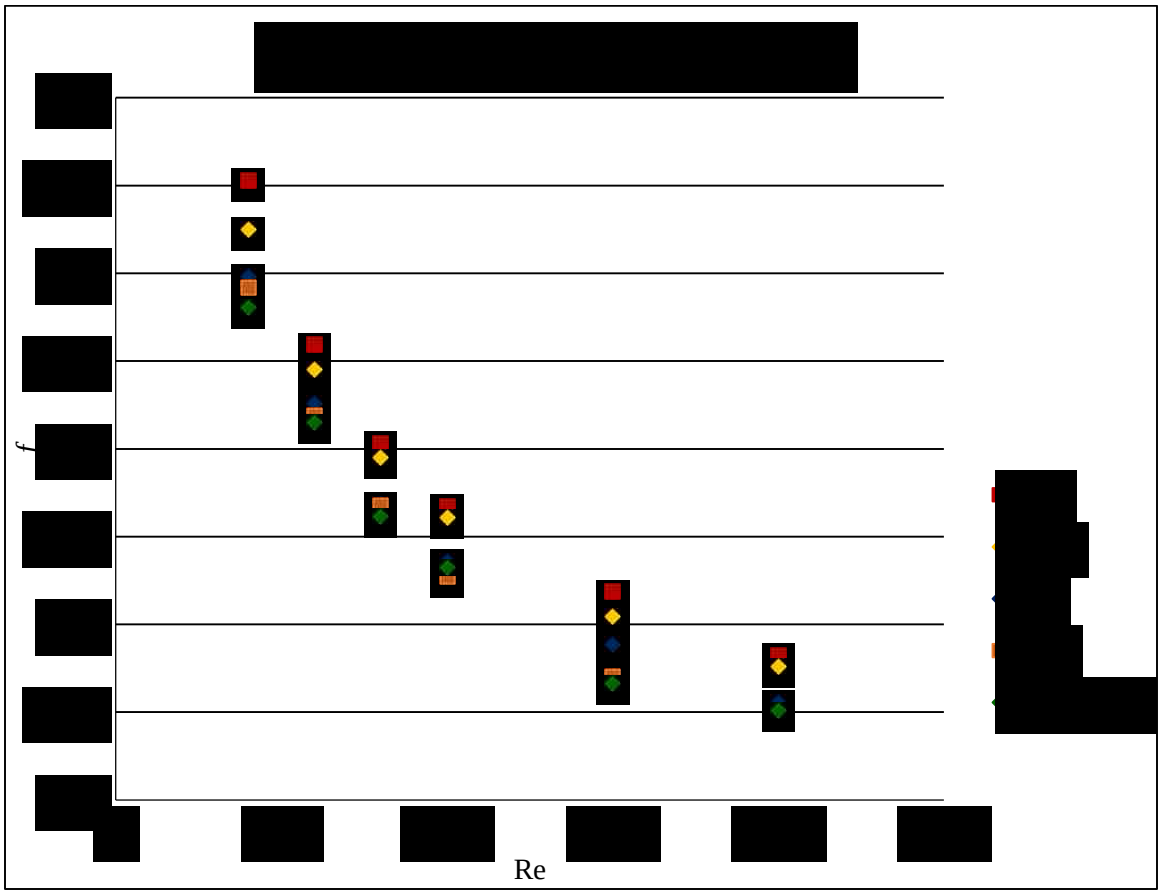


Figure 5.15 Friction Factor as a Function of Reynolds Number for Four Different Grooved Tubes (Pitch Size: 7.1, 12.7, 50 and 130 (mm)) and a Smooth Tube.

.

If the ratio of the groove depth to diameter (e/d=0.028) or pipe, "assumed pipe roughness" is 0.000015 (m) [7] is greater than the thickness of the viscous sub layer, the turbulence effect near the wall, will lead to an increase in pressure drop. Therefore, by decreasing the viscous sublayer thickness and with more disturbance in the flow, the effect of roughness is increasing, so, the friction factors play an important role in heat

enhancement efficiency [6] [9]. Working with higher Reynolds is not always efficient due to more pumping power and cost.

### 5.4.3 Thermal performance

Enhanced surface geometry leads to an increase in heat transfer by promoting turbulence in the flow, but in general there is a penalty of increased pressure drop and increased pumping power that comes with it. Therefore to better quantify the heat enhancement efficiency, the thermal factor should be considered [6]. The performances of grooved tubes were investigated in terms of thermal enhancement factor, $\eta$, which is the ratio of the Nu number of grooved tubes to a smooth tube over the friction factor ratio of an internally grooved tube to a smooth tube. Figure 5.19 shows the η of the studied cases as a function of Re number. Thermal enhancement factor has different definitions with different authors. Some used heat enhancement coefficient ratio ($h/h_s$) or Stanton number ratio ($St/St_s$) instead of Nu number [6].In this study equation 16 is used to evaluate the effect of pitch size on heat enhancement.

$$\eta = \frac{\frac{Nu}{Nu_s}}{\frac{f}{f_s}} \tag{16}$$

Where:

$h_s$ : heat transfer coefficient of a smooth tube

$St_s$: Stanton number of a smooth tube

$Nu_s$: Nusselt of a smooth tube

$f_s$: Friction factor of a smooth tube

First, the heat enhancement factor results of CFD work for tubes with the pitch sizes of 203, 254 and 305 were compared to experimental works [2]. Since, the Nu number and friction factor uncertainty in the study were mentioned to be 18% and 1 % respectively, the Nu number uncertainty can affect the enhancement factor, but the effect of the friction factor uncertainty should not be neglected due to its small magnitude. Therefore, the range of errors reported for the Nusselt number from the experimental study were plotted in Figures 5.16 through 5.18 and compared to CFD enhancement factors. By using an error range of $\pm 18\%$ in the Nu number and considering that this error is random, the range of errors which can be expected to exist in the heat enhancement factor calculation for the experimental data was evaluated. This range is expected to be 32% from calculation of uncertainty of Nusselt number for the reported experiment and is what is shown in the error bars (Figure 5.16-5.18). Although, the thermal enhancement factor for the CFD results is lower than 1 in some cases, it still is in the range of uncertainty of the experimental work. After comparing the CFD results with those of the experimental work, the enhancement factors in the current study with different pitch sizes (7.1, 12.7, 50 pitch and 130 additional CFD runs with no experimental data for comparison) were also calculated and are shown in Figure 5.19. η increases by increasing Reynolds number in the range of 4000 to 15000.

If the $\eta$ >=1 , it means the increase in heat transfer is more or about the same as the increase in friction factor which indicate that the tube design is efficient to be used for enhancement purposes [22]. Since the highest enhancement factor for all grooved tubes achieved in Re number equal to 15000, the Re of the 15000 is a critical point for enhancement factor in the current work. By increasing Re to 20,000 the enhancement

decreases which indicates the augmentation of heat transfer is not efficient for higher Re due to higher pressure drop [6]. The enhancement observed in all cases, for tubes with smaller pitch size such as 7.1, 12.7 (mm) the factor was higher. Figure 5.19 shows the grooved tube design is efficient for being utilized in heat exchanger devices for heat augmentation.

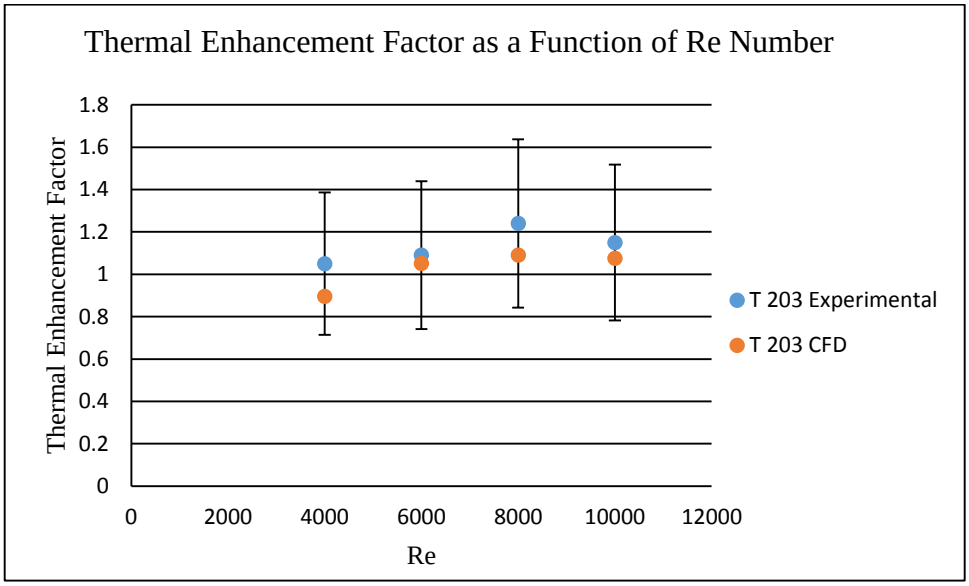


Figure 5. 16 Thermal Enhancement Factor for Grooved Tube with 203 (mm) Pitch Size

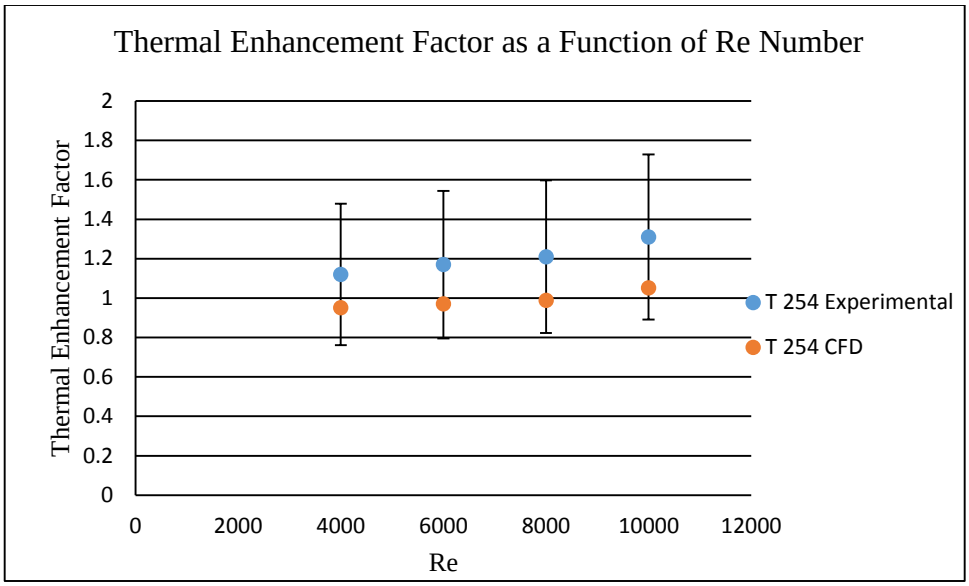


Figure 5.17 Thermal Enhancement Factor for Grooved Tube with 254 (mm) Pitch Size

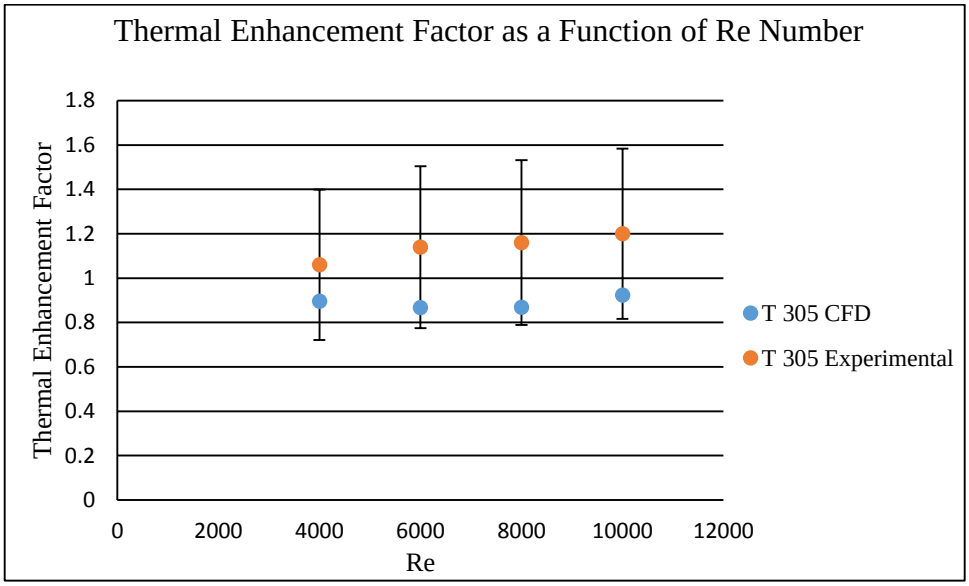


Figure 5.18 Thermal Enhancement Factor for Grooved Tube with 305 (mm) Pitch Size

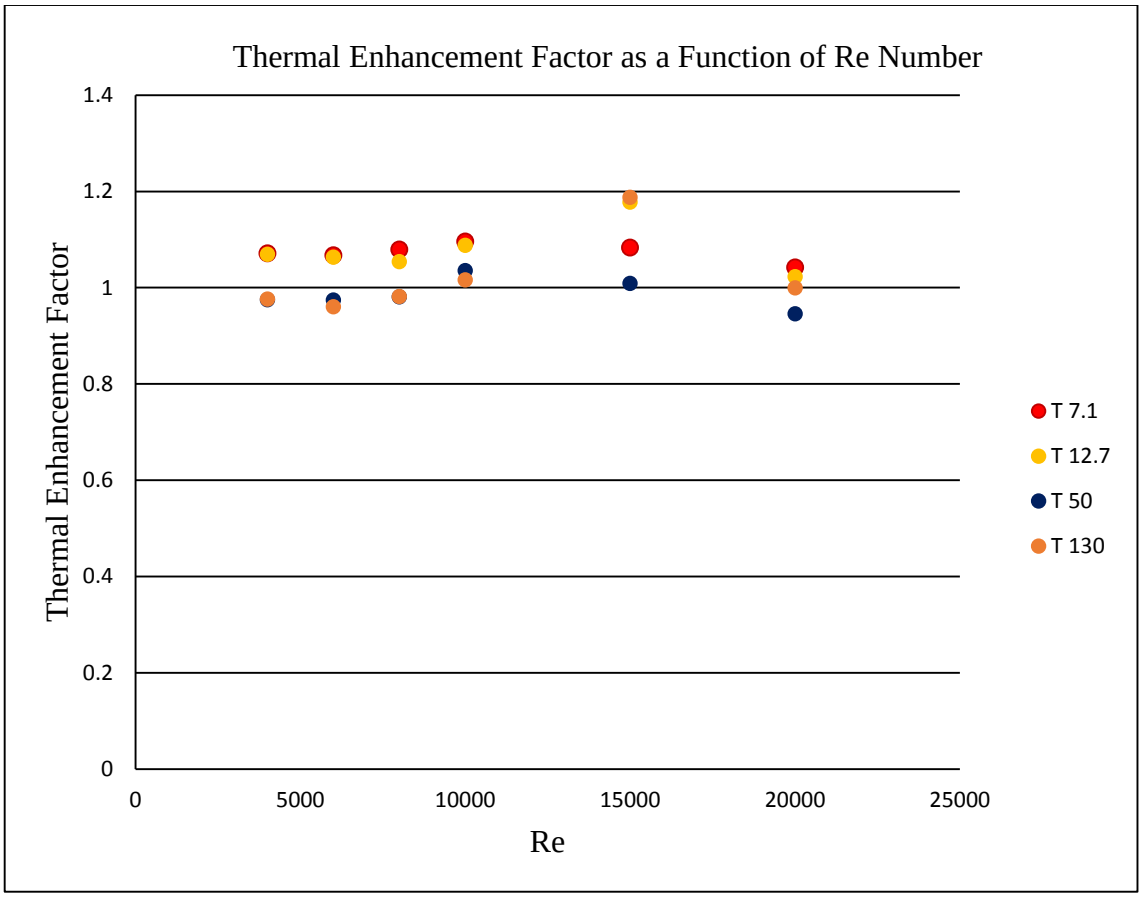


Figure 5.19 Thermal Enhancement Factor as a Function of Reynolds Number for Four Grooved Tubes

5.5 Center plane plots of temperature for tube pitch 12.7

In the current study, mean bulk temperature was one of the important parameters to obtain. The thermal contours of the center plane of the tube with a 12.7 mm pitch for various Re numbers are shown in Figures 5.20 through 5.24 along with one plot of the temperature field around the grooved area of the tube in Figure 5.21. The center plane is along the whole length of the tube and includes the tube axis from inlet to outlet. The inlet temperature is considered a constant at 24 ◦C similar to that of the experimental study. Constant heat flux is assumed to occur along the length of the tube. By increasing the Reynolds number, the mean bulk temperature at the outlet is decreasing (Table 5.5)

Table 5.5 Average Outlet Temperatures in all cases

| Reynolds number | $T_o$ave 7.1 | $T_o$ave 12.7 | $T_o$ave 50 | $T_o$ave 130 |
|---|---|---|---|---|
| 4000 | 25.94 | 25.75 | 25.72 | 25.72 |
| 6000 | 25.29 | 25.16 | 25.14 | 25.14 |
| 8000 | 24.97 | 24.87 | 24.86 | 24.86 |
| 10000 | 24.77 | 24.69 | 24.69 | 24.69 |
| 15000 | 24.59 | 24.56 | 24.46 | 24.47 |
| 20000 | 24.46 | 24.35 | 24.35 | 24.34 |

The higher outlet temperatures are expected for lower flow rate to satisfy energy balance. For the given Re numbers and the applied heat flux the average temperature difference was expected to be approximately in the neighborhood of 2.0 C. Figure 5.20 shows the detail of the temperature field near the groove, close to the outlet of the tube, where as expected the higher temperatures are in the transverse direction. Also disruption in thermal boundary layer is shown.

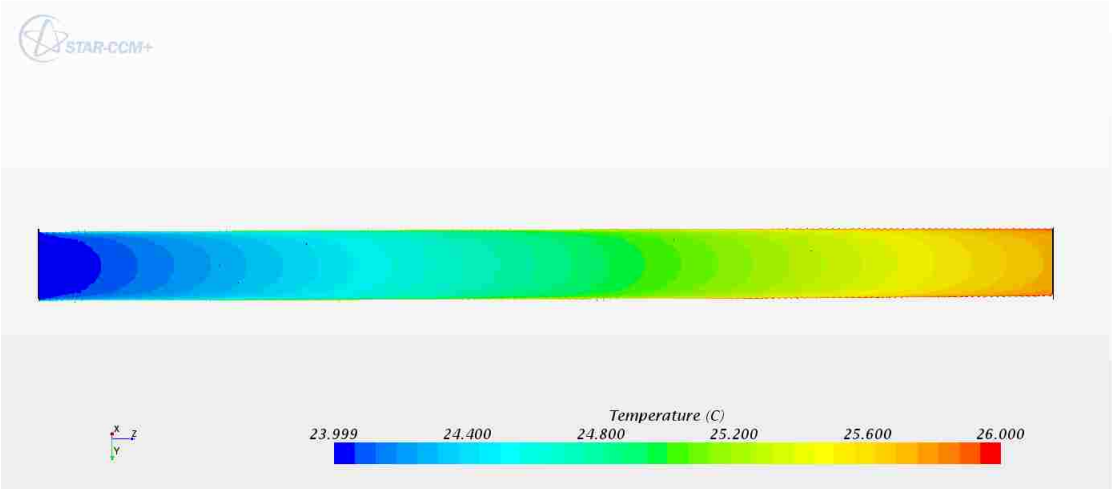


Figure 5.20 Center-plane Temperature Profile of Tube with12.7 (mm) Pitch at 4000 Re Number

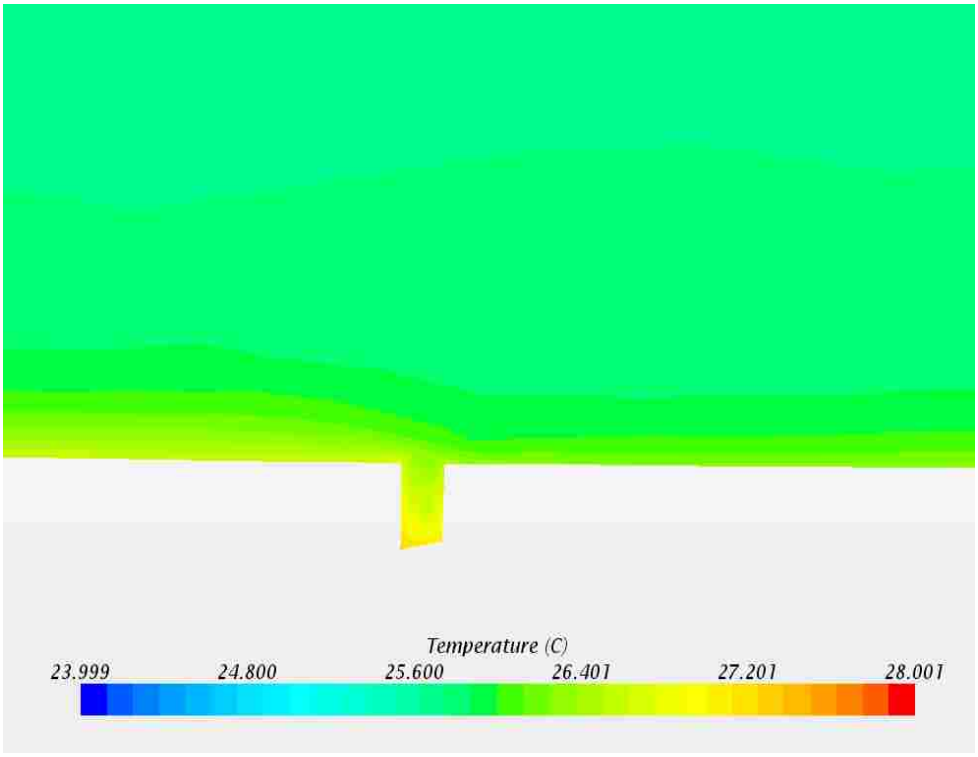


Figure 5.21 Temperature Profile Near the Groove for Tube with 12.7 (mm) Pitch Size and Re: 4000

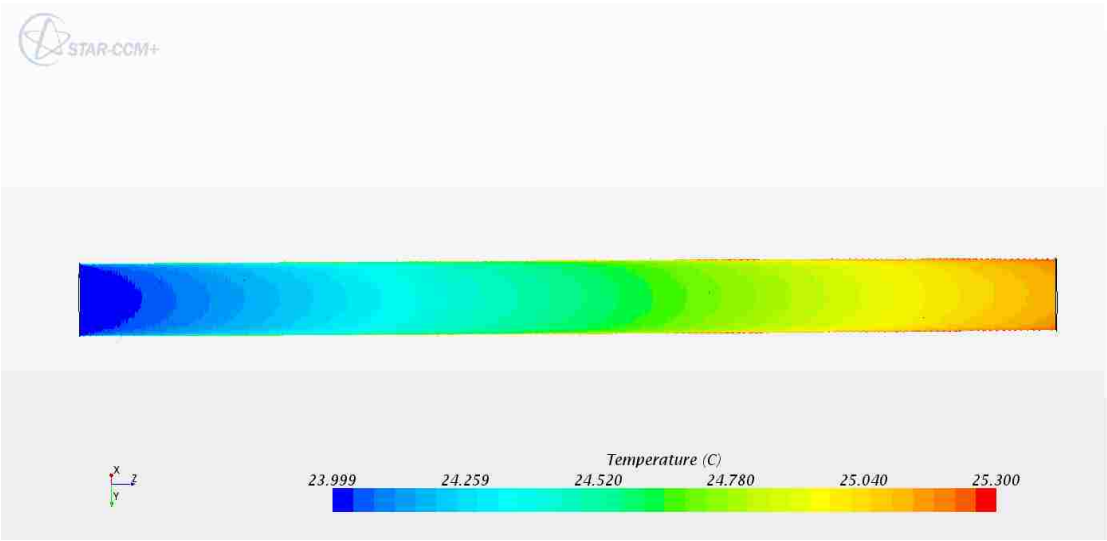


Figure 5.22 Center-plane Temperature Profile of Tube with12.7 (mm) Pitch at 6000 Re Number

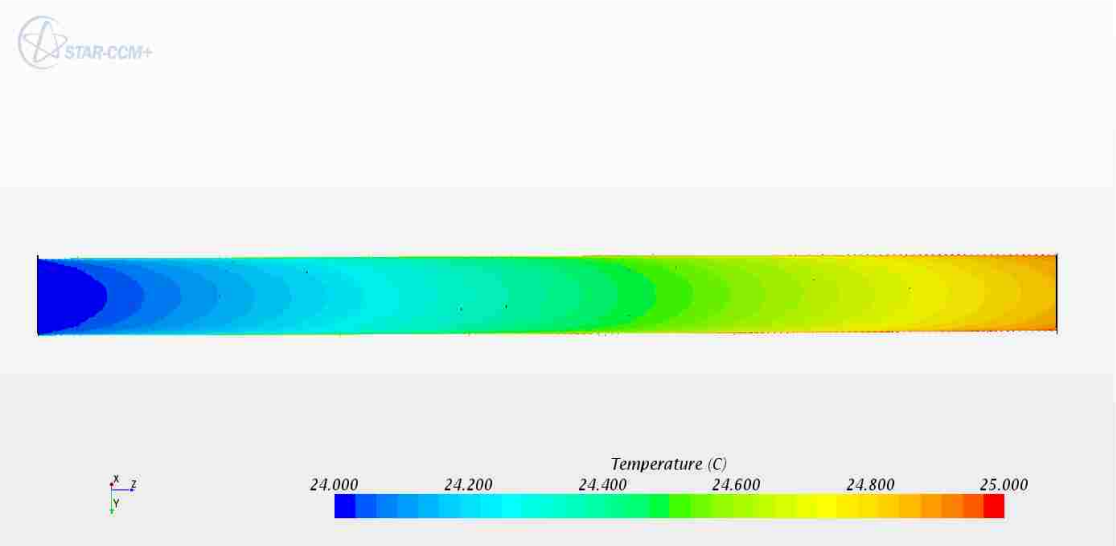


Figure 5.23 Center-plane Temperature Profile of Tube with12.7 (mm) Pitch at 8000 Re Number

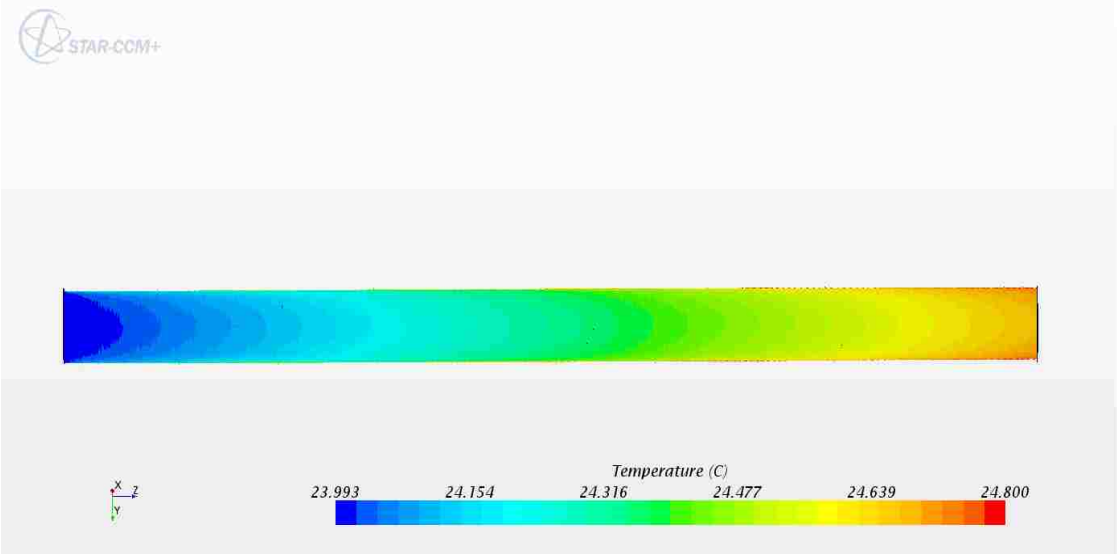


Figure 5.24 Center-plane Temperature Profile of Tube with12.7 (mm) Pitch at 10000 Re Number

## 5.6 Streamlines for Re number of 10000

To visualize the effect of pitch size on the flow pattern, streamlines were plotted for smooth tube and grooved tube with a Re number of 10000. Streamlines were plotted along the entire length of the heat exchanger. Figures 5.25 and 5.26 depict the generation of a swirl in the flow inside the tubes. The starting point of this plot is at the inlet of the tube and locations are chosen randomly on the cross-sectional area at the inlet. Streamlines which were observed at the mid center of the tubes are smoother (less wavy) because they were not as affected by the grooves. Since the Re number is the same in all cases, by decreasing the pitch size an increase in the swirl in path lines is noticed and also the velocity magnitude is increased somewhat indicating that there is an increase in the transverse component of the flow, as the average axial velocity should be the same for these cases since the Re number is assumed the same. In cases with larger pitch size such as tubes with 50 and 130 mm, the streamlines were almost parallel such as in a smooth tube and swirl in the flow was not as noticeable.

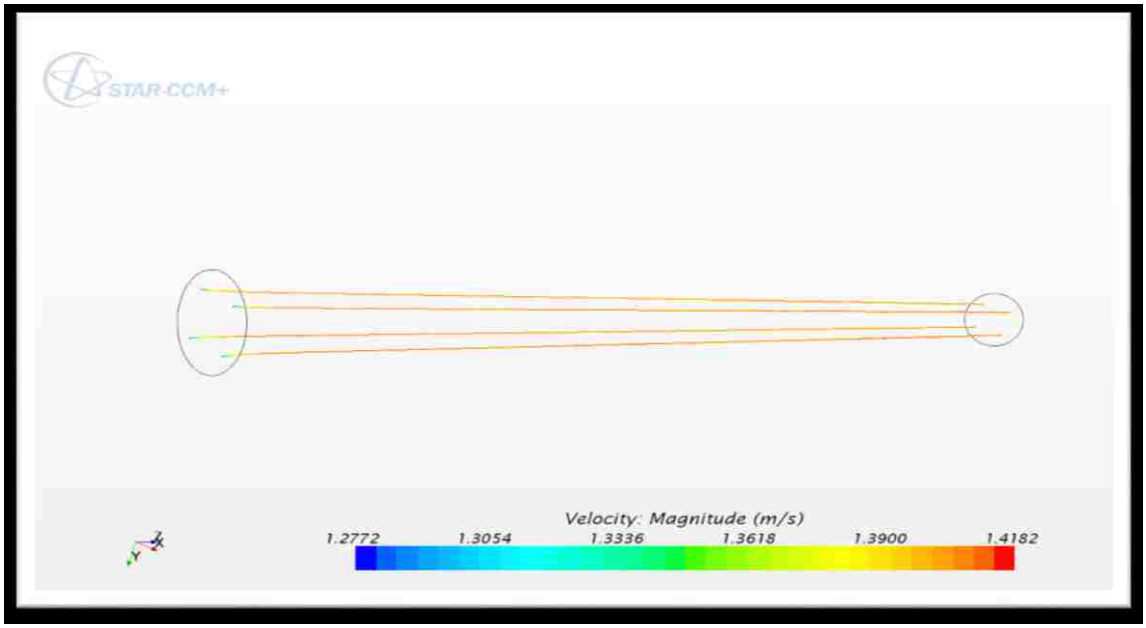


Figure 5.25 Streamlines within the Fluid Region in Tube without Groove.

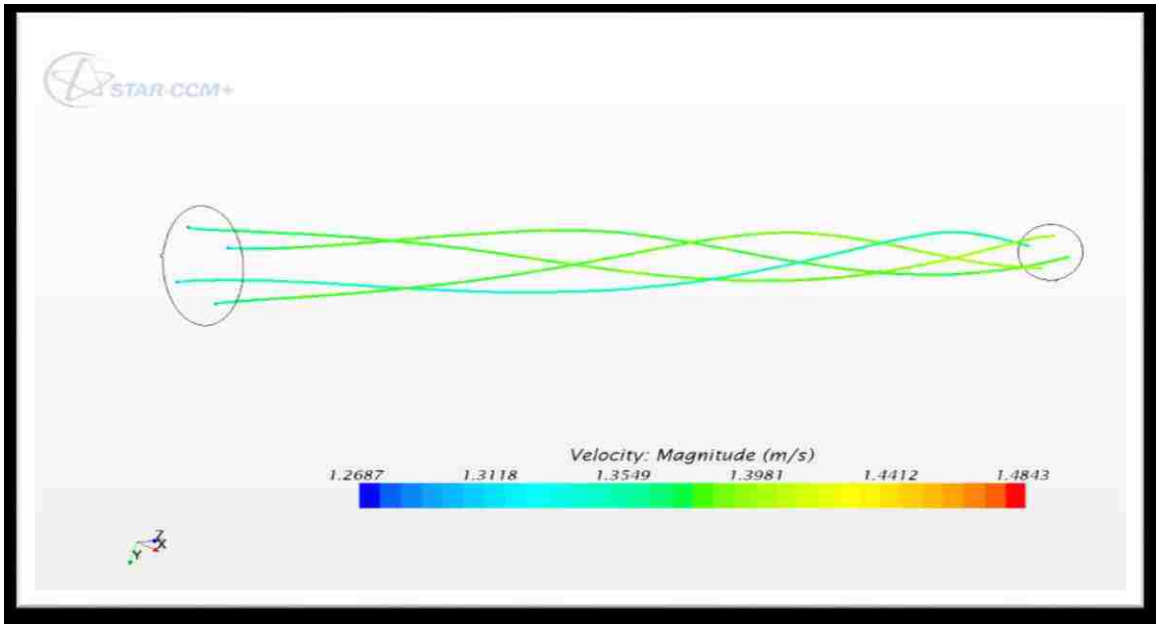


Figure 5. 26 Streamlines within the Fluid Region in Tube with 7.1 mm Pitch Size

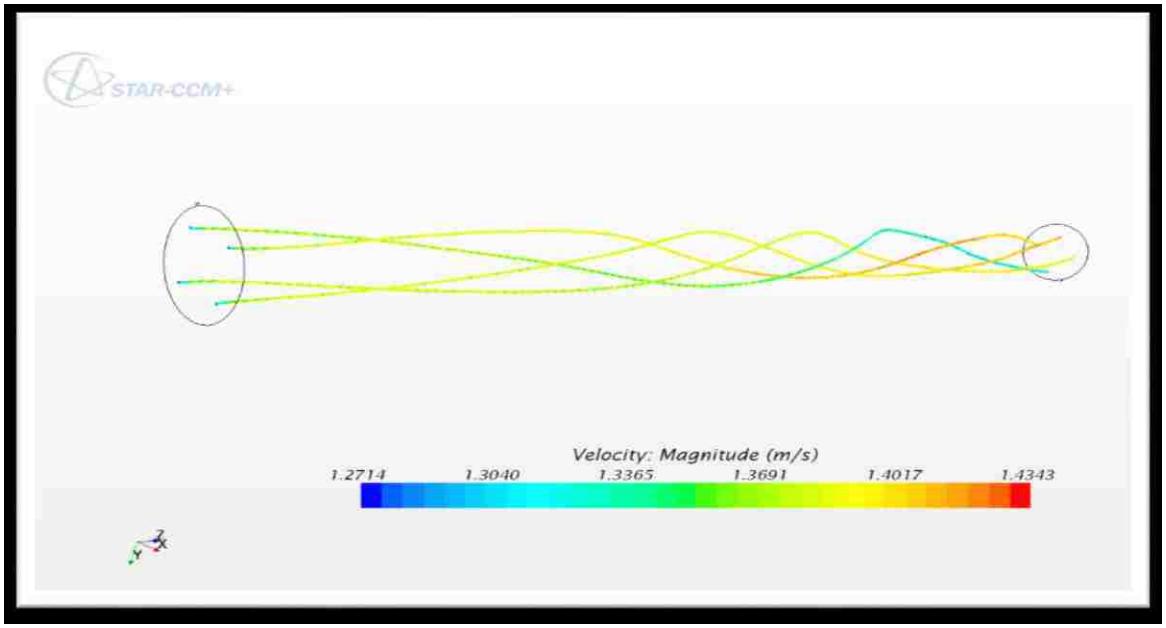


Figure 5.27 Streamlines within the Fluid Region in Tube with 12.7 mm Pitch Size

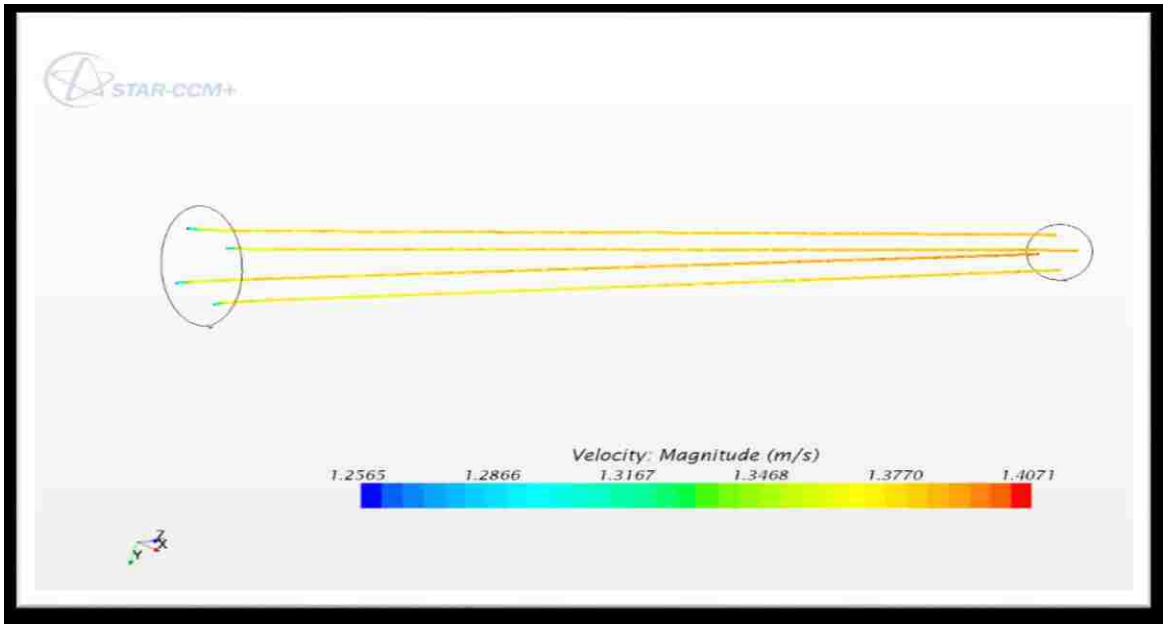


Figure 5.28 Streamlines within the Fluid Region in Tube with 50 mm Pitch Size

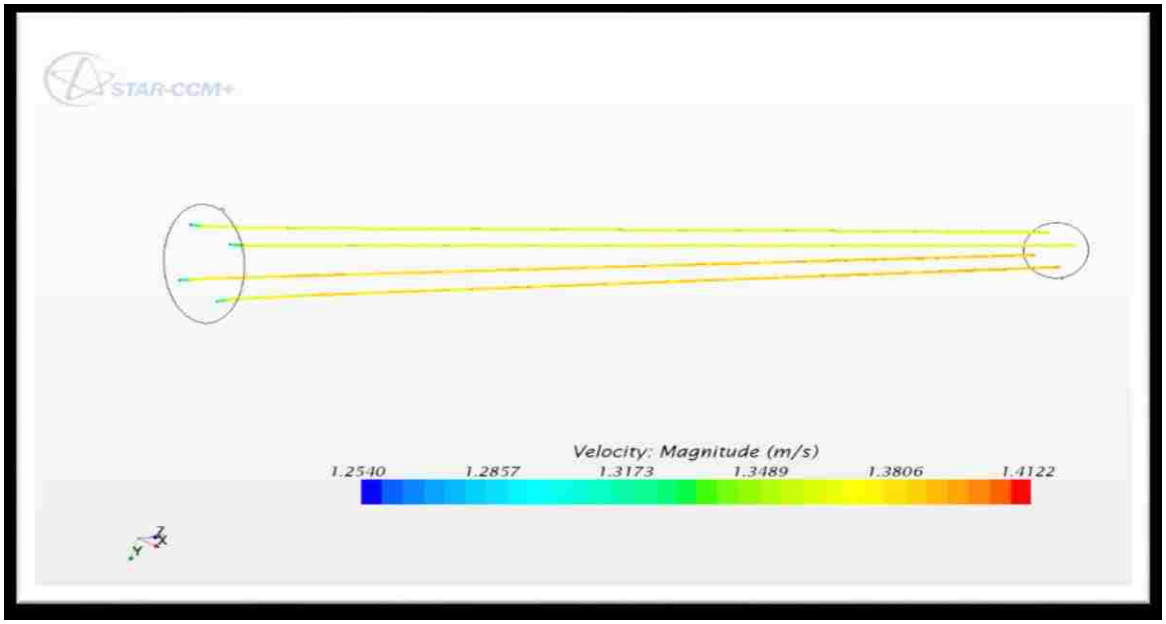


Figure 5.29 Streamlines within the Fluid Region in Tube with 130 mm Pitch Size

## 5.7 Swirl Effect

Adding a helical groove generates swirl effect on the flow close to the wall [2]. The vector velocities of [i]+[j] were plotted to show the swirl motion for tube pitches of 7.1 and 12.7 at a cross section plane, which is placed by 1(m) distance from the inlet. The vectors show the rate of change in the position of each volume of cells. Also, the color bar illustrates the magnitude of the speed at each position and the arrow of the vectors point the direction of their movement [25]. Figures 5.30 and 5.31 show the swirl effect which in the experimental study is too complicated to display. For tubes with higher pitch size, the swirl effect is insignificant.

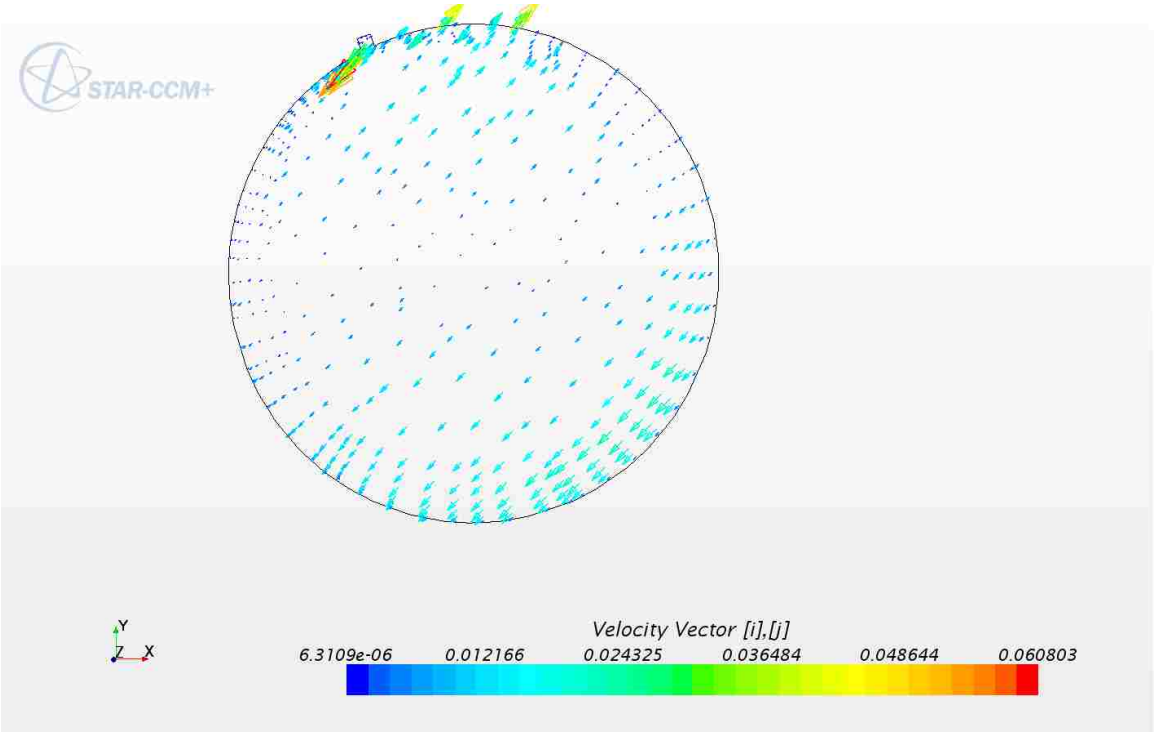


5.30 Vector Velocity of [i]+[j] at Re of 10000 for Tube with 7.1 mm Pitch Size

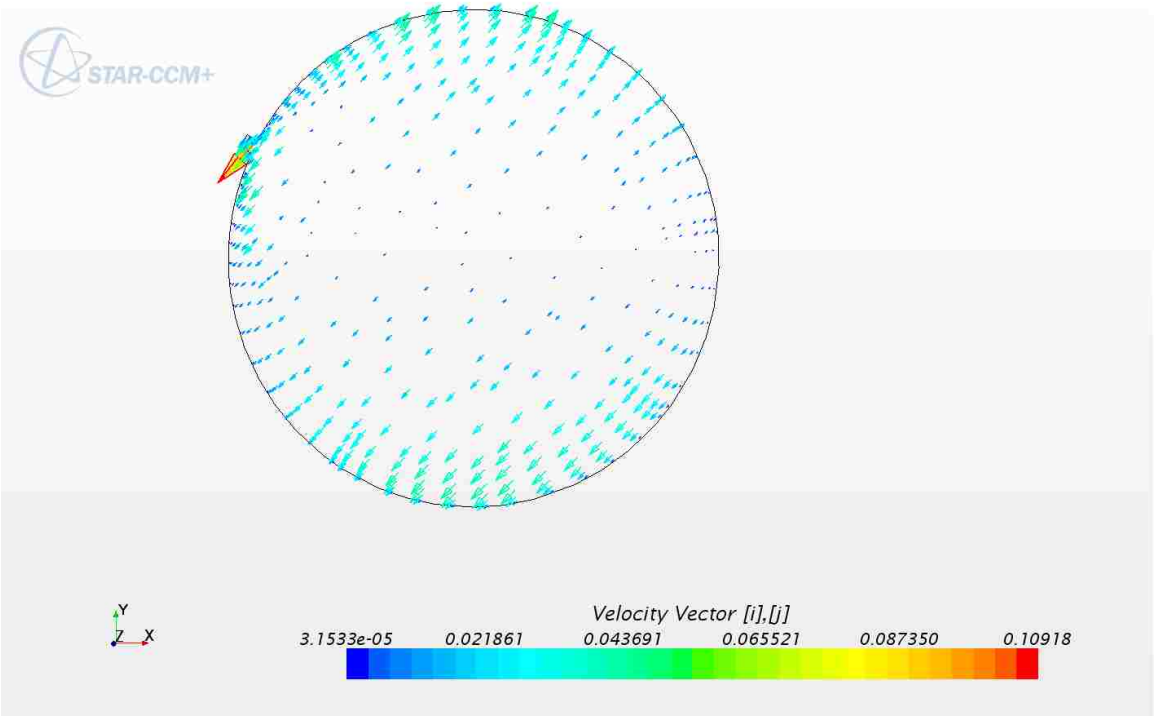


5.31 Vector Velocity [i]+[j] Direction at Re of 10000 for Tube with 12.7 mm Pitch Size

## 5.8 Turbulent Kinetic Energy

Turbulent Kinetic Energy (TKE) values in the flow field can be considered an indicator of increased turbulence and hence increased heat transfer [8]. An increasingly monotonic value of the average TKE value is observed as a function of increasing Re number. This can be discerned from the maximum TKE values presented in the legend of colors underneath each plot. It has already been revealed that an increased Re is shown to increase the Nu and hence the heat transfer between the tube surface and the bulk of the fluid. In Figures 5.32 through 5.37 the TKE pattern of flow in a tube with 12.7 mm pitch size has been shown for various Re numbers. The turbulence intensity is predicted by the k−ε model and in subsequent figures indicates that the peak values are in the downstream region of grooves and the minimum turbulence intensity is observed in the upstream of grooves. The lowest TKE zone is found to be in the core region of the tube flow as would be expected as it is furthest from the wall region. The basic structure of the contours of turbulent kinetic energy remains the same but the scale changes with the change in Reynolds number. It can be seen that the maximum turbulent kinetic energy increases from 0.0058 to 0.20 (j/kg) with an increase in Re number from 4000 to 20000.

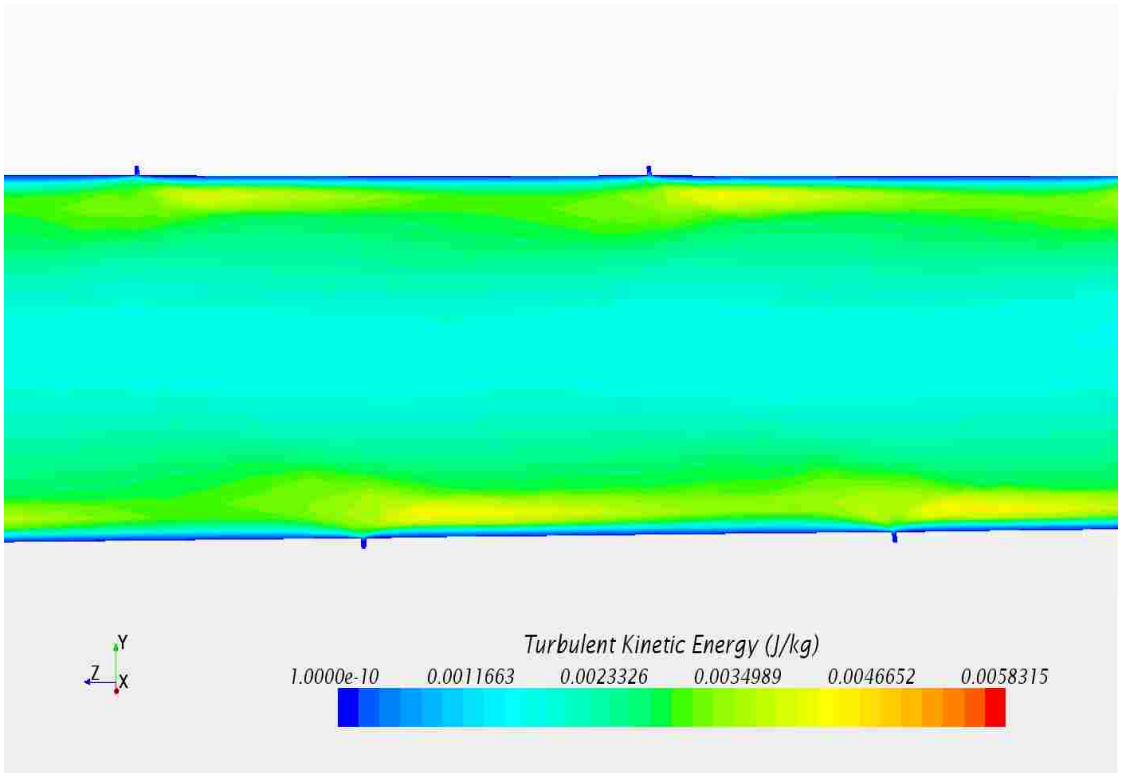


5.32 Contour Plot of TKE for Tube with 12.7 Groove at Re Number of 4000

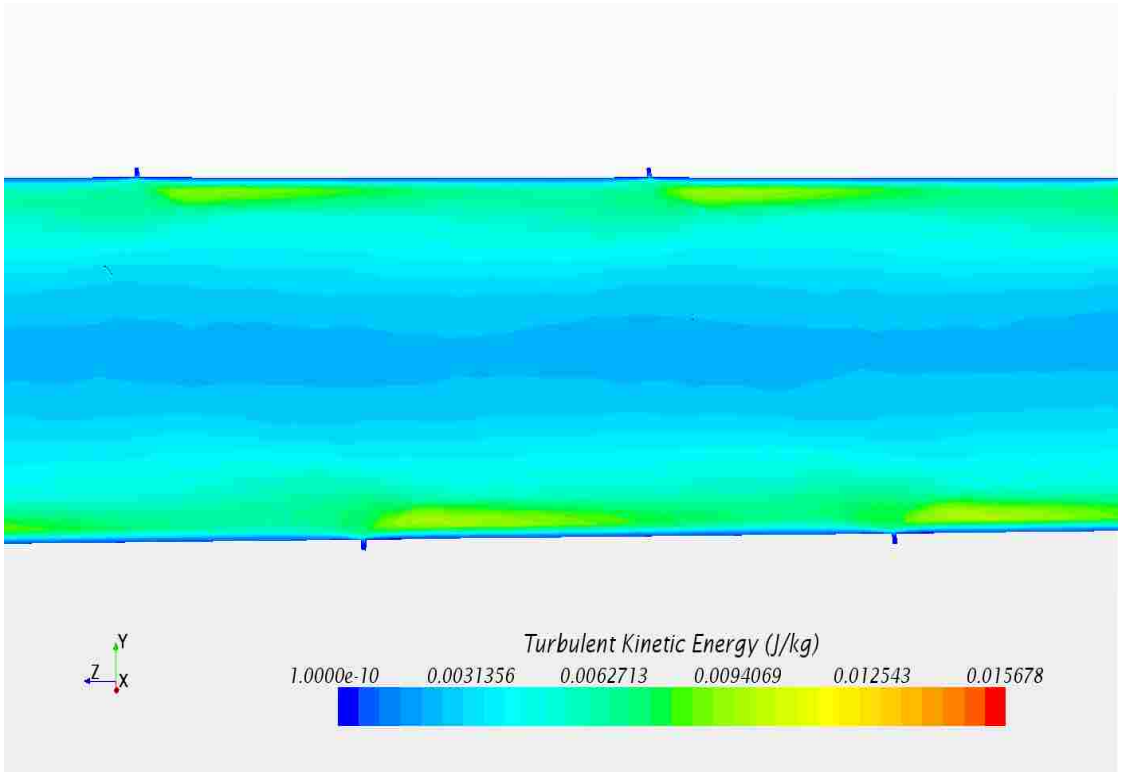


Figure 5.33 Contour Plot of TKE for Tube with 12.7 Groove at Re Number of 6000

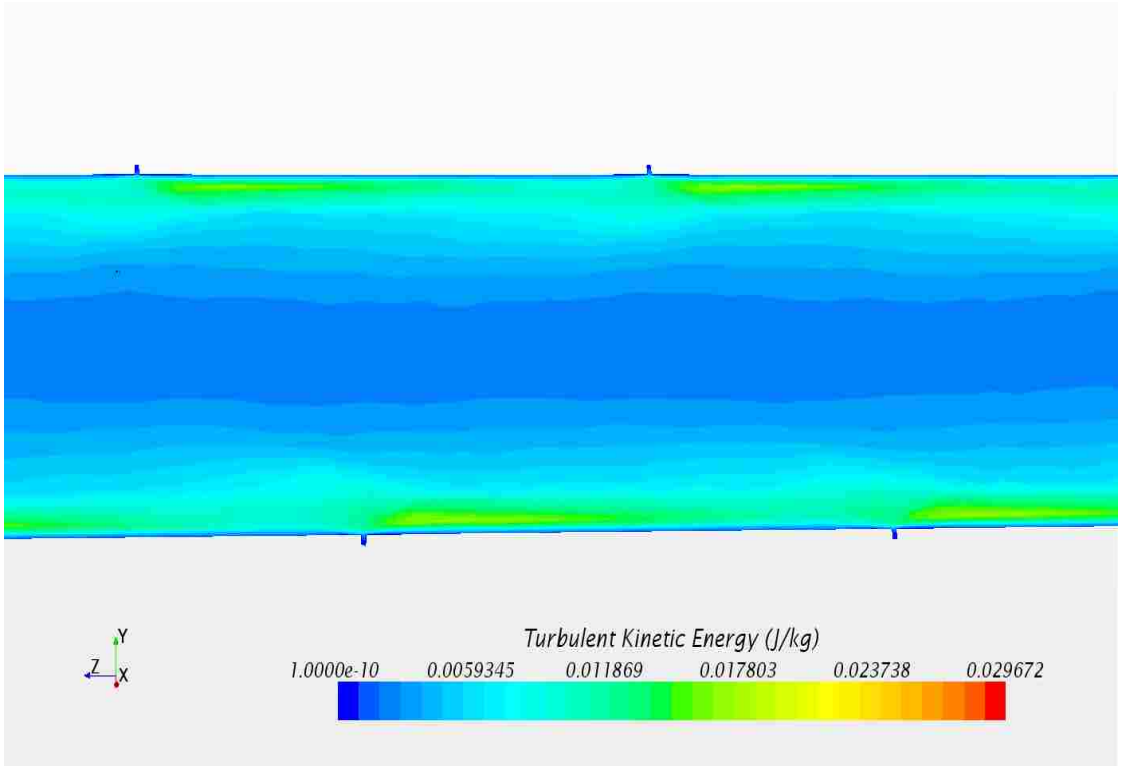


Figure 5.34 Contour Plot of TKE for Tube with 12.7 Groove at Re Number of 8000

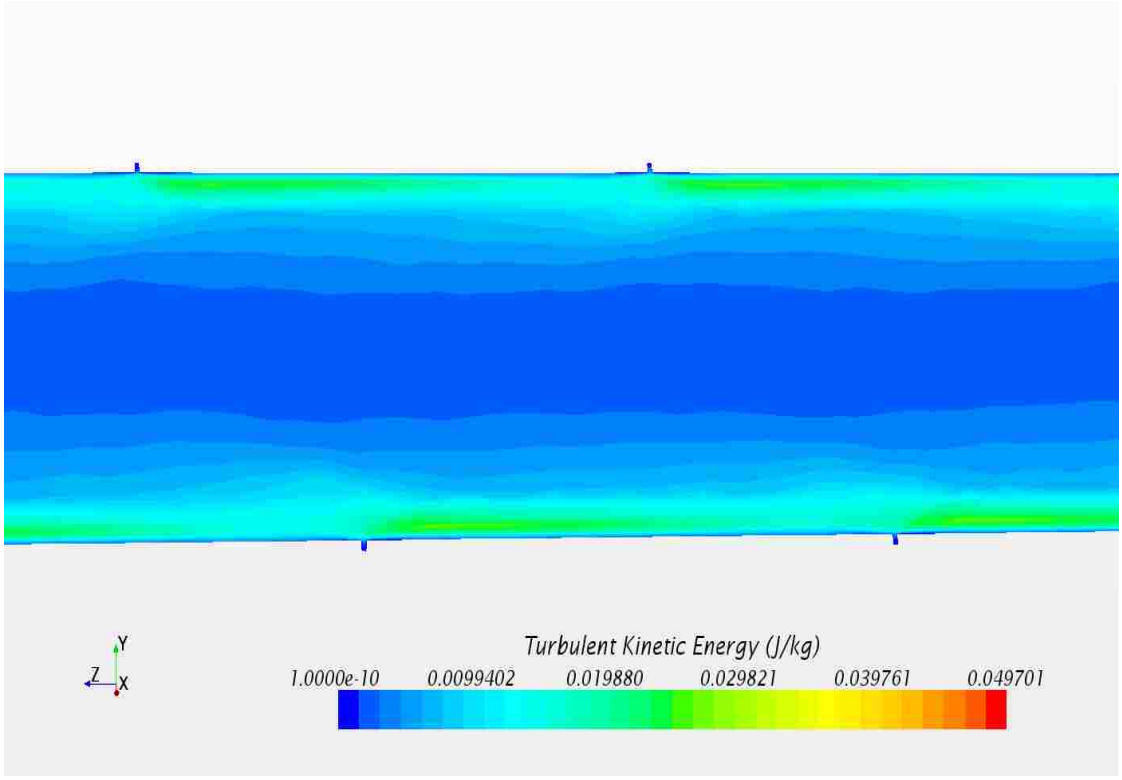


Figure 5.35 Contour Plot of TKE for Tube with 12.7 Groove at Re Number of 10000

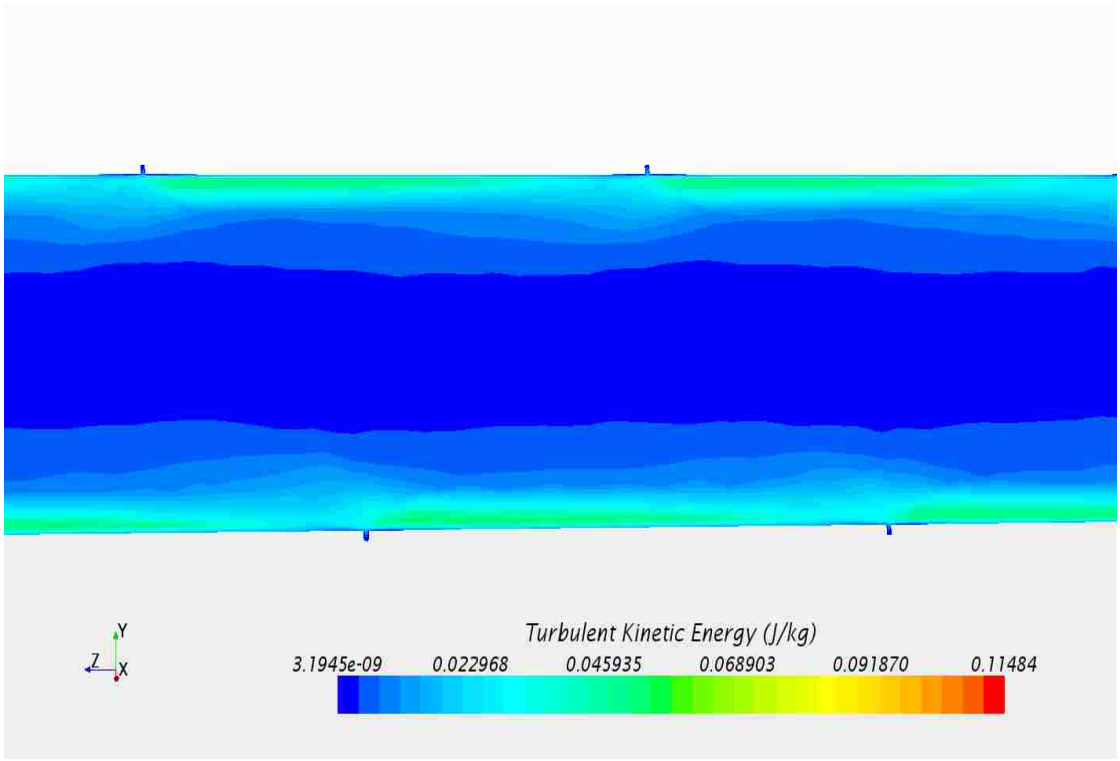


Figure 5.36 Contour Plot of TKE for Tube with 12.7 Groove at Re Number of 15000

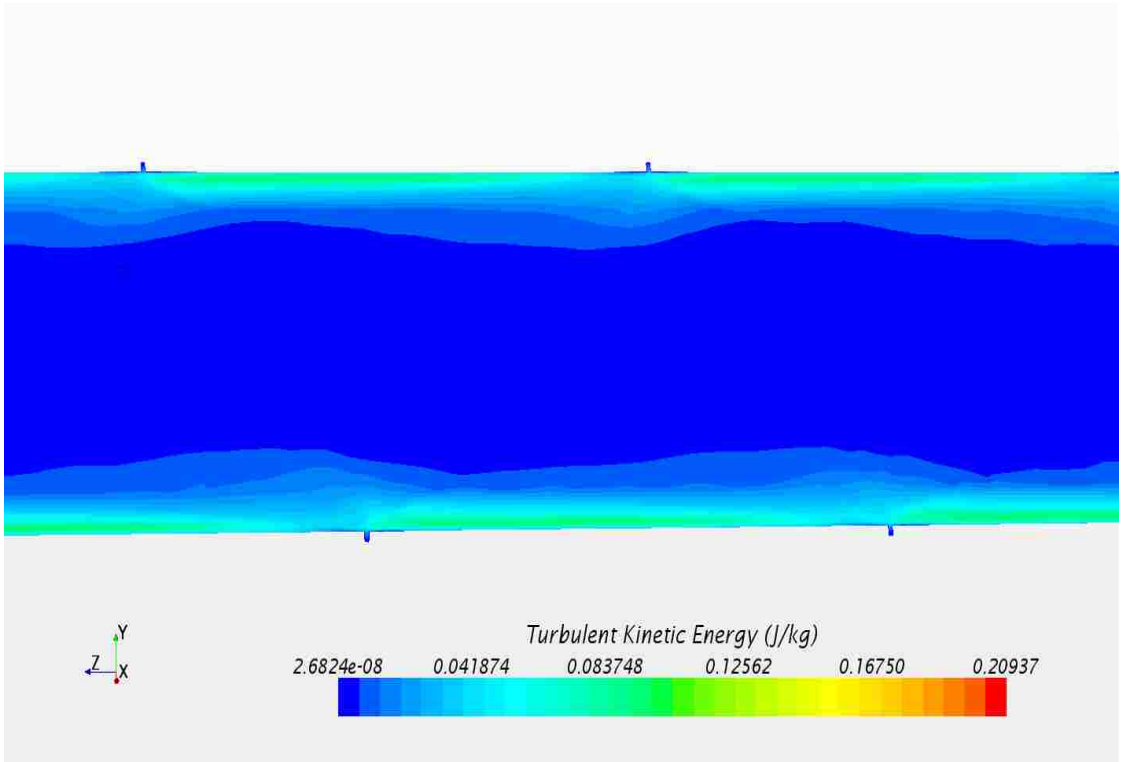


Figure 5.37 Contour Plot of TKE for Tube with 12.7 Groove at Re Number of 2000

## 5.9 Heat Transfer Coefficient

### 5.9.1 Local heat transfer coefficient as calculated by STAR-CCM+

The (local) heat transfer coefficient, which is calculated by the software, is based on the local wall surface temperature of the cell in question and a reference fluid temperature ($T_{ref}$) used of 24 ◦C, which is the inlet fluid temperature for all runs, as seen in equation 18 :

$$h = \frac{q''}{(T_{wall} - T_{ref})} \quad [18]$$

where q'' is the heat flux and $T_{wall}$ is the temperature of the surface cell directly attached to the wall and $T_{fluid}$ the reference fluid temperature. The variation of these coefficients is shown in Figures 5.38 to 5.43. The heat transfer coefficient seems to increase just upstream of the groove location as seen by the red color of the plots This could be partially explained by the anticipated disturbance of the boundary layer in that region leading to more fluid transverse mixing. It is evident from this visual presentation that there is a sudden increase in that value very close to the groove by about a factor of 2 from the heat transfer coefficient values shown between the grooves (green color). This indicates physically the rapid interruption of the local thermal boundary layer in that region and the periodic effect of that pattern over the whole tube. Also it is noticed that with an increase in the Re number, the local heat transfer coefficient increases as indicated by the maximum legend color values of red in these figures. The range of values of this heat transfer coefficient is noted to increase also by increasing Re number in the same grooved tube as shown in the subsequent figures.

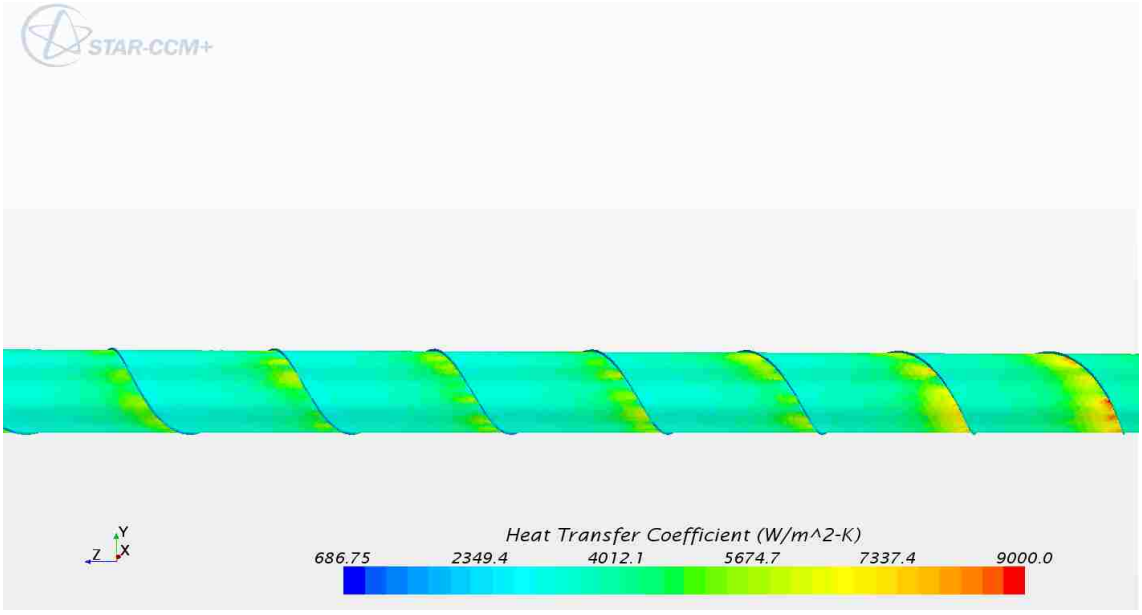


5.38 Local Heat Transfer Coefficient on Surface of the Tube with 12.7 mm Pitch Size at Re Number of 4,000

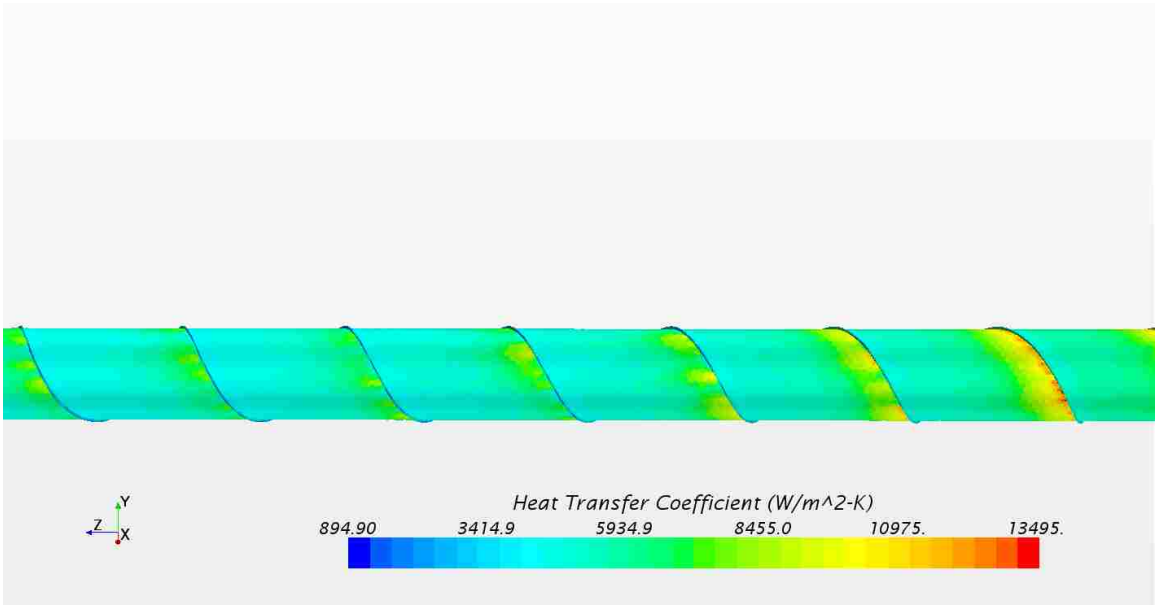


5.39 Local Heat Transfer Coefficient on Surface of the Tube with 12.7 mm Pitch Size at Re Number of 6,000

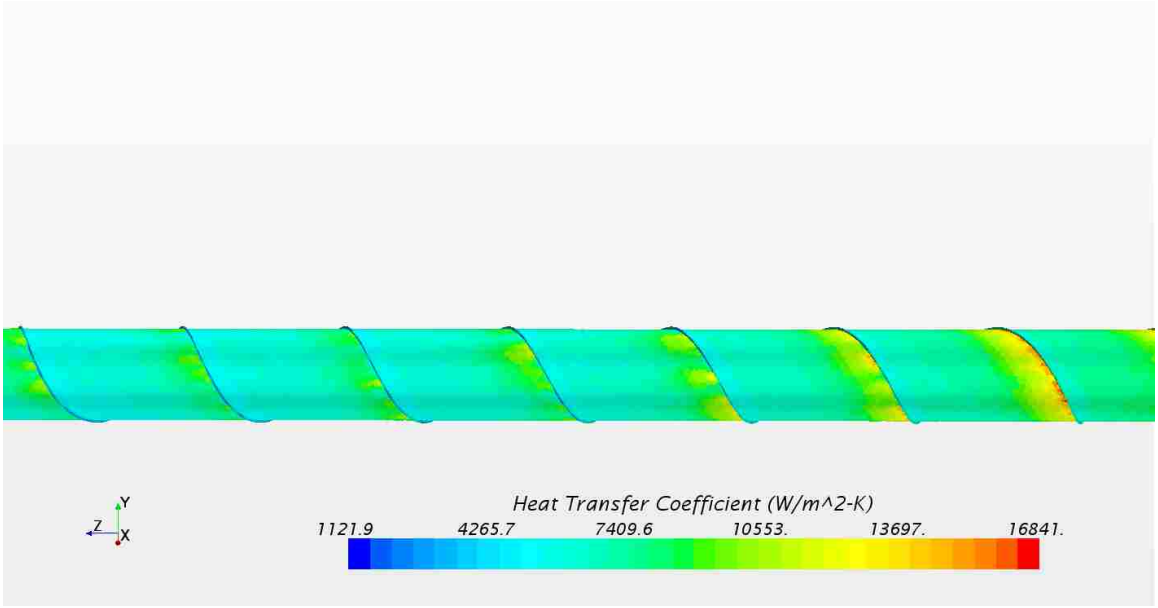


5.40 Local Heat Transfer Coefficient on Surface of the Tube with 12.7 mm Pitch Size at Re Number of 8,000

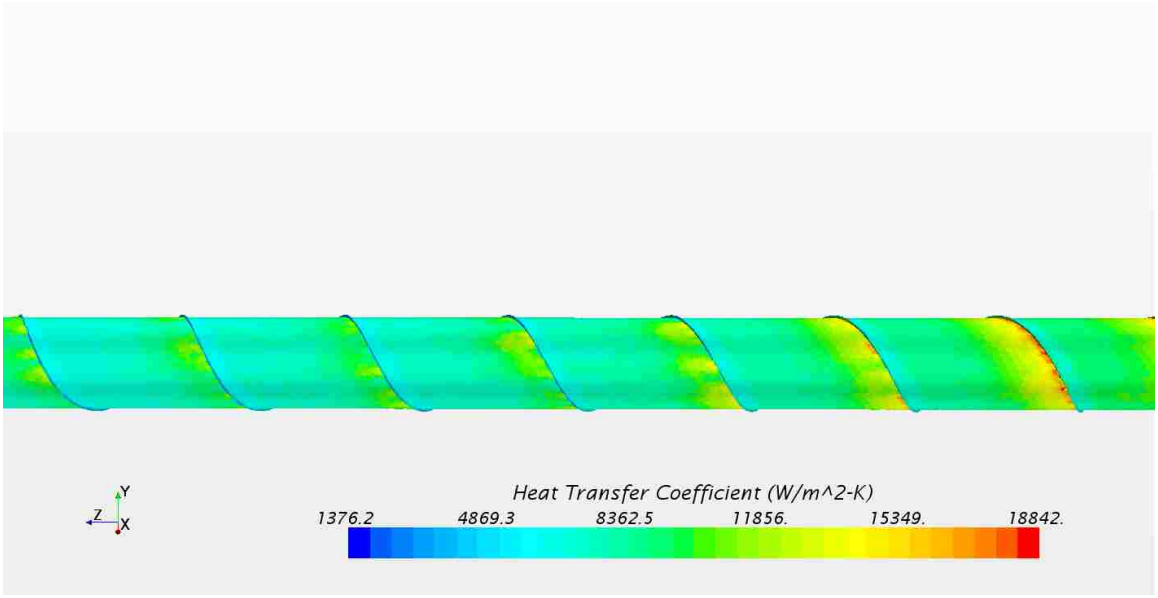


5.41 Local Heat Transfer Coefficient on Surface of the Tube with 12.7 mm Pitch Size at Re Number of 10,000

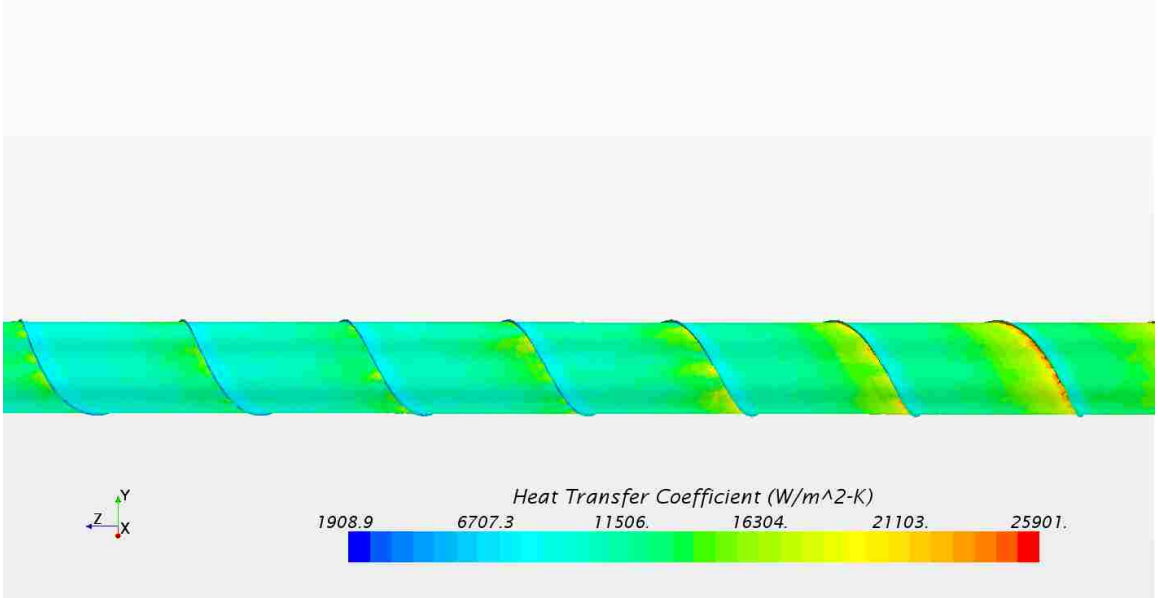


5.42 Local Heat Transfer Coefficient on Surface of the Tube with 12.7 mm Pitch Size at Re Number of 15,000

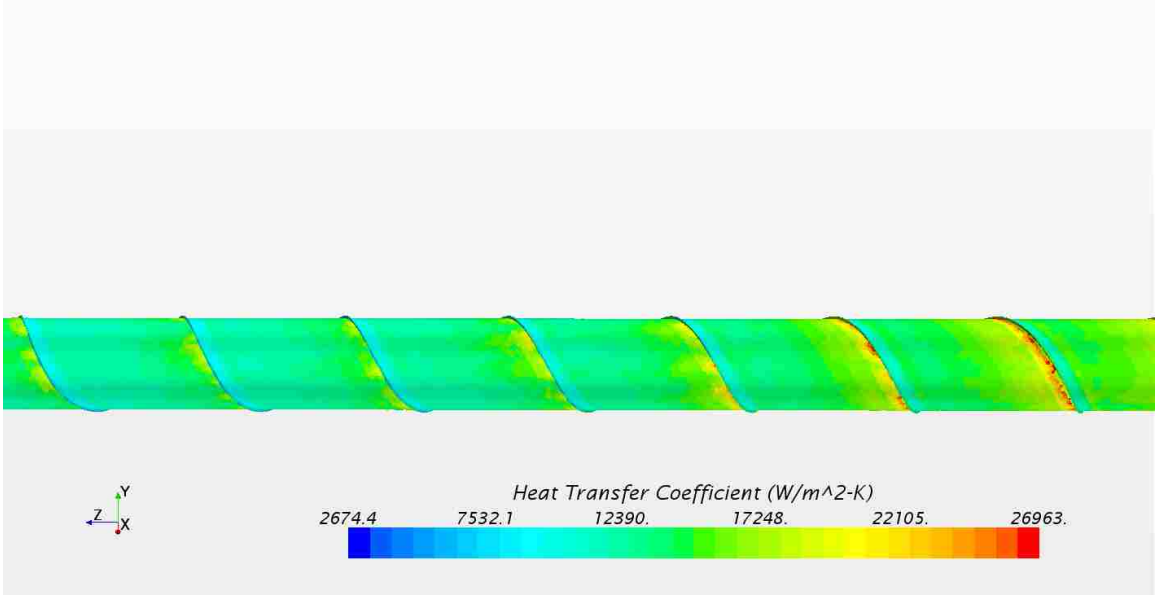


5.43 Local Heat Transfer Coefficient on Surface of the Tube with 12.7 mm Pitch Size at Re Number of 20,000

### 5.9.2 Circumferentially Averaged Value for the Heat Transfer Coefficient

In addition to the heat transfer coefficient which was obtained by software, seven axial cross sections (Figure 5.44) were considered along the tube to take another look at the variation of what might be called the "circumferential averaged calculated heat transfer coefficient". The same equation 18 was considered again, but instead of $T_{wall}$, the average temperature of the circumference of each section was inserted in the formula and the mean bulk temperature of each section was calculated by STAR-CCM+ and was substituted as $T_{fluid}$. The results are summarized in table 5.6 and 5.7 which indicate that this heat transfer coefficient decreases by increasing the pitch size at the same Re number. Also, the heat transfer coefficient in the grooved tube with same pitch size is increased by increasing the Re. And, it is fairly uniform regardless of their axial position along the pipe for the same Re and pitch as summarized and shown in Table 5.6. and 5.7 and Figure 5. 45, respectively. This could be partially explained by the fact that the helical grooves reduce the developing length distance in these flow situations, since the groove starts from the beginning of the tube length.

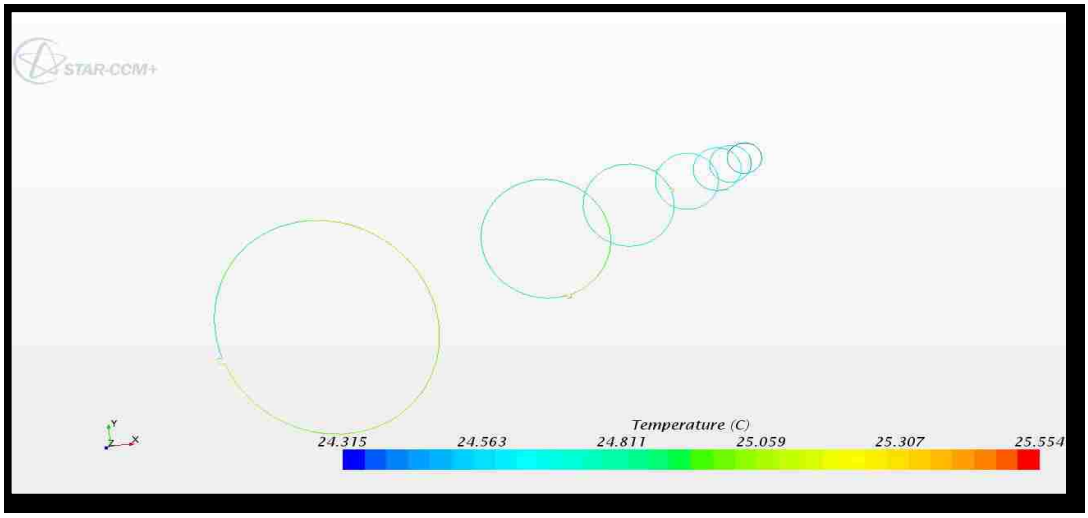


5.44 Schematic Diagram of Cross Sections at Different Axial Position along Different Grooved Tubes.

Table 5.6 Calculated Local Heat Transfer for Reynolds of 10000 in Grooved Tube with Different Pitch Size (7.1, 12.7, 50 and 130 (mm))

| Position (Re 10000) | Tube 7.1 | Tube 12.7 | Tube 50 | Tube 130 |
|---|---|---|---|---|
| z=0.035 | 9460 | 8750 | 7954 | 7777 |
| z=0.2 | 9210 | 9210 | 8139 | 7777 |
| Z=0.5 | 9722 | 9210 | 8333 | 7954 |
| Z=0.7 | 9210 | 9722 | 8536. | 7954 |
| Z=1 | 9722 | 9722 | 8333 | 7954 |
| z=1.3 | 8750 | 9210 | 8536 | 8139 |
| z=1.5 | 9722 | 8974 | 8536 | 7954 |
| z=1.7 | 9459 | 9459 | 8536 | 8139 |

Table 5.7 Calculated Local Heat Transfer for Grooved Tube with 12.7 (mm) Pitch

| Position ( Tube Pitch length 12.7 mm) | Re= 4000 | Re 6000 | Re 8000 | Re 10000 |
|---|---|---|---|---|
| z=0.2 | 3365 | 5833 | 7446 | 9210 |
| Z=0.5 | 3846 | 6034 | 7446 | 9210 |
| Z=0.7 | 3431 | 6363 | 8750 | 9722 |
| Z=1 | 3333 | 6250 | 7777 | 9722 |
| z=1.3 | 3608 | 5932 | 7446 | 9210 |
| z=1.5 | 4430 | 5932 | 7446 | 8974 |
| z=1.7 | 4605 | 6250 | 7777 | 9459 |

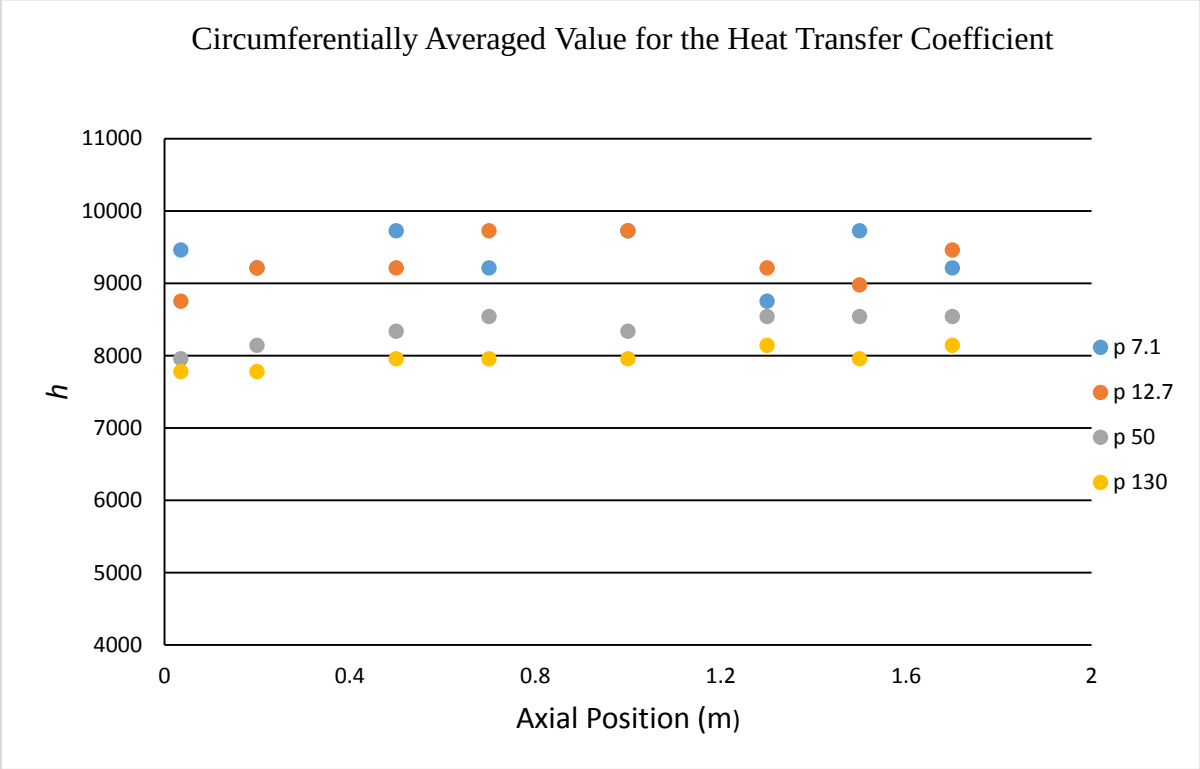


Figure 5.45 Circumferentially Averaged Heat Transfer for Reynolds of 10000 in Grooved Tube with Different Pitch Size (7.1, 12.7, 50 and 130 (mm))

5.9 Axial Pressure Drop along the Tube

The axial pressure drop profile was calculated along different cross-sections of the tube from the inlet to the outlet. The pressure drop was plotted for smooth tubes and grooved tubes with pitch sizes of (7.1,12.7, 50 and 130(mm)) and with Reynolds of 4000 to 20000 as shown in Figures 5.45 through 5.49. The plot shows that the pressure drop is higher for higher Re numbers as expected (Table 5.7). Also, pressure drop is higher for the grooved tube in comparison with the smooth tube (Figure 5.50). The calculated axial pressure drop for smooth and grooved tubes for various Reynolds numbers is shown in Table 5.7.

Table 5.8 Axial Pressure Drop for Smooth and Grooved Tube along the Length of Tubes

| Pressure (pa) / Re | Smooth tube | Grooved tube 7.1(mm) | Grooved tube 12.7(mm) | Grooved tube 50(mm) | Grooved tube 130(mm) |
|---|---|---|---|---|---|
| 4000 | 1714 | 1972 | 1873 | 1778 | 1756 |
| 6000 | 3314 | 3668 | 3554 | 3401 | 3348 |
| 8000 | 5126 | 5720 | 5604 | 5226 | 5220 |
| 10000 | 7381 | 8152 | 8003 | 7453 | 7261 |
| 15000 | 13176 | 15652 | 15220 | 14178 | 13286 |
| 20000 | 22270 | 25004 | 24496 | 23176 | 22747 |

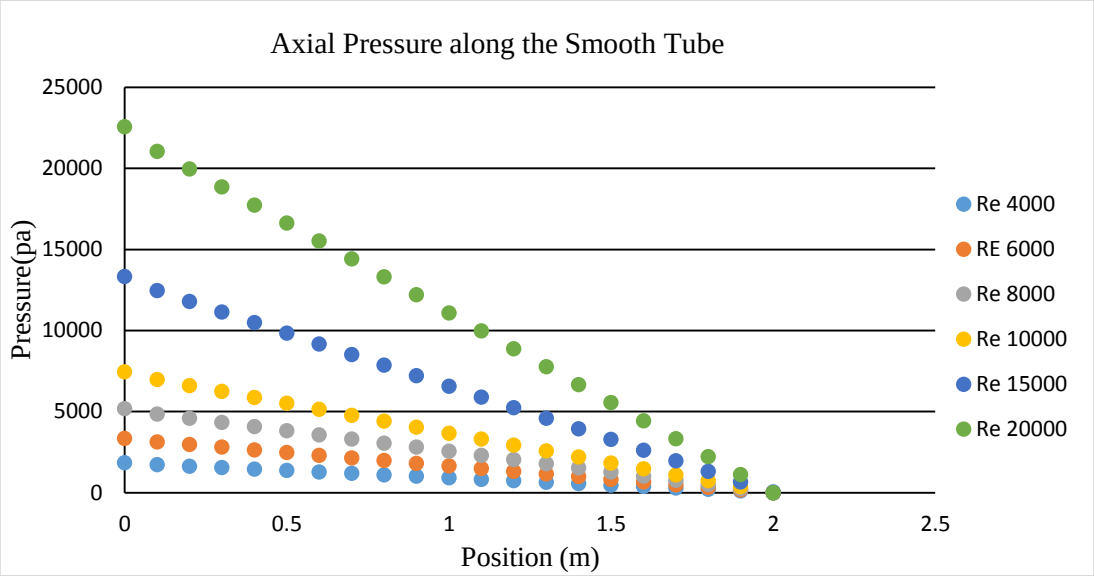


Figure5.46 Pressure Drop along the Smooth Tube for Reynolds Number Ranges between 4000-20000

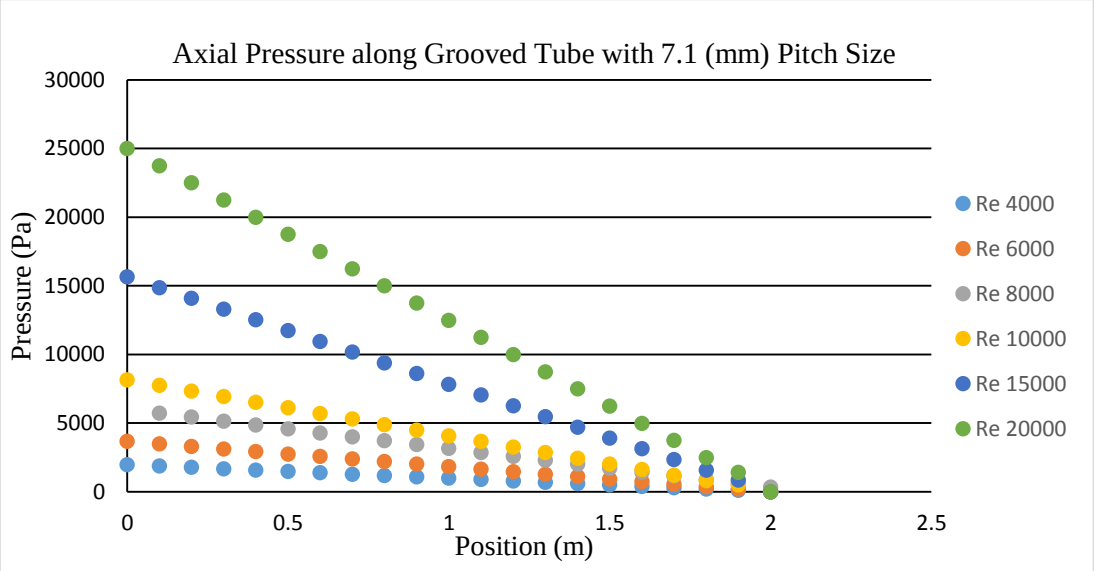


Figure 5.47 Pressure Drop along the Grooved Tube with Pitch Size of 7.1 (mm) for Reynolds Number Ranges between 4000-20000

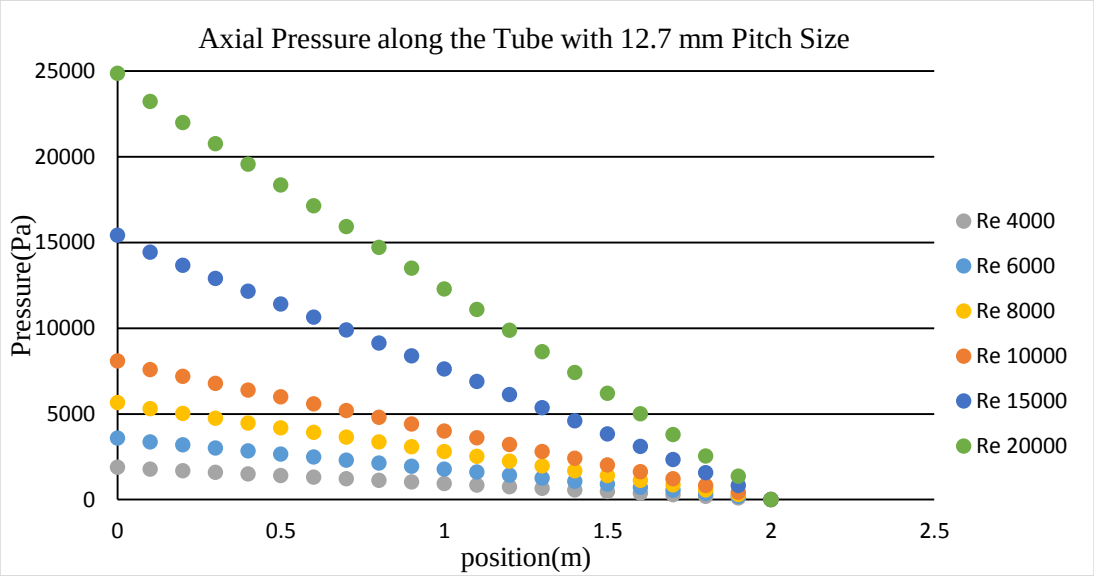


Figure 5.48 Pressure Drop along the Grooved Tube with Pitch Size of 12.7 (mm) for Reynolds Number Ranges between 4000-20000

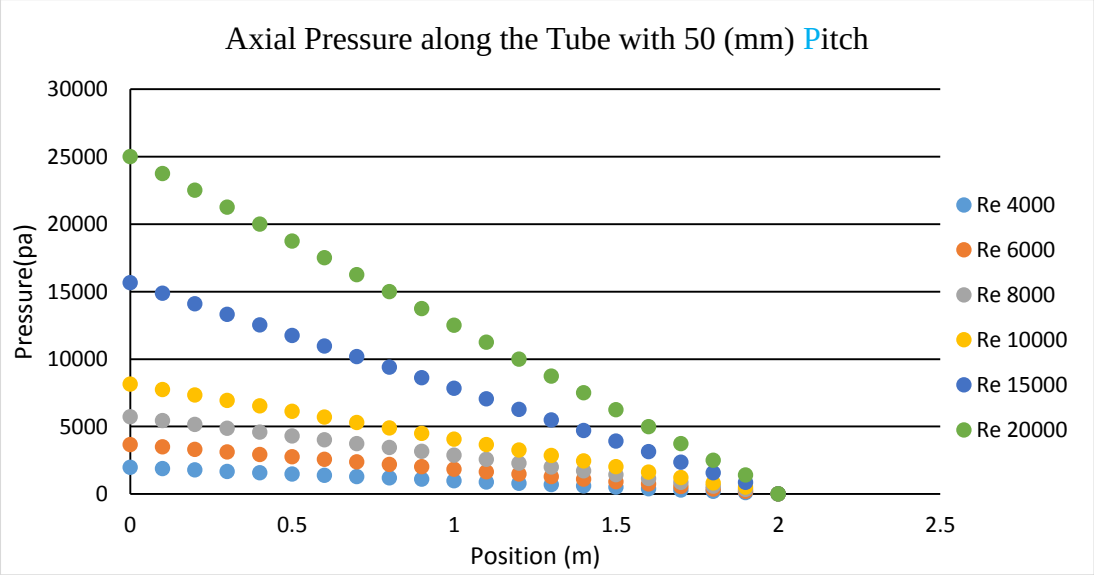


Figure 5.49 Pressure Drop along the Grooved Tube with Pitch Size of 50 (mm) for Reynolds Number Ranges between 4000-20000

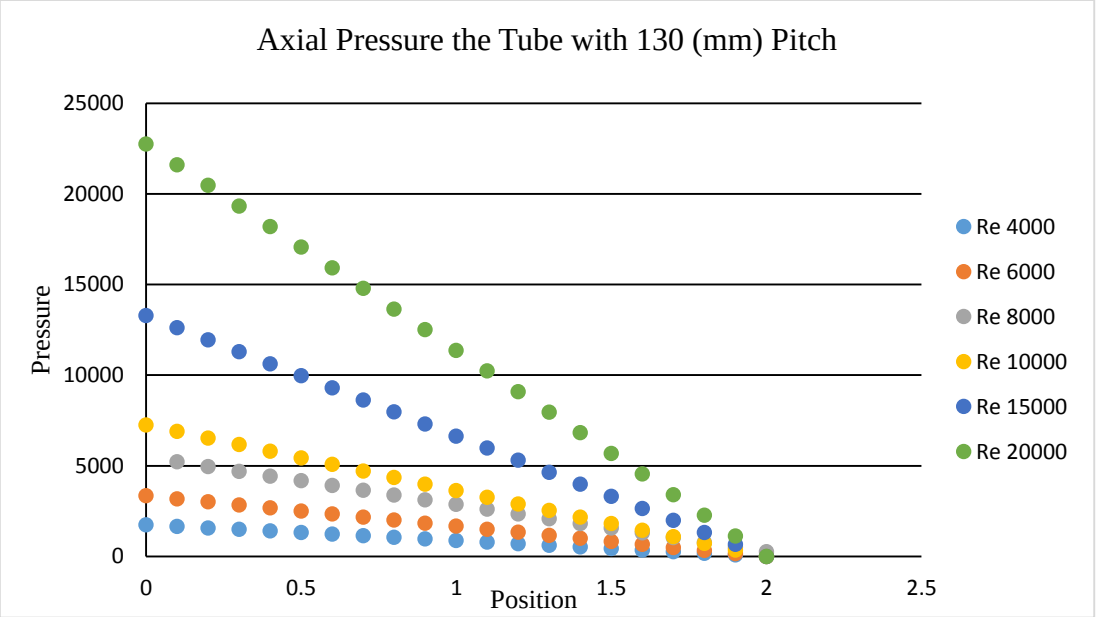


Figure 5.50 Pressure Drop along the Grooved Tube with Pitch Size of 130 (mm) for Reynolds number ranges between 4000-20000

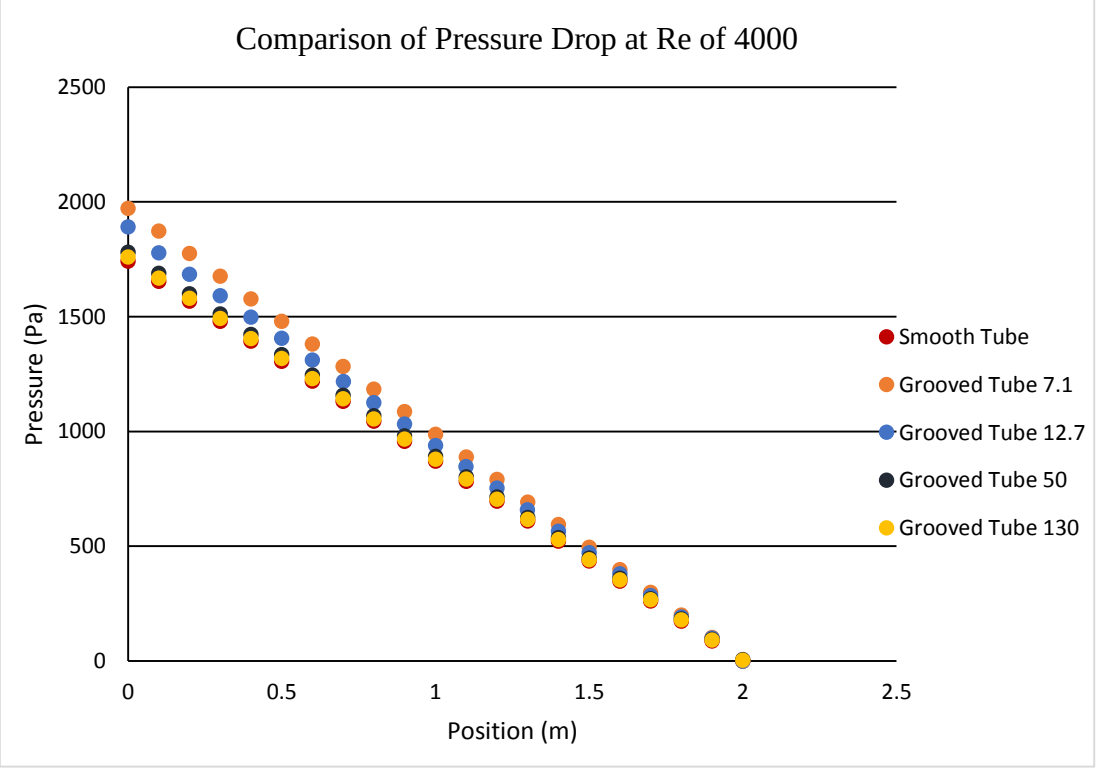


Figure 5.51 Comparison of Pressure Drop along the Grooved Tubes and Smooth Tube

# CHAPTER 6

# CONCLUSION

The CFD study on heat enhancement characteristics of water flowing inside grooved tubes with different pitch size were evaluated (7.1 mm, 12.7 mm, 50 mm and 130 mm). The study shows that the CFD results were in good agreement with the experimental data of a published paper [2]. Therefore, CFD modeling with commercial CFD software, STAR-CCM+, is a reliable method to be used to predict heat transfer characteristics of flow.

These CFD simulations present the effects of groove size and inlet mass flow rate on increasing the heat transfer in internally grooved tubes. This study shows that 3D CFD modeling can be used to accurately predict the Nusselt number and friction factor relative to the experimental data [1]. In the experimental study, the difference between the temperature of the pipe surface and fluid temperature were calculated by averaging the temperature of eight thermocouples on the surface and center-point temperature probe at outlet, then the CFD simulations were compared with the experimental data in a similar situation. Thus the results were within the uncertainty of the experimental values except for Reynolds of 4000. Additionally, for improving the accuracy of the results, d bulk temperature was evaluated instead of center-point temperature probe for finding the heat transfer coefficient of the current CFD work.

This study also provides insight into the hydrodynamic and thermal properties of the internally grooved tube which can be used in heat exchangers for heat enhancement purposes. High heat augmentation observed in an internally grooved tube with pitch size

of 7.1mm, shows that reducing the pitch size is effective in heat enhancement for internally grooved tubes. Additionally, increasing Reynolds number leads to increased heat transfer but at the penalty of pressure drop. Therefore, the proper Reynolds number and pitch size should be considered for better performance. Also, mean bulk temperature, streamlines, turbulent kinetic energy and pressure drop were evaluated to show the fluid heat enhancement characteristics by changing the pitch size and mass flow rate at the inlet. The conclusions are as follows:

1- The Nusselt number and friction factors obtained from current CFD works for grooved tubes were higher than smooth tubes. By decreasing the groove pitch size from 130 mm to 7.1, the Nusselt number and friction factor increased. The results for higher pitch size such as 50 and 130 mm shows insignificant effect on heat enhancement. Therefore, pitch size plays an important role in heat enhancement and should be chosen wisely.

2- By increasing the Reynolds number, the Nusselt number is increased in all cases due to more turbulence which led to mixing the flow. The highest Nusselt number belongs to a Reynolds number of 20000 in all cases. The Nusselt number increased about 10 t0 34% in grooved tubes in comparison to smooth tubes.

3- The thermal enhancement factor for grooved tubes tended to increase by increasing the Reynolds number and the overall highest thermal factor belongs to a pitch size of 7.1 mm. Also, the Reynolds of 15000 showed the highest value in all cases. Since increasing the Reynolds number, leads to more pressure drop, in the case of Reynolds of 20000, the thermal factor drops down. Results concluded that the augmentation of heat transfer is not efficient for a Reynold number more than 15000 due to higher pressure drop.

## 6.1 Future Work

Further studies can be done using this study as a base. Some of the possibilities are mentioned below:

1. This thesis utilized some basic assumptions to simplify the analysis. Water was used as the working fluid for all the tubes; therefore, Future CFD works can be done by using a different type of flow such as refrigerants in internally grooved tubes. Moreover, study can be made of adding additives to the main flow to determine increase of heat transfer, for example, some nanoparticles such as Al2O3, CuO,SiO2, and ZnO

2. In the current work, the effect of only pitch size on heat enhancement was investigated. Therefore, the effects of different geometry parameters such as width, height and helix angle for current groove tubes can be studied by commercial CFD software.

3. Instead of Rectangular groove shapes, circular or trapezoidal can be chosen for the internally grooved tubes.

4. The proposed designs can be used for cooling purposes such as air-cooled heat exchangers devices.

5. Investigation of cost and energy for using helical groove tube in heat exchangers.

6- Using the grooved pipe in the collector of parabolic trough solar power plants can be examined.

REFERENCES

[1] Al-Shamani, A.N., Sopian K., Mohammed, H.A., Mat,S., Ruslan, M.H. & Abed. A.M, (2015), Enhancement heat transfer characteristics in the channel with Trapezoidal rib–groove using nano fluids, *Case Studies in Thermal Engineering*, 5, 48–58

[2] Aroonrat, k., Jumpholkul, C., Leelaprachakul, R., Dalkilic. A.S., Mahian, O., & Wongwises, S., 2013, Heat transfer and single-phase flow in internally grooved tubes, *International Communications in Heat and Mass Transfer*, 42, 62–68.

[3] Bharadwaj, P., Khondge, A.D., Date, A.W., (2009), Heat transfer and pressure drop in a spirally grooved tube with twisted tape insert, *International Journal of Heat and Mass Transfer*, 52, 1938–1944.

[4] Bilen, K., Cetin, M., Gul, H., Balta,T., (2009), The investigation of groove geometry effect on heat transfer for internally grooved tubes, *Applied Thermal Engineering*, 29, 753–761.

[5] Blazek, J., 2001, computational fluid Dynamics: principle and applications, Alstom power Ltd, Switzerland, Elsevier.

[6] Ceylan, K., Kelbaliyev, G., (2003), The roughness effects on friction and heat transfer in the fully developed turbulent flow in pipes, *Applied Thermal Engineering* ,23, 557–570.

[7] Chaurette, J. PIPE ROUGHNESS VALUES, (2003, February) Retrieved from www.lightmypump.com February 2003

[8] Eiamsa-ard, S., Promvonge, P., (2008), Numerical study on heat transfer of turbulent channel flow over periodic grooves, *International Communications in Heat and Mass Transfer*, 35, 844-852.

[9] Elyyan, M.A. (2008). Heat Transfer Augmentation Surfaces Using Modified

Dimples/Protrusions (Dissertation). Virginia Polytechnic Institute and State University, Virginia.

[10] Georgi Kalitzin,G., Medic, G., Iaccarino,G., Durbin,P., (2005) Near-wall behavior of RANS turbulence models and implications for wall functions, *Journal of Computational Physics*, 204, 265–291.

[11] Graham, D., Chato, J.C., Newell, T.A., (1999), Heat transfer and pressure drop during condensation of refrigerant 134a in an axially grooved tube, *International Journal of Heat and Mass Transfer*, 42,1935-1944.

[12] Jiji, L.M. (2009). *Heat Convection* (2nd ed.). Germany: Springer.

[13] Johar, G. & Hasda, V., (2010) EXPERIMENTAL STUDIES ON HEAT TRANSFER AUGMENATATION USING MODIFIED REDUCED WIDTH TWISTED TAPES (RWTT) AS INSERTS FOR TUBE SIDE FLOW OF LIQUIDS Thesis, Department of Chemical Engineering, National Institute of Technology Rourkela.

[14] Kaji, R., Yoshioka, S., Fujino, H., (2012) The Effect of Inner Grooved Tubes on the Heat Transfer Performace of Air-Cooled Heat Exchangers of Co2 Heat Pump System at International Refrigeration and Air Conditioning Conference, Purdue e-Pubs.

[15] Liu,J., Xie, G.& Simon, T.W., (2015), Turbulent flow and heat transfer enhancement in rectangular channels with novel cylindrical grooves, *International Journal of Heat and Mass Transfer*, 81, 563–577.

[16] Liu, S. & Sakr, M., (2013) A comprehensive review on passive heat transfer enhancements in pipe exchangers, *Renewable and Sustainable Energy Reviews*, 19, 64–81.

[17] Manjunath, K. & Kaushik, S.C., (2014), Second law thermodynamic study of heat exchangers: A review, *Renewable and Sustainable Energy Reviews*, 40, 348–374.

[18] Oliver, J.A. (2009) , SINGLE PHASE HEAT TRANSFER AND PRESSURE DROP OF WATER COOLED AT A CONSTANT WALL TEMPERATURE INSIDE A HORIZONTAL CIRCULAR SMOOTH AND ENHANCED TUBES WITH DIFFERENT INLET CONFIGURATION IN THE TRANSITIONAL FLOW REGION, dissertation, university of Pretoria, South Africa.

[19] Rahman, M., Zhen & Kadir A.K., (2013), Numerical simulation of fluid flow and heat transfer in enhanced copper tube, 4th International Conference on Energy and Environment (ICEE), Malaysia, IOP Publishing Ltd.

[20] Salman, S. D., Kadhum, A.A.H., Takriff, M.S., Mohamad, A.B., (2014),CFD Simulation of Heat Transfer Augmentation in a Circular Tube Fitted with Alternative Axis Twisted Tape in Laminar Flow under a Constant Heat Flux, *Heat Transfer—Asian Research*, 43, 4.

[21] Salman, S.D., Kadhum, A.A.H., Takriff, M.S., Mohamad, A.B, (2013), CFD Analysis of Heat Transfer and Friction Factor Characteristics in Circular Tube Fitted with Quadrant-Cut Twisted Tape Inserts, *Mathematical Problems in Engineering*, Hindawi Publishing Corporation.

[22] San, J. Y. & Huang, W.C., (2006), Heat transfer enhancement of transverse ribs in circular tubes with consideration of entrance effect, *International Journal of Heat and Mass Transfer, 49*, 2965–2971.

[23] Shih, T.H., Liou, W.W., Shabbir, A., Yang, Z., Zhu, J. (1994). A New k- Eddy Viscosity Model for High Reynolds Number Turbulent Flows -- Model Development and Validation. *NASA*, TM- 106721.

[24] Singh,S., Singh,B., Hans,V.S., Gill, R.S. (2015),CFD (computational fluid dynamics) investigation on Nusselt number and friction factor of solar air heater duct roughened with non-uniform cross-section transverse rib, *Journal of Energy* ,84, 509-517.

[25] STAR-CCM+ user manual, version 9.04.009. CD-Adapco.

[26] Webb, R.L. & Kim, N.H., (2005), Principles of Enhanced Heat Transfer (2nd ed.), New York: Taylor & Francis.

[27] Xinyi, T & Dongsheng, Z., (2012), Experimental and Numerical Study on Heat Transfer Enhancement of a Rectangular Channel with Discontinuous Crossed Ribs and Grooves, *Chinese Journal of Chemical Engineering*, 20(2), 220-230.

[28] Zikanov, O. (2010). *Essential Computational Fluid Dynamics* (1st ed.). New Jersey: John Wiley & Sons.

.

# CURRICULUM VITAE

Graduate College

University of Nevada, Las Vegas

Sogol, Pirbastami

Degrees:

Bachelor of Science, Biomedical Engineering, 2011

University of Science and Research Iran

Thesis Title: CFD Simulation of Heat Enhancement in Internally Helical Grooved Tubes

Thesis Examination Committee:

Chairperson, Dr. Samir F. Moujaes, Ph.D.

Committee Member, Dr. Brendan O'Toole, Ph.D.

Committee Member, Dr. Darrell Pepper, Ph.D.

Graduate Faculty Representative, Dr. Samaan Ladkany, Ph.D.